Networks and gelation

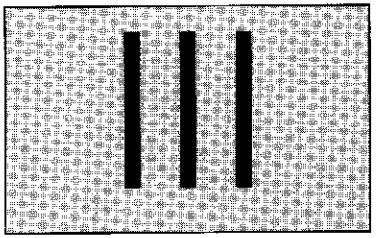

Random branching and gelation

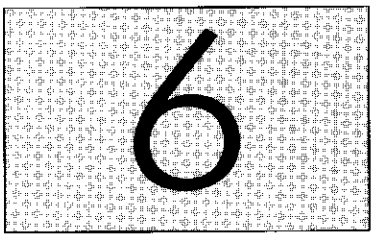

6.1 Introduction

Everyday life encounters many materials in transition from liquid to solid, examples are preparing Jello® gelatin or mixing Epoxy glue. This fascinating phenomenon is called gelation and it is caused by the formation of **crosslinks** between polymer chains. In the above examples, these crosslinks are induced either by microcrystallization upon cooling (Jello®) or by covalent bonds formed on mixing (Epoxy). The final state after crosslinking consists of linear polymer **strands** connected by crosslinks.

Linking chains together leads to progressively larger branched polymers [see Fig. 6.1(a)]. The polydisperse mixture of branched polymers obtained as the result of such a process is called the **sol** (since the molecules are soluble). As the linking process continues, still larger branched polymers are obtained [Fig. 6.1(b)]. At a certain extent of reaction a molecule spanning the whole system appears. Such a huge molecule will not dissolve in a solvent, but may only swell in it. This 'infinite polymer' is called the **gel** or **network** and is permeated with finite branched polymers [Fig. 6.1(c)]. The transition from a system with only finite branched polymers (exclusively sol) to a system containing also an infinite molecule (gel) is called the **sol–gel transition** (or **gelation**) and the critical point where gel first appears is called the **gel point**.

The early studies of the sol–gel transition date back to the dawn of polymer science. The first quantitative theories of gelation—the mean-field theories—were formulated in the 1940s by Flory and Stockmayer. Critical percolation theory was successfully applied to gelation in the 1970s. A number of growth models (diffusion limited aggregation, cluster–cluster aggregation, kinetic gelation) have been developed in the 1980s to describe the kinetic aspects of aggregation and gelation.

Different types of gelation transitions are summarized in Fig. 6.2. Gelation can occur either by physical linking (as in the Jello® gelatin example above) or by chemical crosslinking (as in the Epoxy glue example). The first type is called **physical gelation**, while the second type is called **chemical gelation**.

It is convenient to distinguish between strong and weak physical gels. **Strong physical gels** have **strong physical bonds** between polymer chains that are effectively permanent at a given set of experimental conditions.

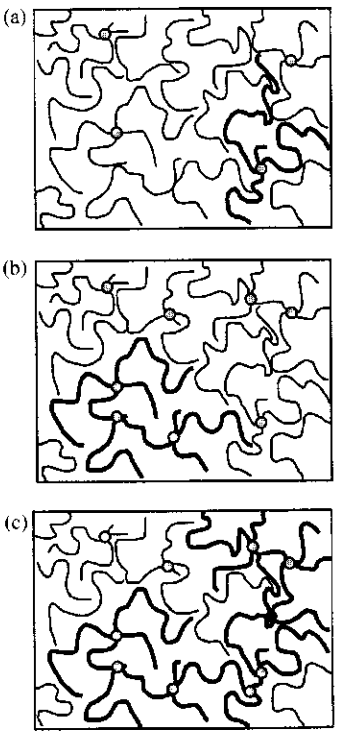

Fig. 6.1
Crosslinking of linear chains: (a) four crosslinks; (b) eight crosslinks; (c) 10 crosslinks. The largest branched polymer is highlighted and the 10th crosslink (dark) formed an incipient gel.

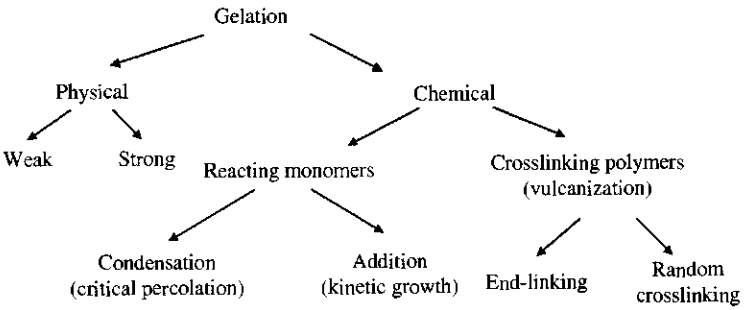

Fig. 6.2
Classification of gelation transitions (and the models describing them).

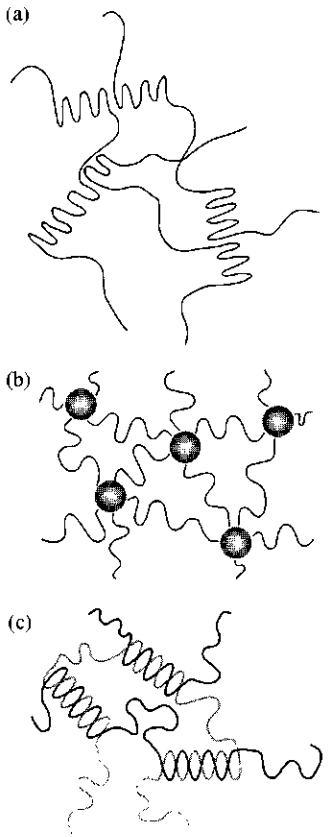

Fig. 6.3
Examples of strong physical gels with crosslinks that are: (a) lamellar microcrystals; (b) glassy nodules; (c) double helices.

Examples of strong physical bonds are glassy and microcrystalline nodules, or double and triple helixes (see Fig. 6.3). The strong physical gels formed by these bonds are solids and can only melt and flow when the external conditions change (such as changing temperature for **thermoreversible gels** like Jello®). Hence, strong physical gels are analogous to chemical gels (discussed below).

The difference between strong physical gels and chemical gels has important industrial applications. **Thermoplastic elastomers** are examples of strong physical gels. Triblock copolymers of styrene–isoprene–styrene flow like liquids at high temperature (far above the polystyrene glass transition temperature of 100 °C). However, at room temperature the polystyrene blocks are immobilized in glassy nodules [Fig. 6.3(b)] that act as effective crosslinks for polyisoprene, whose glass transition temperature is −60 °C. These elastomers are reformable by simply heating above 100 °C, and hence are called thermoplastic.

Weak physical gels have reversible links formed from temporary associations between chains. These associations have finite lifetimes, breaking and reforming continuously. Examples of weak physical bonds are hydrogen bonds, block copolymer micelles above their glass transition, and ionic associations (Fig. 6.4). Such **reversible gels** are never truly solids but if the association lifetime is sufficiently long they can appear to be solids on certain time scales. Hence, whether a reversible gel is weak or strong depends on the time scale over which it is observed. Paint is a good example of a reversible gel. The weak hydrophobic associations in a water-based paint give it properties of a weak network at short time scales, but these associations have short lifetime and allow paint to flow at long times. These weak associations can also be easily broken by stirring, spraying, or brushing.

In contrast, chemical gelation involves formation of covalent bonds and always results in a strong gel. There are three main chemical gelation processes: condensation, vulcanization, and addition polymerization.

Condensation reactions typically start from a melt or solution of monomers that are capable of reacting with each other. If all monomers are

bifunctional (able to react with at most two other monomers) then only linear chains result and no network can be formed. Condensation of bifunctional monomers and the molar mass distribution of the resulting linear chains are discussed in Section 1.6.2. If at least some of the starting monomers have functionality three or higher, so that they can form bonds with three or more other monomers, then branched polymers are formed and a sol–gel transition is possible. An example is a condensation reaction of a difunctional acid (any molecule with two acid groups, A_2) with a trifunctional alcohol (any molecule with three alcohol groups, B_3).[1] Each trifunctional alcohol can become a branch point leading to randomly branched polyesters and ultimately networks. Condensation of monomers with functionality greater than two, like the $A_2 + B_3$ system, in the melt (meaning that there is no non-reactive diluent present) is well described by the **critical percolation** model. This model is discussed in Section 6.5. Condensation polymerization of monomers with one acid group and $f-1$ alcohol groups, AB_{f-1} with functionality f higher than 2 produces randomly branched polymers that are **hyperbranched**, but does not lead to gelation, as will be discussed in Section 6.2.1.

Vulcanization refers to crosslinking of long linear chains that start out strongly overlapping each other. This process is well described by the **mean-field percolation** model, discussed in Section 6.4. Condensation and vulcanization are two closely related processes. By increasing the fraction of bifunctional alcohol monomers in the first process (i.e., increasing the fraction of B_2 in an $A_2 + B_2 + B_3$ system) or by decreasing the molar mass of linear chains in vulcanization it is possible to study the crossover between them. In vulcanization, one usually distinguishes end-linking [multifunctional units crosslinking the ends of the chains—see Fig. 6.5(a)] from random crosslinking with bonds formed between monomers along the chains [see Fig. 6.5(b)]. This random crosslinking vulcanization process was invented by Goodyear in 1839 to crosslink natural rubber (*cis*-polyisoprene) using sulphur. In Section 6.5.4, we will learn that the overlap of the branched polymers diminishes as the vulcanization proceeds, and consequently vulcanization crosses over to critical percolation sufficiently close to the gel point.

In **addition polymerization**, a free radical transfers from one vinyl monomer to another, leaving behind a trail of chemical bonds (Fig. 6.6). The distinction of addition polymerization, compared with condensation polymerization, is the high correlation of the formed bonds along the path of a free radical. Certain monomers (with two double bonds, such as divinylbenzene) can be visited twice by free radicals and become crosslinks (black circles in Fig. 6.6). As the neighbouring trails of formed bonds begin to overlap, the system approaches its gel point. The model describing branching and network formation via addition polymerization is called **kinetic gelation**.

[1] In this notation, A groups only react with B groups.

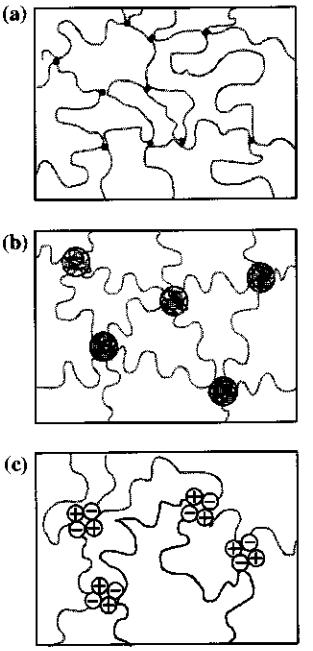

Fig. 6.4
Weak physical bonds: (a) hydrogen bonds; (b) block copolymer micelles; (c) ionic associations.

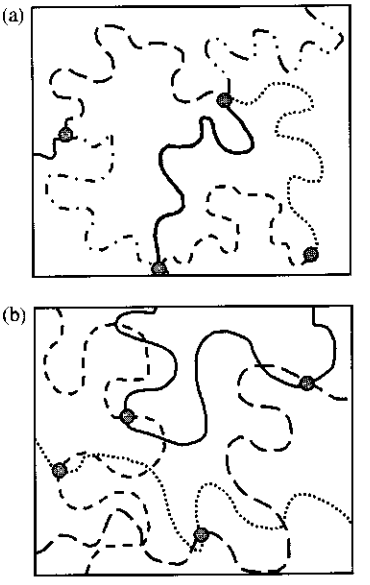

Fig. 6.5
Examples of vulcanization: (a) end-linking; (b) random crosslinking. Different lines represent different chains.

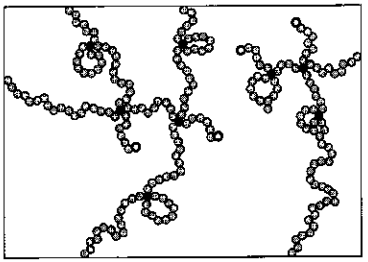

Fig. 6.6
Addition polymerization with branching. Free radicals are denoted by open circles and crosslinks by black circles.

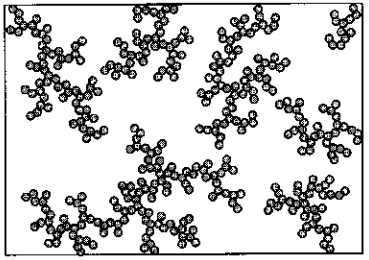

Fig. 6.7
Cluster–cluster aggregation leading to gelation.

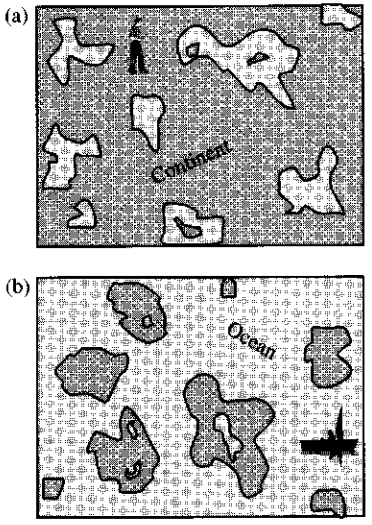

Fig. 6.8
Percolation transition from a continent with lakes to an ocean with islands.

The condensation reaction in solution can, at early stages, be **diffusion-controlled**, meaning that the time it takes for molecules to diffuse towards each other in order to react controls the reaction time. This diffusion-limited process is described by kinetic models such as **diffusion-limited aggregation** and **cluster–cluster aggregation**. During aggregation, highly ramified clusters are formed that are fractals with fractal dimension $\mathcal{D} < 3$, as depicted in Fig. 6.7. At first, only small clusters are formed and the monomer density inside each cluster is higher than the overall monomer density in solution. Since $\mathcal{D} < 3$, as the clusters grow by coalescing with other clusters, the monomer density inside them decreases and finally reaches the overall solution density. At this point the clusters overlap and their growth at later stages and the sol–gel transition itself is described by the critical percolation model. Examples are aggregation of colloidal gold and silica, the latter being a low-temperature method of making glasses.

It is very important to distinguish the equilibrium gelation models (such as mean-field gelation and critical percolation) where kinetics only affect reaction rates but not the structures formed, from the growth models (such as cluster–cluster aggregation and kinetic gelation) in which rate processes strongly influence the structures formed. All of these processes have at least a small region near the gel point (called the critical region) where the reacting structures are just at overlap, which is described by the critical percolation model. However, in many cases this region is too small to be experimentally accessible. In Section 6.5.4, the size of this small critical region in vulcanization is estimated using the Ginzburg criterion.

6.1.1 Percolation around us

Before considering the details of the gelation process, it is useful to mention the broad spectrum of other systems undergoing similar connectivity transitions and therefore described by mathematically similar percolation models. Familar examples are water percolating through sand and coffee percolating through ground coffee beans.

6.1.1.1 Deluge

The first written reference to a percolation-related process can be found in the Old Testament (Genesis 7–10). It describes a continent, different parts of which are at different heights above the sea level. Rain begins to fall and the sea level rises, submerging the low-lying parts of the continent under water. At the early stages of the deluge it is still possible to walk across the continent, travelling around numerous puddles, lakes, and perturbing bays [Fig. 6.8(a)]. As the water level rises above some critical point called the **percolation threshold**, the continent ceases to exist as it is broken into an archipelago of islands [Fig. 6.8(b)]. At the later stages of the deluge it is no longer possible to travel large distances over land and it becomes necessary to sail between the islands by boat. This transition from a continent containing lakes and bays [Fig. 6.8(a)] to an ocean containing islands [Fig. 6.8(b)] is an example of a percolation transition. When the deluge

stops and the sea level lowers, an opposite transition takes place from an ocean with islands to a continent with lakes.

6.1.1.2 Forest fires

Another example of a percolation-related process is the spreading of a fire in a forest without wind. Consider a forest represented by a set of trees, as sketched in Fig. 6.9. Smokey the Bear goes into hibernation, leaving an unextinguished campfire under one of the trees and the tree catches fire. A burning tree can ignite a neighbouring tree with some probability p. A very important question is whether the fire will propagate and burn most of the forest or stop after burning only a small copse of trees.

The ignition probability p depends on the distance between the trees, the size of the trees, and on how dry the season is. Depending on these conditions, there are two possible outcomes resulting from Smokey's carelessness:

(1) An accident—If the trees are small and grow far apart and the season is relatively wet, the ignition probability p is low and the fire would stop after burning only a small cluster of trees.
(2) A major disaster—If the trees are large, grow close together and the season is dry, the ignition probability p is large and the fire would spread across the forest burning a significant fraction of the trees.

The transition between these two possible outcomes—an 'island' and a 'continent' of burned trees—is another example of a percolation transition. In the present example of a forest fire we have described percolation on a discrete set of trees, while in the example of a deluge we dealt with a continuously varying water level on a constant terrain. The two problems are quite different, but both are described by percolation models.

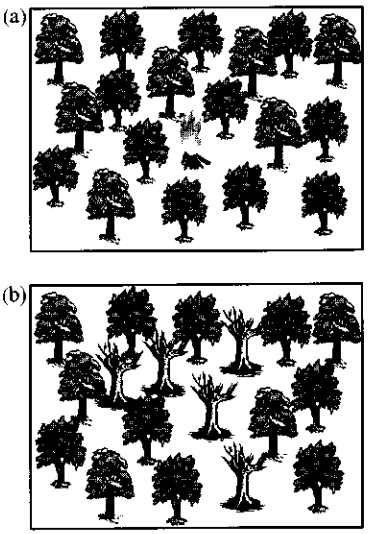

Fig. 6.9
Spreading of a fire in a forest.

6.1.1.3 Spreading of a contagious disease

Another problem related to percolation and analogous to forest fires is the spreading of a disease in an apple orchard. In an orchard, the trees grow on a regular lattice [Fig. 6.10(a)]. A sick tree can contaminate its neighbour with probability p. Just as in the above example, for small values of p the disease remains contained and will only strike a finite cluster (island) of trees. For higher values of the disease transmission probability p above the percolation threshold, p_c, the disease will spread through the whole orchard, affecting a large fraction of its trees [Fig. 6.10(b)]. This problem is an example of bond percolation that was described by Hammersley in 1956. In a **bond percolation** model, all sites are occupied (in the present example, all lattice sites are occupied by trees). The percolation process is determined by the presence or absence of bonds between two neighbouring sites (in the present example, a bond corresponds to the spreading of the disease between two neighbouring trees). The island of sick trees corresponds to a cluster of sites connected by bonds. The spreading of a disease in an orchard is an example of bond percolation on a regular two-dimensional lattice. For a triangular lattice, the percolation threshold is $p_c \cong 0.34729$ and for the

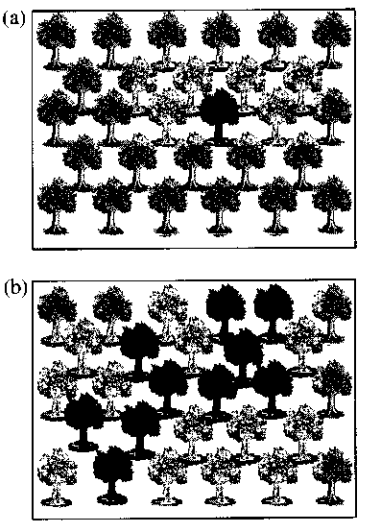

Fig. 6.10
Spreading of a disease in an orchard.

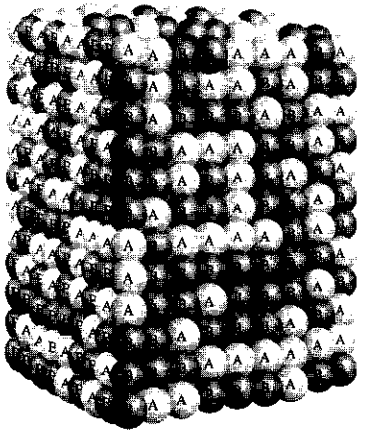

Fig. 6.11
A random three-dimensional substitutional alloy $A_{1-q}B_q$.

square lattice it is $p_c = 1/2$. In contrast, the forest fire is an example of two-dimensional bond percolation on a random set of points (trees in a forest).

6.1.1.4 Substitutional alloy

Consider a substitutional alloy $A_{1-q}B_q$ with A and B atoms randomly occupying sites of a regular lattice (see Fig. 6.11). A B cluster is defined as a set of neighbouring B atoms. For low values of the fraction q of B atoms in the $A_{1-q}B_q$ alloy, the B clusters are small. With increasing fraction q of B atoms, B clusters become progressively larger and above some critical value q_c a macroscopic B cluster spanning the whole crystal appears. This transition from a set of finite B clusters (for $q < q_c$) to a crystal with a macroscopic B cluster in addition to finite clusters (for $q > q_c$) is an example of **site percolation** on a lattice. In site percolation, only some sites of the lattice are occupied (in the present example—by B atoms). The neighbouring occupied sites are always connected into a cluster (in the language of the bond percolation model, the bond between neighbouring occupied sites is always present with probability $p = 1$). If B atoms are ferromagnetic, the B clusters would form magnetic domains. In this case, the percolation model gives a necessary condition for a transition from a paramagnet with only small magnetic domains to a ferromagnet with a macroscopic domain and finite spontaneous magnetization.

Note that for $q < q_c$ only A percolates, for $q_c < q < 1 - q_c$ both A and B percolate, and for $q > 1 - q_c$ only B percolates. Copper and gold form substitutional alloys on a face-centred cubic lattice ($Cu_{1-q}Au_q$). For $q < 0.2$, there are isolated gold islands in an ocean of copper. Conversely, for $q > 0.8$, there are isolated copper islands in an ocean of gold. For $0.2 < q < 0.8$ both copper and gold are co-continuous. There are still isolated islands of each metal but there are also continuous pathways across the macroscopic material consisting only of each individual metal.

6.1.1.5 Classes of percolation models

We have given four examples of connectivity transitions described by percolation models. Other examples include the conductor–insulator transition for a random resistor network, oil recovery through a porous rock, and communication networks (the world wide web).

The percolation transition can be defined on a continuous manifold (deluge) or on a discrete set of objects. This discrete set can be either random (such as trees in a forest) or regular (such as rows of trees in an orchard). Two types of percolation models have been distinguished: bond percolation (spreading of a disease) and site percolation (substitutional alloy). These can also be combined into a **site-bond percolation** model, where only some sites are occupied and bonds may only be placed between occupied adjacent sites. For example, if a fraction $1 - q$ of the trees in the orchard are randomly cut down, the spreading of a disease between the trees of the remaining fraction q with the spreading probability p could be studied using site-bond percolation.

The value of the percolation threshold depends on many details of the model, including the type of lattice. Table 6.1 compares site and bond

Table 6.1 Values of site and bond percolation thresholds on selected lattices

Lattice	d	f	q_c (site)	p_c (bond)
Honeycomb	2	3	0.696	0.652
Square	2	4	0.592	0.5
Triangular	2	6	0.5	0.347
Diamond	3	4	0.43	0.388
Simple cubic	3	6	0.312	0.249
BCC	3	8	0.246	0.180
FCC	3	12	0.198	0.119

The dimension of space is d and the coordination number of the lattice is f. BCC is body-centred cubic and FCC is face-centred cubic.

percolation thresholds for three two-dimensional lattices and four three-dimensional lattices. In each dimension, as the coordination number of the lattice increases, the percolation threshold decreases.

6.1.2 Percolation in one dimension

The percolation transition can be described in space of any dimension. Examples of two-dimensional percolation are deluge, forest fire, spreading of a contagious disease in an orchard, and gelation of a polymer at an air–water interface. Examples of three-dimensional percolation are substitutional alloys and bulk polymer gelation. A problem analogous to one-dimensional percolation is the condensation polymerization of bifunctional monomers described in Section 1.6.2.

Consider the condensation polymerization of bifunctional monomers, each with two different reactive groups A and B, where A is only allowed to react with B in an intermolecular fashion. For example, if group A were –OH and group B were –COOH, the resulting polymers would be polyesters with the link B–A denoting –COO–. For simplicity of notation, we call the unreacted monomer AB. The bonds allowed between groups A and B can be formulated as bond percolation on a one-dimensional lattice by simply placing the unreacted monomers on every site of the lattice and randomly connecting (or reacting) them with probability p.

AB–AB AB–AB–AB AB AB–AB–AB–AB AB–AB AB

There is exactly one unreacted A group (and one unreacted B group) per molecule. The number density of molecules $n_{tot}(p)$ (number of molecules per monomer) is therefore equal to the fraction $1-p$ of unreacted groups:

$$n_{tot}(p) = 1 - p. \tag{6.1}$$

The number-average degree of polymerization (the number of monomers per molecule) is [see Eq. (1.55)] the reciprocal of the number density of molecules:

$$N_n(p) = \frac{1}{n_{tot}(p)} = \frac{1}{1-p}. \tag{6.2}$$

A linear polymer (N-mer) is a cluster of N monomers (sites) connected by $N-1$ bonds and containing one unreacted A group and one unreacted B group. *The number fraction distribution (mole fraction of N-mers) is given by the probability that a chosen unreacted* A *group is part of an N-mer.* This number fraction of N-mers is the probability of $N-1$ formed bonds (p^{N-1}) and one unreacted B group ($1-p$) [Eq. (1.52)]:

$$n_N(p) = p^{N-1}(1-p). \tag{6.3}$$

For one-dimensional percolation, the system can either be below the percolation threshold ($p < p_c = 1$) with finite polymers or at the threshold ($p = p_c = 1$) with one infinite polymer, but not above the threshold. States above the threshold exist only for percolation in dimensions higher than one.

In a real polymerization reaction, monomers are distributed in three-dimensional space rather than on a one-dimensional lattice. An important consequence is that cyclic structures of various numbers of monomers can be created. Unlike their linear counterparts, these ring polymers have no reactive ends and never grow longer as reaction proceeds. They are not accounted for in the simple theory presented here.

6.2 Branching without gelation

6.2.1 Hyperbranched polymers

Another reaction that does not lead to gelation is the polymerization of hyperbranched polymers from AB_{f-1} monomers (each with a single functional group of type A and $f-1$ functional groups of type B) in which A can only react with B. For functionality $f=2$, this reduces to the condensation polymerization of linear chains, described above. For $f>2$, such a process leads to formation of highly branched molecules.

Let p be the fraction of reacted B groups. The fraction of reacted A groups is $p(f-1)$ (the same number of reacted A and B groups, but $f-1$ times smaller total number of A groups in AB_{f-1} molecules). Therefore, the fraction of unreacted A groups is $1-p(f-1)$. There is one unreacted A group per molecule, giving the total number of molecules per monomer:

$$n_{\text{tot}}(p) = 1 - p(f-1). \tag{6.4}$$

The number-average degree of polymerization (the average number of monomers per molecule) is the reciprocal of $n_{\text{tot}}(p)$:

$$N_{\text{n}}(p) = \frac{1}{1-p(f-1)}. \tag{6.5}$$

This number-average degree of polymerization diverges at $p_{\text{c}} = 1/(f-1)$. This maximum possible fraction of reacted B groups corresponds to complete reaction of all A groups $(f-1)p_{\text{c}} = 1$.

Each N-mer in a condensation polymerization of AB_{f-1} monomers consists of $N-1$ reacted A–B bonds and exactly one unreacted A group, as shown in Fig. 6.12. There are $(f-1)N$ total B groups, of which $N-1$ have reacted, so there are $(f-2)N+1$ unreacted B groups in each N-mer. The probability that an unreacted A group is a part of an N-mer is proportional to the probability that $N-1$ B groups have reacted (p^{N-1}), while $(f-2)N+1$ B groups have not $(1-p)^{(f-2)N+1}$. The number fraction of N-mers is given by a product of probabilities:

$$n_N(p) = a_N p^{N-1}(1-p)^{(f-2)N+1}. \tag{6.6}$$

The **degeneracy** a_N is the number of unique ways of arranging N monomers AB_{f-1} into an N-mer. The number of ways of selecting the first B to form a bond out of $(f-1)N$ possible B groups of the N-mer is $(f-1)N$. The number of ways of selecting the second B group for the second bond out of

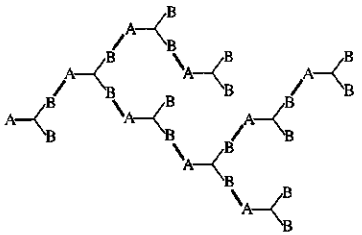

Fig. 6.12
A hyperbranched polymer. Darker lines correspond to bonds between monomers.

the remaining B groups is $(f-1)N-1$. Each successive reaction has one less B group to choose from, all the way up to the last bond of an N-mer, leading to the total number of structurally different arrangements for all $N-1$ bonds:

$$(f-1)N[(f-1)N-1]\cdots[(f-1)N-(N-2)] = \frac{[(f-1)N]!}{[(f-2)N+1]!}. \quad (6.7)$$

Since all monomers of the N-mer are indistinguishable, the number of structurally different arrangements has to be reduced by $N!$ permutations of monomers leading to the number of unique N-mers:

$$a_N = \frac{[(f-1)N]!}{N![(f-2)N+1]!}. \quad (6.8)$$

Using this degeneracy in Eq. (6.6) gives the number fraction of N-mers at any extent of reaction p for hyperbranched polymers:

$$n_N(p) = \frac{[(f-1)N]!}{N![(f-2)N+1]!} p^{N-1}(1-p)^{(f-2)N+1}. \quad (6.9)$$

Comparing Eqs (6.3) and (6.9), we see that for $f \geq 3$, hyperbranched polymers have a quite different form for their number fraction distribution than linear polymers. The large number of unreacted B groups (Fig. 6.12) on large hyperbranched N-mers broadens the distribution because the larger molecules have a higher probability of growing than smaller molecules do.

In order to evaluate different moments, this number fraction distribution is rewritten as

$$n_N(p) = a_N \frac{1-p}{p} x^N \quad (6.10)$$

using the following definition of x:

$$x \equiv p(1-p)^{f-2}. \quad (6.11)$$

The number fraction is a normalized distribution:

$$\sum_{N=1}^{\infty} n_N(p) = \frac{1-p}{p} \sum_{N=1}^{\infty} a_N x^N = 1. \quad (6.12)$$

The k-moment of the number fraction distribution is related to the k-moment of the sum Σ_k:

$$m_k = \sum_{N=1}^{\infty} N^k n_N(p) = \frac{1-p}{p} \sum_{N=1}^{\infty} N^k a_N x^N = \frac{1-p}{p} \Sigma_k. \quad (6.13)$$

The consecutive moments of the sum

$$\Sigma_k \equiv \sum_{N=1}^{\infty} N^k a_N x^N \tag{6.14}$$

are related to each other through the derivative with respect to the variable x:

$$\Sigma_k = x\frac{\partial \Sigma_{k-1}}{\partial x} = x\frac{\partial \Sigma_{k-1}}{\partial p}\frac{\partial p}{\partial x}. \tag{6.15}$$

The rate of change of extent of reaction p with variable x can be evaluated from Eq. (6.11):

$$\begin{aligned}\frac{\partial p}{\partial x} &= \frac{1}{\partial x/\partial p} = \frac{1}{(1-p)^{f-2} - p(f-2)(1-p)^{f-3}} \\ &= \frac{p(1-p)}{p(1-p)^{f-1} - p^2(f-2)(1-p)^{f-2}} = \frac{p(1-p)}{x[(1-p) - p(f-2)]} \\ &= \frac{p(1-p)}{x[1-p(f-1)]}.\end{aligned} \tag{6.16}$$

From Eq. (6.12), we find the zeroth moment of the sum:

$$\Sigma_0 = \frac{p}{1-p}. \tag{6.17}$$

All higher moments of the sum, Σ_k, can be evaluated from the zeroth moment, using the recurrence relation [Eq. (6.15)]. The first moment of the sum is

$$\begin{aligned}\Sigma_1 &= x\frac{\partial \Sigma_0}{\partial p}\frac{\partial p}{\partial x} = x\frac{1}{(1-p)^2}\frac{p(1-p)}{x[1-p(f-1)]} \\ &= \frac{p}{(1-p)[1-p(f-1)]},\end{aligned} \tag{6.18}$$

leading to the number-average degree of polymerization in agreement with Eq. (6.5):

$$N_n(p) = \sum_{N=1}^{\infty} N n_N(p) = \frac{1-p}{p}\Sigma_1 = \frac{\Sigma_1}{\Sigma_0} = \frac{1}{1-p(f-1)} \qquad \text{for } p < p_c = \frac{1}{f-1}. \tag{6.19}$$

The second moment of the sum is determined similarly:

$$\begin{aligned}\Sigma_2 &= x\frac{\partial \Sigma_1}{\partial p}\frac{\partial p}{\partial x} = x\frac{1-p^2(f-1)}{(1-p)^2[1-p(f-1)]^2}\frac{p(1-p)}{x[1-p(f-1)]} \\ &= \frac{(1-p^2(f-1))p}{(1-p)[1-p(f-1)]^3}.\end{aligned} \tag{6.20}$$

The weight-average degree of polymerization is the ratio of the second and the first moments

$$N_w(p) = \frac{\sum_{N=1}^{\infty} N^2 n_N(p)}{\sum_{N=1}^{\infty} N n_N(p)} = \frac{\Sigma_2}{\Sigma_1} = \frac{1 - p^2(f-1)}{[1-p(f-1)]^2} \quad \text{for } p < p_c = \frac{1}{f-1}. \tag{6.21}$$

This weight-average degree of polymerization $N_w(p)$ diverges at p_c more rapidly than the number-average $N_n(p)$. The polydispersity index of this distribution

$$\frac{N_w(p)}{N_n(p)} = \frac{1 - p^2(f-1)}{1-p(f-1)} \quad \text{for } p < p_c = \frac{1}{f-1} \tag{6.22}$$

also diverges at $p_c = 1/(f-1)$. All of the above results reduce for $f=2$ to those for condensation polymerization of linear chains (Section 1.6.2) and for $f>2$ correspond to the random branching that creates hyperbranched polymers. Like the linear condensation of Section 1.6.2, this branched condensation can, in principle, reach the gel point (where all monomers are connected into a single enormous hyperbranched polymer) but the reaction cannot proceed beyond the gel point, since there are no more unreacted A groups. In practice, it is difficult to achieve complete reaction.

Of particular interest is the molar mass distribution of high molar mass hyperbranched polymers that are produced when the reaction of AB_{f-1} monomers is driven close to completion. The number fraction of molecules [Eq. (6.9)] can be approximated for large N, using Stirling's formula:

$$N! \cong \sqrt{2\pi N} N^N \exp(-N). \tag{6.23}$$

The degeneracy a_N [Eq. (6.8)] is approximated for $f>2$ as

$$\begin{aligned} a_N &= \frac{1}{(f-2)N+1} \frac{[(f-1)N]!}{N![(f-2)N]!} \\ &\cong \frac{1}{(f-2)N+1} \frac{\sqrt{2\pi(f-1)N}[(f-1)N]^{(f-1)N}}{\sqrt{2\pi N} N^N \sqrt{2\pi(f-2)N}[(f-2)N]^{(f-2)N}} \\ &\cong \frac{1}{(f-2)N} \sqrt{\frac{f-1}{2\pi(f-2)N}} \frac{(f-1)^{(f-1)N}}{(f-2)^{(f-2)N}}. \end{aligned} \tag{6.24}$$

Let us define the **relative extent of reaction**:

$$\varepsilon \equiv \frac{p - p_c}{p_c} = (f-1)p - 1. \tag{6.25}$$

The limit of interest to us here is small negative values of ε. The fraction p of reacted B groups can be expressed in terms of this relative extent of

reaction ε

$$p = \frac{1+\varepsilon}{f-1}, \tag{6.26}$$

as can the fraction of unreacted B groups:

$$1-p = \frac{f-2-\varepsilon}{f-1} = \frac{f-2}{f-1}\left(1-\frac{\varepsilon}{f-2}\right). \tag{6.27}$$

Consider the p-dependence of Eq. (6.9):

$$\begin{aligned} p^{N-1}(1-p)^{(f-2)N+1} &= \left(\frac{1+\varepsilon}{f-1}\right)^{N-1}\left(\frac{f-2}{f-1}\right)^{(f-2)N+1}\left(1-\frac{\varepsilon}{f-2}\right)^{(f-2)N+1} \\ &= \frac{f-2}{1+\varepsilon}\left(1-\frac{\varepsilon}{f-2}\right) \\ &\quad \times \left[\left(\frac{1+\varepsilon}{f-1}\right)\frac{(f-2)^{f-2}}{(f-1)^{f-2}}\left(1-\frac{\varepsilon}{f-2}\right)^{f-2}\right]^N. \end{aligned} \tag{6.28}$$

The small negative values of ε can be neglected outside the square bracket in Eq. (6.28), $1+\varepsilon \cong 1$ and $1-\varepsilon/(f-2) \cong 1$. Since the square bracket in Eq. (6.28) is taken to a large power N it dominates the ε-dependence. Expanding $[1-\varepsilon/(f-2)]^{f-2} \cong 1-\varepsilon$ to the lowest power in ε we find a simple form:

$$\begin{aligned} p^{N-1}(1-p)^{(f-2)N+1} &\cong (f-2)\left[\frac{(f-2)^{f-2}}{(f-1)^{f-1}}(1+\varepsilon)\left(1-\frac{\varepsilon}{f-2}\right)^{f-2}\right]^N \\ &\cong (f-2)\frac{(f-2)^{(f-2)N}}{(f-1)^{(f-1)N}}[(1+\varepsilon)(1-\varepsilon)]^N \\ &\cong \frac{(f-2)^{(f-2)N+1}}{(f-1)^{(f-1)N}}(1-\varepsilon^2)^N \\ &\cong \frac{(f-2)^{(f-2)N+1}}{(f-1)^{(f-1)N}}\exp(-\varepsilon^2 N). \end{aligned} \tag{6.29}$$

The number fraction of N-mers [Eq. (6.6)] can be approximated by combining Eqs (6.24) and (6.29):

$$\begin{aligned} n_N(p) &= a_N p^{N-1}(1-p)^{(f-2)N+1} \\ &\cong \sqrt{\frac{f-1}{2\pi(f-2)}}N^{-3/2}\exp(-\varepsilon^2 N) \quad \text{for } |\varepsilon| = 1-p(f-1) \ll 1. \end{aligned} \tag{6.30}$$

This number fraction distribution has a form of a power law with an exponential cutoff at the **characteristic degree of polymerization** $N^* = \varepsilon^{-2}$:

$$n_N(p) \approx N^{-3/2}\exp(-N/N^*). \tag{6.31}$$

It is interesting to note that both in linear condensation polymerization (AB) and in condensation polymerization of AB_{f-1}, a similar asymptotic behaviour is predicted for the number-average degree of polymerization

$$N_n = -\varepsilon^{-1} \tag{6.32}$$

and the weight-average degree of polymerization

$$N_w \approx \varepsilon^{-2} \tag{6.33}$$

for small negative relative extents of reaction $\varepsilon = (f-1)p - 1$. The weight-average, z-average, and all higher-order average degrees of polymerization are proportional to the characteristic degree of polymerization N^*:

$$N_w \approx N_z \approx N_{z+1} \approx \cdots \approx N^* = \varepsilon^{-2}. \tag{6.34}$$

Just as for linear condensation polymers, the simple statistics presented above assume there are no intramolecular reactions. This assumption is never really correct. For linear polymers, the assumption gets progressively better for longer chains. However, for hyperbranched polymers it gets worse for species with large degrees of polymerization, since most of the unreacted B groups near an unreacted A will be on the same polymer. Properly including intramolecular reactions is a difficult and important problem. The molar mass distributions of hyperbranched polymers do not follow the simple statistics presented here because of intramolecular reactions.

6.2.2 Regular dendrimers

Another means of preparing branched polymers using condensation chemistry is to systematically grow a very regular structure, called a dendrimer. Dendrimers are typically grown from a B_n monomer core by reacting this core with AB_{f-1} monomers that temporarily have their B groups protected from further reaction. If done properly, this reaction will link each B_n core with n AB_{f-1} monomers, resulting in a first-generation dendrimer. By deprotecting the B groups, this first-generation dendrimer becomes a $B_{n(f-1)}$ core that can react with $n(f-1)$ AB_{f-1} monomers to create a second-generation dendrimer. In principle, this process can be repeated indefinitely, with each subsequent generation having another layer of monomers incorporated, which are connected to the central B_n core by the intermediate generations. For the special case of $f = n$, the dendrimer is a **Cayley tree**, shown in Fig. 6.13 for $f = n = 3$. Since the dendrimer is created one generation at a time, in principle each new generation could utilize different monomers with different functionalities and functional groups. However, in practice if $f \geq 3$ for all generations, real dendrimers cannot exceed a certain largest possible size and remain perfect because they eventually become too congested. To understand this congestion, we count the number of monomers in each generation of the dendrimer in Table 6.2.

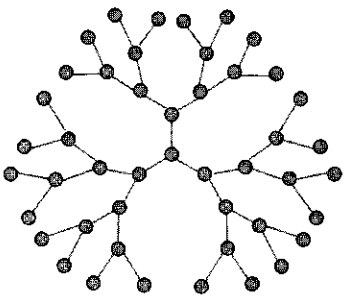

Fig. 6.13
Cayley tree or Bethe lattice with functionality $f = 3$.

Table 6.2 The number of monomers in each generation layer of a dendrimer and the total number of monomers in the dendrimer at each generation

Generation	Number of monomers	Cumulative number of monomers
0	1	1
1	n	$1+n$
2	$n(f-1)$	$1+n+n(f-1)$
3	$n(f-1)^2$	$1+n+n(f-1)+n(f-1)^2$
.	.	
.	.	
g	$n(f-1)^{g-1}$	$1+n+n(f-1)+n(f-1)^2+\cdots+n(f-1)^{g-1}$

The number of monomers in generation g (the last generation) of the dendrimer is $n(f-1)^{g-1}$, while the total number of monomers in the dendrimer (from the core to generation g) is

$$\begin{aligned} N_g &= 1+n+n(f-1)+n(f-1)^2+\cdots+n(f-1)^{g-1} \\ &= 1+n[1+(f-1)+(f-1)^2+\cdots+(f-1)^{g-1}] \\ &= 1+n\left[\frac{(f-1)^g-1}{f-2}\right], \end{aligned} \tag{6.35}$$

where the last step in the derivation used the sum of a geometric series $1+x+x^2+\cdots+x^{g-1}=(x^g-1)/(x-1)$. The number of monomers in the rest of the polymer (from the core to generation $g-1$) is

$$N_{g-1} = 1+n\left[\frac{(f-1)^{g-1}-1}{f-2}\right]. \tag{6.36}$$

The ratio of the number of monomers in the last generation of a very large dendrimer $n(f-1)^{g-1}$ to the number of monomers in the rest of the dendrimer N_{g-1} is

$$\frac{n(f-1)^{g-1}}{1+n[(f-1)^{g-1}-1]/(f-2)} \cong f-2 \quad \text{for } g \gg 1. \tag{6.37}$$

Thus, for $f=3$ approximately half of the monomers are in the last generation of the dendrimer! For higher functionalities ($f>3$), an even larger fraction of monomers are in the last generation of the dendrimer.

The volume occupied by the polymer is $v_0 N_g$, where v_0 is the monomer volume and the maximum accessible volume for a fully stretched dendrimer is $(4\pi/3)(gl)^3$, where l is the monomer size. The occupied volume cannot exceed the maximum accessible volume, leading to the maximum possible generation $g_{\max}$ for a perfect dendrimer:

$$v_0 N_{g_{\max}} \cong \frac{4\pi}{3}(g_{\max} l)^3. \tag{6.38}$$

Using Eq. (6.35) relates the maximum generation for a perfect dendrimer to geometric properties of a monomer:

$$\frac{l^3}{v_0} \cong \frac{n}{f-2}\frac{(f-1)^{g_{max}}}{(4\pi/3)g_{max}^3}.$$

To make a large generation dendrimer, monomers with large aspect ratio are needed,[2] so that $l^3 \gg v_0$. For example, to make a perfect tetrafunctional ($n=f=4$) seventh generation dendrimer requires $l^3/v_0 > 3$.

The regular lattice constructed in this way is called a **Bethe lattice** (see Fig. 6.13). The mean-field model of gelation corresponds to percolation on a Bethe lattice (see Section 6.4). The infinite Bethe lattice does not fit into the space of *any* finite dimension. Construction of progressively larger randomly branched polymers on such a lattice would eventually lead to a congestion crisis in three-dimensional space similar to the one encountered here for dendrimers.

6.3 Gelation: concepts and definitions

Gelation is a **connectivity transition** that can be described by a bond percolation model. Imagine that we start with a container full of monomers, which occupy the sites of a lattice (as sketched in Fig. 6.14). In a simple bond percolation model, all sites of the lattice are assumed to be occupied by monomers. The chemical reaction between monomers is modelled by randomly connecting monomers on neighbouring sites by bonds. The fraction of all possible bonds that are formed at any point in the reaction is called the **extent of reaction** p, which increases from zero to unity as the reaction proceeds. A polymer in this model is represented by a cluster of monomers (sites) connected by bonds. When all possible bonds are formed (all monomers are connected into one macroscopic polymer) the reaction is completed ($p=1$) and the polymer is a fully developed network. Such fully developed networks will be the subject of Chapter 7, while in this chapter we focus on the gelation transition.

At the percolation threshold or gel point p_c, the system undergoes a connectivity transition. Slightly below the gel point, the system is a polydisperse mixture of branched polymers shown in Fig. 6.14(a). Slightly beyond the gel point, the system is still mostly a polydisperse mixture of branched polymers, but one structure percolates through the entire system [Fig. 6.14(b)]. This structure is called the **incipient gel**, which is a tenuous structure quite different from the fully developed network that exists far above p_c. This connectivity transition from a sol below p_c to a gel permeated with sol above p_c is called the gelation transition.

At any specified extent of reaction p, the dimensionless number density of molecules with N monomers is $n(p, N)$, defined as the number of N-mers divided by the total number of monomers. This number density is proportional to the probability that a randomly selected polymer has N

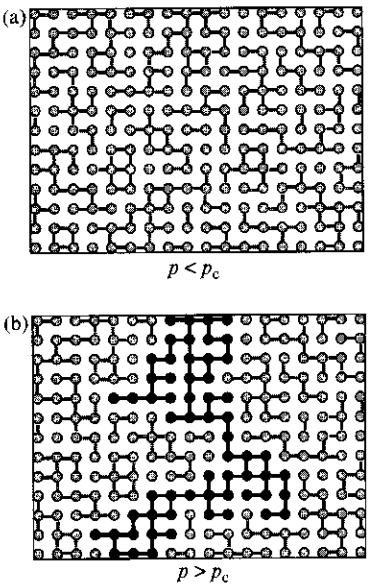

Fig. 6.14
Gelation is a bond percolation transition. The percolation cluster is indicated by darker shading.

[2] Alternatively, short linear chains can be introduced between the f-functional branch points.

monomers, which is the number fraction of N-mers $n_N(p)$ (the number fraction distribution function of Sections 1.6.2 and 6.1.2). The two functions are simply normalized differently [Eq. (1.45)]. The number density $n(p, N)$ is the number of N-mers per monomer. In contrast, the number fraction distribution $n_N(p)$ is normalized by the total number of molecules.

The **sol fraction** is defined as the fraction of all monomers that are either unreacted or belong to finite-size polymers (the sol):

$$P_{\text{sol}}(p) = \sum_{N=1}^{\infty} Nn(p, N) = \sum_{N=1}^{\infty} w(p, N). \tag{6.39}$$

The sum in Eq. (6.39) is only made over the finite-size species, meaning that above the gel point the gel is excluded. The last equality employs the definition of the dimensionless weight density of N-mers:

$$w(p, N) = Nn(p, N). \tag{6.40}$$

Analogous to the weight fraction distribution function $w_N(p)$ of Section 1.6.2, the weight density $w(p, N)$ is the probability that a randomly chosen monomer is part of a polymer with N monomers, but the two functions are normalized differently. The weight density $w(p, N)$ is normalized by the total number of monomers in the system, while the weight fraction $w_N(p)$ is normalized only by the monomers belonging to finite-size polymers [see Eq. (1.23)]. The sum of weight densities $w(p, N)$ of all finite size polymers is the sol fraction [Eq. (6.39)], while the sum of weight fractions $w_N(p)$ is always unity. Therefore, the weight density $w(p, N)$ is equal to the weight fraction $w_N(p)$ times the sol fraction $P_{\text{sol}}(p)$.

The **gel fraction** is defined as the fraction of all monomers belonging to the gel. Every monomer must be either part of the sol or part of the gel, so the sum of the sol and gel fractions is unity:

$$P_{\text{gel}}(p) + P_{\text{sol}}(p) = 1. \tag{6.41}$$

Below the gel point, all monomers are either unreacted or belong to finite sized polymers and therefore the sol fraction is unity and the gel fraction is zero:

$$P_{\text{sol}}(p) = 1, \quad P_{\text{gel}}(p) = 0 \qquad \text{for } p \leq p_c; \tag{6.42}$$

above the gel point, the gel fraction is non-zero and the sol fraction is less than unity.

$$P_{\text{sol}}(p) < 1, \quad P_{\text{gel}}(p) > 0 \qquad \text{for } p > p_c. \tag{6.43}$$

The gel fraction is the probability that a randomly selected monomer belongs to the gel. The gel fraction is the order parameter for gelation. The order parameter tells us whether the reaction has passed the gel point and if above the gel point, it indicates the gel fraction. The growth of the gel fraction is accompanied by a simultaneous decay of the sol fraction, beyond

the gel point p_c as shown in Fig. 6.15. The fact that the order parameter is continuous through the transition means that gelation is analogous to a **continuous phase transition**. Familiar examples of continuous phase transitions are the paramagnetic–ferromagnetic transition of iron at the Curie temperature (where the magnetization changes continuously) and the vapor-liquid transition with increasing pressure at the critical temperature (where the density changes continuously). A great deal is known about continuous phase transitions and the application of those ideas to gelation is discussed in Section 6.5.

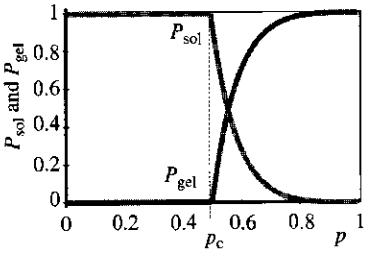

Fig. 6.15
Mean-field prediction of sol and gel fractions for functionality $f = 3$.

The total number density of molecules is the sum of number densities of all finite-size polymers and unreacted monomers. The number density of all finite molecules $n_{tot}(p)$ is the zeroth moment of the number density distribution function:

$$n_{tot}(p) = \sum_{N=1}^{\infty} n(p, N). \tag{6.44}$$

The number-average degree of polymerization [see Eq. (1.27)] is the average number of monomers per finite-size polymer:

$$N_n(p) = \frac{\sum_{N=1}^{\infty} Nn(p, N)}{\sum_{N=1}^{\infty} n(p, N)} = \frac{P_{sol}(p)}{n_{tot}(p)}. \tag{6.45}$$

The weight-average degree of polymerization is the ratio of second and first moments [recall Eq. (1.31)]:

$$N_w(p) = \frac{\sum_{N=1}^{\infty} N^2 n(p, N)}{\sum_{N=1}^{\infty} Nn(p, N)} = \frac{\sum_{N=1}^{\infty} Nw(p, N)}{\sum_{N=1}^{\infty} w(p, N)} = \frac{\sum_{N=1}^{\infty} Nw(p, N)}{P_{sol}(p)}. \tag{6.46}$$

Note that the sums are understood to run only over finite-size molecules. Beyond the gel point, the gel fraction is excluded from such sums.

6.4 Mean-field model of gelation

A convenient way of presenting the mean-field model (though it is not the way it was originally defined) is by placing monomers at the sites of an infinite Bethe lattice, a small part of which is shown in Fig. 6.13. The Bethe lattice has the advantage of directly taking into account the functionality of the monomers f by adopting this functionality for the lattice. For trifunctional monomers (the $f = 3$ Bethe lattice of Fig. 6.13) there are three possible bonds emanating from each lattice site.

In a bond percolation model on a Bethe lattice, we assume that all lattice sites are occupied by monomers and the possible bonds between neighbouring monomers are either formed with probability p or left unreacted with probability $1 - p$. In the simplest version, called the random

bond percolation model, the probability p of forming each bond is assumed to be independent of any other bonds in the system.

The basic assumptions of the mean-field model are implicit in the topology of the Bethe lattice. The most apparent assumption is the absence of closed loops. No intramolecular crosslinking is allowed—bonds can only be formed between monomers belonging to different polymers. This assumption significantly simplifies the analytical treatment of the model, but limits its practical utility.

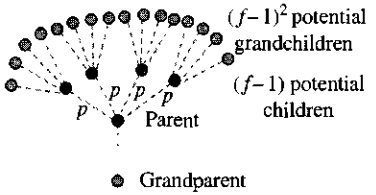

Fig. 6.16
Gel point calculation on a Bethe lattice. Each site that is already connected to the gel from its grandparent has $f-1$ possible additional connections (potential children).

6.4.1 Gel point

To calculate the gel point for bond percolation on an f-functional Bethe lattice, let us choose a single site and work progressively outwards from it, analysing the structure of the polymer obtained by forming bonds. Which site is chosen as the starting point of this procedure makes no difference because they are all statistically identical for an infinite Bethe lattice.

Let us assume that our starting ('parent') site has already formed a bond with one of its neighbours (the 'grandparent' site) as sketched in Fig. 6.16. We would like to calculate the average number of additional bonds the 'parent' site forms with its $f-1$ remaining neighbours (potential 'children'). The probability of each of these bonds being formed is p and is independent of other bonds. Therefore, the average number of bonds between a 'parent' site and its 'children' is $p(f-1)$. Similarly, the average number of bonds between each of its 'children' and their corresponding 'grandchildren' is also $p(f-1)$.

If this probability $p(f-1)$ is less than unity ($p<1/(f-1)$), each new generation has, on average, fewer members and the dynasty does not survive for long (only finite-size branched polymers exist in the system). If this probability $p(f-1)$ is greater than unity ($p>1/(f-1)$), each new generation has, on average, more members and the descendants of some parents multiply indefinitely, forming an infinite genealogical branched family tree.

The transition between these two cases is the gel point:

$$p_c = \frac{1}{f-1}. \tag{6.47}$$

Below the gel point (for $p<p_c$) there are only finite-size branched polymers, while above the gel point (for $p>p_c$) there is also at least one infinite polymer (the gel) in addition to many finite-size branched polymers. The distribution of polymer sizes changes with the fraction of formed bonds p. For small extents of reaction $p \ll p_c$ there are only small polymers, while near the gel point some large branched polymers are present.

A unique feature of percolation on a Bethe lattice is that there are many infinite polymers present in the same system above the gel point. The easiest way to understand this result is to start with a single infinite network

polymer on a fully reacted Bethe lattice at $p = 1$. If a single bond is cut, the infinite polymer breaks into two infinite polymers. As bonds are randomly cut, progressively more infinite polymers are created, as well as many finite-size branched polymers. The reason for the existence of many infinite polymers on the Bethe lattice above the gel point is the absence of intramolecular bonds. This is due to the fact that loops are prohibited for a Bethe lattice. In contrast, on a regular lattice (such as a simple cubic lattice) loops are allowed and there is only one infinite polymer above the gel point. Large overlapping polymers on a regular three-dimensional lattice have many possibilities for potential bonding and therefore high probability of being connected into one larger polymer.

6.4.2 Sol and gel fractions

Each site of the f-functional Bethe lattice has f possible paths to other sites (see Fig. 6.13). We define Q as the probability that a randomly selected site (A in Fig. 6.17) is *not* connected to the gel through a certain randomly selected path (the path from site A to neighbouring site B in Fig. 6.17). There are immediately two possibilities. The bond between sites A and B could be unreacted with probability $1 - p$, and if so this path cannot connect site A to the gel. The second possibility is that the bond between A and B is reacted with probability p. If this bond is formed, there are $f - 1$ remaining paths from site B that could connect to the gel. The probability that none of the $f - 1$ paths connect to the gel is Q^{f-1} and the probability that the bond between A and B is reacted and does not lead to the gel is pQ^{f-1}. Hence, there is a **recurrence relation** for the probability that a randomly selected site is not connected to the gel through a randomly selected potential bond (see Fig. 6.17):

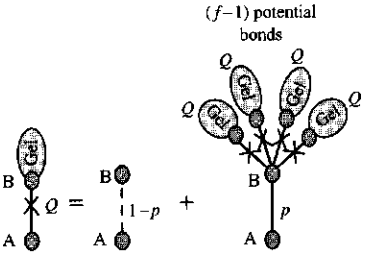

Fig. 6.17
A recurrence diagram for the probability of not being connected to the gel through a given bond.

$$Q = 1 - p + pQ^{f-1}. \tag{6.48}$$

The fraction of monomers in the sol (sol fraction) P_{sol} is the probability that a randomly selected site is not connected to the gel along any of its f paths (Fig. 6.18):

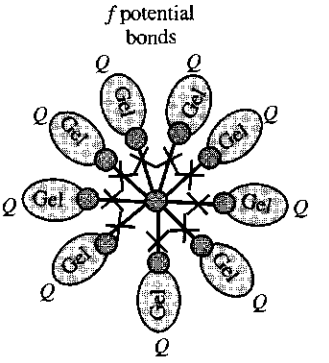

Fig. 6.18
Diagram for the sol fraction.

$$P_{\text{sol}} = Q^f. \tag{6.49}$$

Solving Eq. (6.49) for Q,

$$Q = P_{\text{sol}}^{1/f} \tag{6.50}$$

and substituting into the recurrence relation for Q [Eq. (6.48)] gives a relation between sol fraction and extent of reaction that is valid for any functionality f:

$$P_{\text{sol}}^{1/f} = 1 - p + pP_{\text{sol}}^{(f-1)/f}. \tag{6.51}$$

There is always one solution of this equation [Eq. (6.42)] with zero gel fraction below gel point ($P_{\text{sol}} = 1$). A second solution exists above the gel point for any $f \geq 3$. For $f = 3$ this second solution of Eq. (6.51) can be easily found because it becomes a quadratic equation for $P_{\text{sol}}^{1/3}$:

$$P_{\text{sol}} = \left(\frac{1-p}{p}\right)^3 \quad \text{for } f = 3 \text{ and } p > p_c. \tag{6.52}$$

The gel fraction above the gel point for $f = 3$ is calculated from the sol fraction:

$$P_{\text{gel}} = 1 - P_{\text{sol}} = 1 - \left(\frac{1-p}{p}\right)^3 \quad \text{for } f = 3 \text{ and } p > p_c. \tag{6.53}$$

The sol and gel fractions for functionality $f = 3$ are plotted in Fig. 6.15 as functions of extent of reaction p. For $p > p_c = 1/2$, the $f = 3$ system is beyond the gel point and the gel fraction grows steadily as the reaction proceeds.

6.4.3 Number-average molar mass below the gel point

Before any bonds are formed (at extent of reaction $p = 0$) there are only monomers present and the total number of molecules per site is $n_{\text{tot}}(0) = 1$ (every site is occupied by an unreacted monomer). Each bond reduces the number of molecules by one because there are no intra-molecular bonds. The maximum number of bonds per site on a Bethe lattice with functionality f is $f/2$. The total number of formed bonds per site at extent of reaction p is $pf/2$:

$$n_{\text{tot}}(p) = 1 - \frac{pf}{2} \quad \text{for } p < p_c. \tag{6.54}$$

The number-average degree of polymerization (the average number of sites per molecule) is the reciprocal of the average number of molecules per site.

$$N_n(p) = \frac{1}{n_{\text{tot}}(p)} = \frac{1}{1 - pf/2} \quad \text{for } p < p_c. \tag{6.55}$$

At the gel point $p_c = 1/(f-1)$, the number-average degree of polymerization exhibits no unusual behaviour for $f > 2$ (it is just a finite number):

$$N_n(p_c) = \frac{1}{1 - f/2(f-1)} = \frac{2(f-1)}{f-2}. \tag{6.56}$$

For $f = 3$, $N_n(p_c) = 4$ meaning that a randomly selected molecule at the gel point has an average degree of polymerization of four. The fact that N_n does not diverge at p_c is our first evidence that random branching in gelation leads to very different molar mass distribution than hyperbranched polymers (for which N_n does diverge at p_c), see Eq. (6.5).

6.4.4 Weight-average molar mass below the gel point

The weight-average molar mass at any extent of reaction below the gel point $p < p_c$ can be calculated in a fashion similar to the sol and gel fraction calculations of Section 6.4.2 (see Fig. 6.19). Let Υ be the mean number of monomers connected to a randomly selected site A through one of its f randomly chosen possible bonds (with neighbour B). For $\Upsilon > 0$, the bond connecting A and B must be reacted with probability p and site B contributes one monomer to Υ. Then, each of the remaining paths through $f-1$ remaining potential bonds of B contributes a mean number of monomers Υ, giving the following recurrence relation:

$$\Upsilon = p[1 + (f-1)\Upsilon)]. \tag{6.57}$$

This recurrence relation can be easily solved for Υ:

$$\Upsilon = \frac{p}{1-(f-1)p}. \tag{6.58}$$

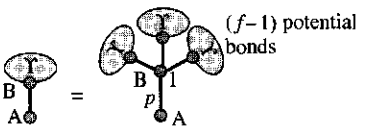

Fig. 6.19
Diagram of the recurrence relation for the average number of monomers connected to site A through a given bond.

The weight-average number of monomers per polymer N_w below the gel point is the average number of monomers in a polymer belonging to a randomly selected site. This number can be written as 1 for the site itself and Υ for each of the f paths emanating from that site (Fig. 6.20):

$$N_w = 1 + f\Upsilon = 1 + \frac{fp}{1-(f-1)p} = \frac{1+p}{1-(f-1)p}$$
$$= \frac{1+p}{1-p/p_c} \quad \text{for } p < p_c. \tag{6.59}$$

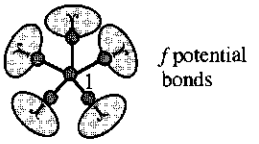

Fig. 6.20
Diagram for the calculation of N_w.

The weight-average degree of polymerization diverges at the gel point, since the denominator of Eq. (6.59) is zero when $p = p_c$. Since the number-average degree of polymerization stays finite at p_c [Eq. (6.56)], the polydispersity index

$$\frac{N_w}{N_n} = \frac{(1+p)(1-pf/2)}{1-(f-1)p} \quad \text{for } p < p_c \tag{6.60}$$

diverges at the gel point $p_c = 1/(f-1)$ for $f > 2$.

6.4.5 Molar mass distribution

The structure of the branched polymers produced by any random branching process is the same. Any individual hyperbranched polymer structure made from reacting AB_{f-1} monomers can also be made by reacting A_f monomers. The difference between these branching processes is the molar mass *distribution*—the relative amounts of each structure produced.

The molar mass distributions resulting from AB_{f-1} and A_f reactions are related in a very simple way. Table 6.3 shows the unique relation between the number of monomers in an N-mer and the number of unreacted A groups in the N-mer. The property of the Bethe lattice not allowing any loops makes this unique relation possible.

Table 6.3 The number of unreacted A groups in an N-mer for A_f condensation on a Bethe lattice

N	Number of unreacted A groups
1	f
2	$2f-2$
3	$3f-4$
4	$4f-6$
...	...
N	$Nf-2N+2=(f-2)N+2$

Regardless of how they are connected, each new monomer brings f more A groups to the molecule, but also reacts two A groups in the process.[3] Each N-mer has exactly $(f-2)N+2$ unreacted A groups.

If any branched structure made from A_f condensation is held by one of its unreacted A groups, it is identical to a structure produced by AB_{f-1} condensation. For the AB_{f-1} reaction, the probability that an unreacted A group is part of an N-mer is given by the number fraction $n_N(p)$ of N-mers because there is only a *single* unreacted A group per molecule for AB_{f-1}. For A_f condensation, the probability $u_N(p)$ that a randomly selected unreacted A group is part of an N-mer is identical to the number fraction $n_N(p)$ of N-mers in the condensation polymerization of AB_{f-1} [Eq. (6.9)]:

$$u_N(p) = \frac{[(f-1)N]!}{N![(f-2)N+1]!} p^{N-1}(1-p)^{(f-2)N+1}. \tag{6.61}$$

The difference between A_f and AB_{f-1} arises from the degeneracy of A_f condensation, since there are $N(f-2)+2$ unreacted A groups on each N-mer (see Table 6.3). The number of N-mers per unreacted A group is obtained by dividing $u_N(p)$ by this degeneracy, since there are $N(f-2)+2$ different ways to select the same N-mer by randomly choosing an unreacted A:

$$\frac{u_N(p)}{(f-2)N+2}.$$

To obtain the number of N-mers per monomer, $n(p, N)$, we simply multiply this number of N-mers per unreacted A group by the average number of unreacted A groups per monomer $f(1-p)$:

$$n(p,N) = \frac{f(1-p)}{(f-2)N+2} u_N(p), \tag{6.62}$$

$$n(p,N) = f\frac{[(f-1)N]!}{N![(f-2)N+2]!} p^{N-1}(1-p)^{(f-2)N+2}. \tag{6.63}$$

[3] Formation of a bond converts two unreacted A groups to two reacted A groups. Since each site has fA groups, there are $f/2$ potential bonds per site.

This number density distribution function is more convenient than the previously used number fraction, when dealing with systems like A_f condensation that can form gels. The reason is that number fraction applies to the randomly branched polymers present but not to the gel, which makes this quantity awkwardly normalized beyond the gel point. The number density $n(p, N)$ avoids this complication since the total number of monomers is independent of extent of reaction.

Simply multiplying $n(p, N)$ by N gives the weight density distribution function, which is the probability of a randomly chosen monomer belonging to an N-mer:

$$w(p, N) = Nn(p, N) = f\frac{[(f-1)N]!}{(N-1)![(f-2)N+2]!}p^{N-1}(1-p)^{(f-2)N+2}. \tag{6.64}$$

The weight density distribution functions are plotted in Fig. 6.21 for functionality $f = 3$ and extents of reaction $p = 0.4$, 0.48, and 0.49.

From these distribution functions, their moments related to sol and gel fractions and to various averages of the degree of polymerization [Eqs (6.45) and (6.46)] may be calculated. Results for functionality $f = 3$ are presented here. The sol fraction is defined as the fraction of all sites belonging to finite molecules

$$P_{\text{sol}}(p) = \sum_{N=1}^{\infty} w(p, N) = \left(\frac{1-|1-p/p_c|}{2p}\right)^3 \quad \text{for } f = 3, \tag{6.65}$$

where $|x|$ denotes the absolute value of x. As expected, the sol fraction is equal to unity below the gel point [Eq. (6.42)]. Above the gel point the sol fraction decreases as the reaction proceeds (see Section 6.4.2 and Fig. 6.15) and Eq. (6.65) reduces to Eq. (6.52) for $p > p_c = 1/2$.

The number of molecules per site can be calculated from Eq. (6.63):

$$n_{\text{tot}}(p) = \sum_{N=1}^{\infty} n(p, N) = P_{\text{sol}}(p)\left(\frac{1}{4} + \frac{3}{4}|1-p/p_c|\right) \quad \text{for } f = 3. \tag{6.66}$$

It decreases linearly below the gel point [recall Eq. (6.54)]:

$$n_{\text{tot}}(p) = 1 - \frac{3p}{2} \quad \text{for } p < p_c = \frac{1}{2} \text{ for } f = 3 \tag{6.67}$$

and non-linearly above the gel point

$$n_{\text{tot}}(p) = \left(\frac{1-p}{p}\right)^3 \frac{3p-1}{2} \quad \text{for } p \geq p_c = \frac{1}{2} \text{ for } f = 3 \tag{6.68}$$

as plotted in Fig. 6.22.

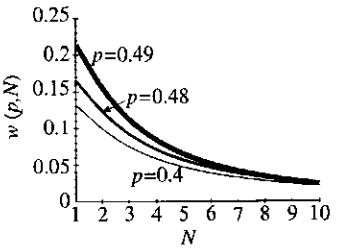

Fig. 6.21
Weight density distribution functions for functionality $f = 3$ at three different extents of reaction.

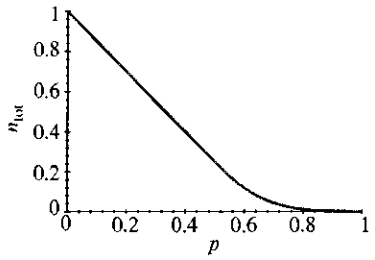

Fig. 6.22
Total number of molecules per site for functionality $f=3$.

The relative extent of reaction ε is defined as a measure of the proximity to the gel point [Eq. (6.25)]. In the mean-field theory, the critical extent of the reaction is given by Eq. (6.47), $p_c = 1/(f-1)$, and the relative extent of the reaction is determined by f and p:

$$\varepsilon = \frac{p}{p_c} - 1 = (f-1)p - 1. \tag{6.69}$$

Using $f=3$ gives the relative extent of reaction for the trifunctional Bethe lattice.

$$\varepsilon = 2p - 1 \quad \text{for } f = 3. \tag{6.70}$$

The number-average degree of polymerization

$$N_n(p) = \frac{\sum_{N=1}^{\infty} Nn(p,N)}{\sum_{N=1}^{\infty} n(p,N)} = \frac{P_{sol}(p)}{n_{tot}(p)} = \frac{4}{1+3|\varepsilon|} \quad \text{for } f = 3 \tag{6.71}$$

grows below the gel point from $N_n(0)=1$ to $N_n(1/2)=4$ [see Eq. (6.55) for a more general expression] and decreases above the gel point, with $N_n(1)=1$ (see Fig. 6.23).

The second moment of the number density distribution [Eq. (6.63)] is

$$\sum_{N=1}^{\infty} N^2 n(p,N) = P_{sol}(p)\frac{3-|\varepsilon|}{2|\varepsilon|} \quad \text{for } f = 3. \tag{6.72}$$

The weight-average degree of polymerization is the ratio of the second and the first moments and diverges at the gel point (see Fig. 6.23):

$$N_w(p) = \frac{\sum_{N=1}^{\infty} N^2 n(p,N)}{\sum_{N=1}^{\infty} Nn(p,N)} = \frac{3}{2|\varepsilon|} - \frac{1}{2} \quad \text{for } f = 3. \tag{6.73}$$

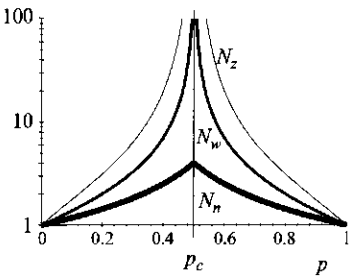

Fig. 6.23
Degree of polymerization averages for functionality $f=3$. N_z—top line, N_w—middle line, and N_n—bottom line.

The third moment of the number density distribution

$$\sum_{N=1}^{\infty} N^3 n(p,N) = P_{sol}(p)\frac{3+9|\varepsilon|-9\varepsilon^2+|\varepsilon|^3}{4|\varepsilon|^3} \quad \text{for } f = 3 \tag{6.74}$$

gives the z-average degree of polymerization at any extent of reaction p:

$$N_z = \frac{\sum_{N=1}^{\infty} N^3 n(p,N)}{\sum_{N=1}^{\infty} N^2 n(p,N)} = \frac{3+9|\varepsilon|-9\varepsilon^2+|\varepsilon|^3}{2\varepsilon^2(3-|\varepsilon|)} \quad \text{for } f = 3. \tag{6.75}$$

It diverges at the gel point faster than the weight-average degree of polymerization (see Fig. 6.23).

Close to the gel point (for $|\varepsilon| \ll 1$) the number density of polymers reaches an asymptotic form for large polymers that can be obtained from the similar expression for condensation polymerization of AB_{f-1} [Eqs (6.30) and (6.61)]:

$$u_N(p) \cong \sqrt{\frac{f-1}{2\pi(f-2)}} N^{-3/2} \exp(-\varepsilon^2 N) \cong n_N(p) \quad \text{for } AB_{f-1} \tag{6.76}$$

using the relation between the two distribution functions [Eq. (6.62)]:

$$\begin{aligned} n(p,N) &= \frac{f(1-p)}{(f-2)N+2} u_N(p) \cong \frac{f}{(f-2)N} \frac{f-2}{f-1} u_N(p) \\ &\cong \frac{f}{\sqrt{2\pi(f-1)(f-2)}} N^{-5/2} \exp(-\varepsilon^2 N). \end{aligned} \tag{6.77}$$

In this conversion we made use of the fact that $p \cong p_c = 1/(f-1)$ near the gel point, so $(1-p)$ was replaced with $(f-2)/(f-1)$. The polymer number density near the gel point on the Bethe lattice decays as a power of the number of monomers in a polymer:

$$n(p,N) \approx N^{-5/2} f_{\pm}(N/N^*). \tag{6.78}$$

The **cutoff function** $f_{\pm}(N/N^*)$ is an exponential

$$f_{\pm}(N/N^*) \approx \exp(-N/N^*) \tag{6.79}$$

with the cutoff at the characteristic degree of polymerization:

$$N^* \approx \varepsilon^{-2}. \tag{6.80}$$

The number density of polymers is plotted in Fig. 6.24 for several different extents of reaction p.

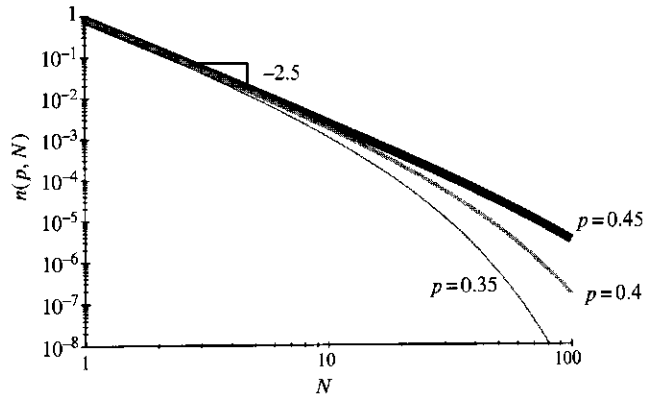

Fig. 6.24
Number density distribution function $n(p,N)$ for trifunctional randomly branched polymers at three different extents of reaction below the gel point ($p_c = 0.5$).

It is important to point out that this characteristic degree of polymerization is proportional to the z-average degree of polymerization near the gel point for any functionality f:

$$N^* \cong 2N_z \quad \text{for } |\varepsilon| \ll 1 \text{ and } f = 3. \tag{6.81}$$

The characteristic degree of polymerization diverges at the gel point, so the number density distribution becomes a power law with no cutoff:

$$n(p_c, N) \sim N^{-5/2}. \tag{6.82}$$

Similar relations with different coefficients and different exponents hold in all percolating systems near the transition point, not just in the mean-field case of percolation on a Bethe lattice, as will be shown in Section 6.5.

6.4.6 Size of ideal randomly branched polymers

So far we have discussed the distribution of degrees of polymerization of molecules both below and above the gel point. In the present section, we will describe their spacial sizes in the polymerization reactor. The Bethe lattice introduced above for the mean-field gelation model properly describes the connectivity of monomers into tree-like branched molecules, but is not designed to describe the location of these monomers in space. Indeed, the Bethe lattice has *infinite* fractal dimension because the number of sites grows exponentially with the number of generations [see Eq. (6.35) and Table 6.2] and would not fit into space with any finite dimension without significant overlap between different sites.

Here we calculate the size of ideal randomly branched polymers, ignoring excluded volume interactions and allowing each molecule to achieve the state of maximum entropy (recall the discussion of ideal chains in Chapter 2). Since branched molecules have many ends, the mean-square end-to-end distance used to characterize the size of linear chains is not appropriate for them. The simplest quantity describing the size of branched molecules is their mean-square radius of gyration R_g [see Eq. (2.44) for the definition].

In Chapter 2 we have presented a proof of the Kramers theorem for branched molecules containing N monomers of size b, but no loops (Eq. 2.65). The mean-square radius of gyration of these molecules is

$$R_g^2 = b^2 \frac{\langle N_1(N - N_1)\rangle}{N}, \tag{6.83}$$

where the average is taken over all possible ways of cutting these molecules into two parts containing N_1 and $N - N_1$ monomers, respectively (see Fig. 2.7).

The Kramers theorem relates the ideal size of molecules to a purely structural property—the number of ways of dividing a molecule into two

branches. The probability that a given bond is connected to a branch of N_1 monomers through a chosen one of the two ends of the bond is the same as the probability $u_{N_1}(p)$ that a given unreacted A group is a part of an N_1-mer [Eq. (6.61)]:

$$u_{N_1}(p) = \frac{[(f-1)N_1]!}{N_1![(f-2)N_1+1]!} p^{N_1-1}(1-p)^{(f-2)N_1+1}. \tag{6.84}$$

The probability that a chosen bond divides a molecule into two branches—the first one with N_1 monomers and the second one with $N-N_1$ monomers is $u_{N_1}(p)u_{N-N_1}(p)$. Therefore, the Kramers theorem can be rewritten:

$$R_g^2 = \frac{b^2}{N} \frac{\sum_{N_1=1}^{N-1} N_1(N-N_1)u_{N_1}(p)u_{N-N_1}(p)}{\sum_{N_1=1}^{N-1} u_{N_1}(p)u_{N-N_1}(p)}. \tag{6.85}$$

The denominator of this equation is the probability that an occupied bond is a part of an N-mer. It is related to the number density of N-mers $n(p, N)$ by the ratio of sites to bonds on the Bethe lattice $2/f$, the number of occupied bonds per N-mer $(N-1)$ and the probability of the chosen bond to be formed p. The number of N-mers per bond is $(2/f)n(p, N)$, while the number of N-mers per occupied bond is larger by the factor $1/p$ and is equal to $(2/f)n(p, N)/p$. The probability that an occupied bond is a part of an N-mer is the number of bonds of all N-mers per occupied bond, which is larger than the number of N-mers per occupied bond by the number of bonds per N-mer $(N-1)$:

$$\begin{aligned}\sum_{N_1=1}^{N-1} u_{N_1}(p)u_{N-N_1}(p) &= \frac{2}{f}\frac{N-1}{p} n(p, N) \\ &= \frac{2(N-1)[(f-1)N]!}{N![(f-2)N+2]!} p^{N-2}(1-p)^{(f-2)N+2}.\end{aligned} \tag{6.86}$$

In the second relation, we used Eq. (6.63) for $n(p, N)$. Close to the gel point [for $\varepsilon = (f-1)p - 1 \ll 1$] this probability can be rewritten for large degree of polymerization $(N \gg 1)$ using Stirling's approximation [Eq. (6.23)]:

$$\sum_{N_1=1}^{N-1} u_{N_1}(p)u_{N-N_1}(p) \cong \sqrt{\frac{2(f-1)}{\pi(f-2)}} N^{-3/2} \exp(-\varepsilon^2 N). \tag{6.87}$$

Each individual branch probability can be approximated in a similar way [recall Eq. (6.76)].

The summation in the numerator of Eq. (6.85) is dominated by the middle of the interval and can be evaluated by replacing the summation by integration using the asymptotic expression for $u_N(p)$ [Eq. (6.76)]:

$$\begin{aligned}
&\sum_{N_1=1}^{N-1} N_1(N-N_1)u_{N_1}(p)u_{N-N_1}(p) \\
&\quad \cong \int_1^{N-1} N_1(N-N_1)u_{N_1}(p)u_{N-N_1}(p)\,\mathrm{d}N_1 \\
&\quad \cong \frac{(f-1)}{2\pi(f-2)}\exp(-\varepsilon^2 N)\int_1^{N-1}\frac{N_1(N-N_1)\,\mathrm{d}N_1}{N_1^{3/2}(N-N_1)^{3/2}} \\
&\quad \cong \frac{f-1}{2\pi(f-2)}\exp(-\varepsilon^2 N)\int_{-1}^{1}\frac{\mathrm{d}x}{\sqrt{1-x^2}} \\
&\quad \cong \frac{f-1}{2(f-2)}\exp(-\varepsilon^2 N), \qquad (6.88)
\end{aligned}$$

where we have introduced a new variable of integration $x = -1 + 2N_1/N$, and the integral over x is π.

Substituting Eqs (6.87) and (6.88) into the Kramers theorem expression [Eq. (6.85)] gives the mean-square radius of gyration for an ideal randomly branched N-mer:

$$\langle R_g^2\rangle \cong \sqrt{\frac{\pi(f-1)}{8(f-2)}}\,b^2 N^{1/2}. \qquad (6.89)$$

A similar relation was derived by Zimm and Stockmayer in 1949.[4]

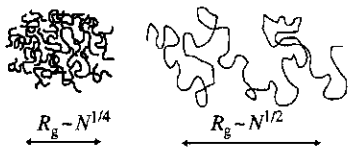

Fig. 6.25
The branched polymer is smaller than the linear polymer with the same number of monomers.

As expected, the radius of gyration of an ideal randomly branched polymer is much smaller than that of an ideal linear chain with the same number and size of monomers (see Fig. 6.25). It is important to note that the dependence of the size on the degree of polymerization for randomly branched polymers

$$R_g \approx bN^{1/4} \quad \text{for ideal randomly branched} \qquad (6.90)$$

is weaker than for ideal linear polymers [Eq. (2.54)]:

$$R_g \approx bN^{1/2} \quad \text{for ideal linear.} \qquad (6.91)$$

The fractal dimension of an ideal randomly branched polymer is $\mathcal{D} = 4$ (because its degree of polymerization is proportional to its size to the fourth power $N \sim R_g^4$). In spaces with dimension $d < 4$ (in two-dimensional and three-dimensional spaces), ideal randomly branched polymers have

[4] The difference is that in Eq. (6.89) N is the number of monomers (occupied sites of an N-mer), while in the treatment of Zimm and Stockmayer N_{lin} is the number of linear segments per N-mer. Their asymptotic values are related to each other by $N = N_{\mathrm{lin}}/(f-1)$. Therefore, the Zimm–Stockmayer prediction is $\langle R_g^2\rangle \cong b^2 N_{\mathrm{lin}}\sqrt{\pi/[8(f-1)(f-2)N]}$.

monomer volume fractions inside them *increasing* with degree of polymerization, as reflected in the overlap parameter:

$$P = \frac{Nb^d}{R_g^d} \approx \frac{N}{N^{d/4}} \approx N^{(4-d)/4}. \tag{6.92}$$

An important difference between randomly branched and linear polymers is that the fractal dimension of branched polymers is larger than the dimension of space ($d = 3$). This severely limits the applicability of the mean-field theory to the crosslinking of long linear chains, called vulcanization. Long chains in the melt have a fractal dimension of $\mathcal{D} = 2$, which leaves lots of room inside the pervaded volume of the chain (i.e., filled by other chains in a polymer melt). The extra room created by the linear sections between crosslinks allows the fractal dimension of $\mathcal{D} = 4$ to exist in three-dimensional space *on a certain range of length scales* (see Section 6.5.4).

6.5 Scaling model of gelation

6.5.1 Molar mass distribution and gel fraction

It is possible to generalize the results, derived in Section 6.4 for the Bethe lattice, to any percolation problem. Of particular interest is gelation (percolation) in two-dimensional and three-dimensional spaces. Unlike mean-field percolation (on a Bethe lattice) there is no simple relation between the number of unreacted groups on a branched polymer and its degree of polymerization. Consequently, general percolation problems have no simple analytical solution, but have been solved by computer simulations and by analytical approximations. For example, polymerization of multifunctional monomers can be modeled on a three-dimensional lattice, while polymerization at a surface can be simulated on a two-dimensional lattice. In this section, we follow the scaling approach developed for treating continuous phase transitions, first applied to gelation by Stauffer and de Gennes.

Near the gel point, the system consists of a highly polydisperse distribution of polymers. One of the most important features of gelation is that the number density of polymers near the gel point has a power law dependence on the degree of polymerization, as was found for the Bethe lattice [Eq. (6.78)]. However, the cutoff function is more complicated than the simple exponential of the mean-field theory. In fact, it is asymmetric, having different form below and above the gel point. Therefore, we define the cutoff function $f_+(N/N^*)$ above the gel point and the cutoff function $f_-(N/N^*)$ below the gel point. These cutoff functions have the property of truncating the power law at the characteristic branched polymer with N^* monomers. In addition, $f_-(N/N^*)$ assures that the first moment of the distribution [the sol fraction, Eq. (6.39)] is unity below the gel point:

$$n(p, N) = N^{-\tau} f_-(N/N^*) \quad \text{for } p < p_c, \tag{6.93}$$

$$n(p, N) = N^{-\tau} f_+(N/N^*) \quad \text{for } p > p_c. \tag{6.94}$$

The critical exponent τ is the same above and below the gel point and is called the **Fisher exponent**. The number of monomers N^* in the characteristic branched polymer increases as the gel point is approached (from either side) and diverges as a power of the distance from the gel point, characterized by the relative extent of reaction ε [Eq. (6.25)]:

$$N^* \approx |\varepsilon|^{-1/\sigma}. \tag{6.95}$$

The values of the critical exponents τ and σ and the cutoff functions $f_+(N/N^*)$ and $f_-(N/N^*)$ depend only on the dimension of space in which gelation takes place. The percolation model has been solved analytically in one dimension ($d=1$, see Sections 1.6.2 and 6.1.2) and critical exponents have been derived for two dimensions ($d=2$). The mean-field model of gelation corresponds to percolation in spaces with dimension above the upper critical dimension ($d>6$). The cutoff function in the mean-field model [see Eq. (6.77)] is approximately a simple exponential function [Eq. (6.79)]. The exponents characterizing mean-field gelation are $\sigma=1/2$ and $\tau=5/2$ (see Section 6.4). The exact values of the critical exponents and the exact functional form of the cutoff functions for three-dimensional percolation are not known, but good estimates exist from computer simulations (see Table 6.4 for the values of critical exponents). In three-dimensional percolation, $\sigma\cong 0.45$ and $\tau\cong 2.18$. Both computer simulations and experiments have also verified that the cutoff function is sharp.

Together, Eqs (6.93)–(6.95) predict that plotting $n(p,N)\,(N^*)^\tau$ against N/N^* constructs a **universal scaling curve** that reduces all molar mass distributions at different extents of reaction below the gel point to a single curve. Two such scaling curves are shown in Fig. 6.26.

The moments of the molar mass distribution $n(p,N)$ were defined in Section 1.6:

$$m_k = \sum_{N=1}^{\infty} N^k n(p,N) \approx \int_1^{\infty} N^{k-\tau} f_{\pm}(N/N^*)\,\mathrm{d}N, \tag{6.96}$$

where $f_{\pm}(N/N^*)$ refers to $f_-(N/N^*)$ below the gel point and $f_+(N/N^*)$ above the gel point. It is important to note that, while the sum and integral in Eq. (6.96) extend to infinity, they *only include the sol molecules*. Above the gel point, the gel is not included in $n(p,N)$ and hence does not affect the calculation of the moments.

Table 6.4 Summary of exponents for percolation in d-dimensions

Exponent	$d=1$	$d=2$	$d=3$	$d=4$	$d=5$	$d\geq 6$
β	0	5/36	0.41	0.64	0.84	1
γ	1	43/18	1.82	1.44	1.18	1
σ	1	36/91	0.45	0.48	0.49	1/2
τ	2	187/91	2.18	2.31	2.41	5/2
ν	1	4/3	0.88	0.68	0.57	1/2
$\mathcal{D}$	1	91/48	2.53	3.06	3.54	4

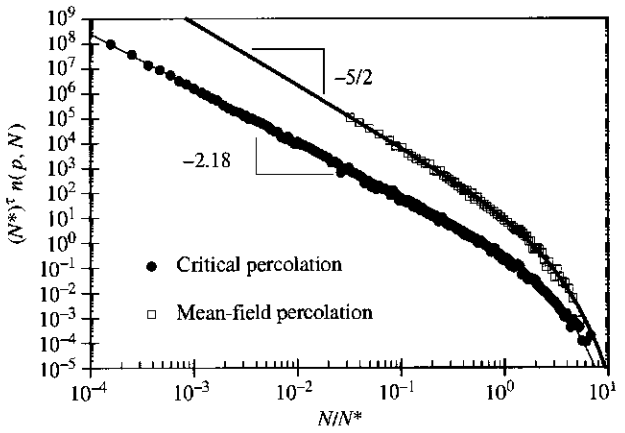

Fig. 6.26
Universal scaling curves for the molar mass distribution of randomly branched polyesters with many different samples in each class. The filled symbols have $N_0 = 2$ monomers between branch points and correspond to critical percolation in three dimensions. The open symbols have $N_0 = 900$ monomers between branch points and obey the mean-field percolation model. Data of C. P. Lusignan *et al., Phys. Rev. E* **52**, 6271 (1995); **60**, 5657 (1999).

Since the Fisher exponent τ for percolation in any dimension is limited to the interval $2 \leq \tau \leq 5/2$, the first two moments of the distribution m_0 and m_1 do *not* diverge at the gel point. These two moments are dominated by the smaller polymers with a small contribution from the larger ones. Below the gel point, the sol fraction is unity [$P_{\text{sol}}(p) = m_1 = 1$, see Eq. (6.42)] and the gel fraction is zero [$P_{\text{gel}}(p) = 1 - P_{\text{sol}}(p) = 0$]. Above the gel point, we can approximate the cutoff function as a step function that goes to zero abruptly at N^*:

$$m_1 \approx \int_1^\infty N^{1-\tau} f_+(N/N^*)\, \mathrm{d}N \approx \int_1^{N^*} N^{1-\tau}\, \mathrm{d}N. \tag{6.97}$$

The integral of a power law is easily evaluated,

$$P_{\text{sol}} = m_1 \approx \int_1^{N^*} N^{1-\tau}\, \mathrm{d}N = 1 - C(N^*)^{2-\tau}, \tag{6.98}$$

where C is a constant. The gel fraction increases with extent of reaction beyond the gel point:

$$P_{\text{gel}}(p) = 1 - P_{\text{sol}}(p) = 1 - m_1 \approx C(N^*)^{2-\tau}.$$

Since $2 - \tau < 0$, the gel fraction is zero right at the gel point (where N^* diverges) and grows steadily with extent of reaction above the gel point:

$$P_{\text{gel}} \sim (N^*)^{2-\tau} \sim \varepsilon^\beta \quad \text{for } p > p_c. \tag{6.99}$$

The exponent β, defined for the growth of the gel fraction, is related to the two exponents τ and σ by a **scaling relation**, obtained by combining Eqs (6.95) and (6.99):

$$\beta = \frac{\tau - 2}{\sigma}. \tag{6.100}$$

The absolute value of ε is not needed when discussing the gel fraction because the growth of P_{gel} only occurs above the gel point, where $\varepsilon > 0$. The mean-field value of this exponent is $\beta = 1$, since $\tau = 5/2$ and $\sigma = 1/2$. However, in three-dimensional percolation this exponent is $\beta \cong 0.41$.

The number-average degree of polymerization is given by the ratio of the first to the zeroth moments of the number density distribution ($N_n = m_1/m_0$) and does *not* diverge (stays finite) at the gel point.

Making the change of variables $x = N/N^*$ in the integral for the moments of the distribution function [Eq. (6.96)] allows us to extract the diverging part from the integral:

$$m_k \approx (N^*)^{k-\tau+1} \int_{1/N^*}^{\infty} x^{k-\tau} f_{\pm}(x)\, dx. \tag{6.101}$$

The cutoff function $f_{\pm}(x)$ assures that the integral in the above equation converges to a number. This approach therefore determines the way in which the moments of the distribution function scale with the proximity to the gel point *without specifying the details of the cutoff function* $f_{\pm}(x)$:

$$m_k \sim (N^*)^{k-\tau+1} \sim |\varepsilon|^{-(k-\tau+1)/\sigma} \quad \text{for } k > \tau - 1. \tag{6.102}$$

The weight-average degree of polymerization of the finite-size branched polymers is the ratio of the second and first moments. Since the first moment is finite and almost constant near the gel point, the weight-average degree of polymerization is proportional to the second moment of the distribution [Eq. (6.102) with $k = 2$]:

$$N_w = \frac{m_2}{m_1} \sim (N^*)^{3-\tau} \sim |\varepsilon|^{-\gamma}. \tag{6.103}$$

Combining Eqs (6.95) and (6.103) leads to a scaling relation for the exponent γ, defined from the divergence of the weight-average degree of polymerization:

$$\gamma = \frac{3-\tau}{\sigma}. \tag{6.104}$$

The mean-field value of this exponent is $\gamma = 1$ [see Eq. (6.59) or substitute $\tau = 5/2$ and $\sigma = 1/2$ in the above equation] and $\gamma \cong 1.82$ in three dimensions. Experimental data on weight-average molar mass of branched polyurethanes in Fig. 6.27 clearly demonstrate that the experimental value of $\gamma = 1.7 \pm 0.1$ is in reasonable agreement with the expectation of three-dimensional percolation.

Moments of the distribution with $k \geq 2$ diverge at the gel point (because $2 \leq \tau \leq 5/2$ and $\sigma > 0$ always). The z-average degree of polymerization of the finite-size branched polymers is the ratio of the third and second moments:

$$N_z = \frac{m_3}{m_2} \sim N^* \sim |\varepsilon|^{-1/\sigma}. \tag{6.105}$$

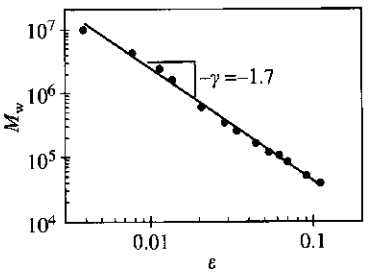

Fig. 6.27
Correlation of weight-average molar mass and relative extent of reaction for trifunctionally branched polyurethanes. Data from M. Adam *et al.*, *J. Phys. France* **48**, 1809 (1987).

Equation (6.80) gives the identical relation for the mean-field model (with $\sigma = 1/2$). Higher-order averages of the distribution are ratios of higher moments (m_{k+1}/m_k with $k \geq 3$). These higher-order averages are all proportional to the degree of polymerization of the characteristic branched polymer N^* and diverge at the gel point with the same exponent $-1/\sigma$.

Note that whenever a new exponent is defined, there is also a scaling relation that calculates this exponent from τ and σ. There are only two independent exponents that describe the distribution of molar masses near the gelation transition, with the other exponents determined from scaling relations. Table 6.4 summarizes the exponents in different dimensions that have been determined numerically, along with the exact results for $d = 1$, $d = 2$, and $d \geq 6$. It turns out that $d = 6$ is the upper critical dimension for percolation, and the mean-field theory applies for all dimensions $d > 6$.

Each set of exponents corresponds to the **universality class** for percolation in space of a particular dimension. These exponents do not depend on the type of lattice (square vs. hexagonal) type of percolation (site vs. bond) and even whether it is on a lattice or not, as long as there are no long-range correlations. Of course, the value of the gel point p_c depends on all the above-mentioned details.

The cutoff functions $f_+(N/N^*)$ and $f_-(N/N^*)$ are expected to only depend on space dimension. In dimensions $1 < d < 6$, the cutoff functions are different above and below the gel point. This asymmetry makes the values of diverging quantities above and below the gel point differ. The ratio of a given quantity below and above the gel point defines an amplitude ratio. For example, the ratio of the weight-average degree of polymerization below and above the gel point by the same small extent x,

$$\lim_{x \to 0} \frac{N_w(p_c - x)}{N_w(p_c + x)}, \tag{6.106}$$

is believed to be universal. In the mean-field theory (and dimensions $d \geq 6$), the transition is symmetric and the amplitude ratios are equal to unity. In general, the percolation transition is not symmetric and the amplitude ratio defined by Eq. (6.106) is of order 10 in three dimensions and even larger (of order 200) in two dimensions.

6.5.2 Cutoff functions

The cutoff functions $f_-(N/N^*)$ and $f_+(N/N^*)$ defined in Eqs (6.93) and (6.94) are both simple exponentials in the mean-field gelation theory [Eq. (6.79)]:

$$\begin{aligned} f_-(N/N^*) = f_+(N/N^*) &\approx \exp[-N/N^*] \approx \exp[-\varepsilon^2 N] \\ &\approx \exp[-(\varepsilon N^{1/2})^2]. \end{aligned} \tag{6.107}$$

Let us define a scaling parameter z,

$$z \equiv \varepsilon N^{\sigma}, \tag{6.108}$$

that combines the two cutoff functions $f_-(N/N^*)$ and $f_+(N/N^*)$ into a single general cutoff function $\hat{f}(z)$. Positive values of z correspond to the system above the gel point, while negative values apply to the system below the gel point. At the gel point, $z = 0$. The absolute value of the scaling parameter z is proportional to $(N/N^*)^{\sigma}$. The cutoff function in the mean-field theory is a Gaussian function of z with its maximum at the gel point:

$$\hat{f}(z) \approx \exp(-z^2). \tag{6.109}$$

The scaling variable z can be used to construct universal plots of molar mass distributions. There are two approaches to making these universal plots. To study the cutoff function itself, multiply both sides of Eqs (6.93) and (6.94) by N^{τ}.

$$N^{\tau} n(p, N) = \hat{f}(z) = \begin{cases} f_-(N/N^*) & \text{for } p < p_c, \\ f_+(N/N^*) & \text{for } p > p_c. \end{cases} \tag{6.110}$$

To study the universal properties of the distribution of molar masses, multiply both sides of Eqs (6.93) and (6.94) by $(N^*)^{\tau}$:

$$(N^*)^{\tau} n(p, N) = z^{-\tau/\sigma} \hat{f}(z) = \left(\frac{N}{N^*}\right)^{-\tau} \begin{cases} f_-(N/N^*) & \text{for } p < p_c, \\ f_+(N/N^*) & \text{for } p > p_c. \end{cases} \tag{6.111}$$

The analytical form of the cutoff function in three-dimensional critical percolation is not known. However, experimental and numerical universal plots have been constructed using the methods described above and constitute a convincing proof of the validity of the scaling ansatz (see Fig. 6.26).

Similar methods can be used to construct universal plots for molar mass distributions of linear and hyperbranched condensation polymers. The number distribution function $n(p, N)$ for linear condensation polymers is obtained from the number fraction distribution [Eq. (1.66)]:

$$n(p, N) = \frac{n_N(p)}{N_n} = \frac{1}{N_n^2} \exp\left(-\frac{N}{N_n}\right). \tag{6.112}$$

Identifying the characteristic degree of polymerization for linear condensation (with $\sigma = 1$ and $p_c = 1$)

$$N^* = N_n = \frac{p_c}{p_c - p} = \frac{1}{\varepsilon} \tag{6.113}$$

the distribution function $n(p, N)$ can be rewritten in the scaling ansatz form:

$$n(p, N) = N^{-2} \left(\frac{N}{N^*}\right)^2 \exp\left(-\frac{N}{N^*}\right). \tag{6.114}$$

Comparing this expression with Eq. (6.93) identifies $\tau = 2$ and the one-dimensional percolation cutoff function

$$\hat{f}(z) = z^2 \exp(z) \tag{6.115}$$

for scaling variable

$$z = -\frac{N}{N^*} \tag{6.116}$$

that is never positive for linear condensation because $p \leq p_c = 1$. The scaled molar mass distribution for linear condensation is a simple exponential

$$n(p, N)N_n^2 = \exp\left(-\frac{N}{N_n}\right) \tag{6.117}$$

that does not have any power law features, even though the Fisher exponent for this case is $\tau = 2$. This is different from the scaled molar mass distribution in gelation that decays as a power law with exponent equal to the Fisher exponent. The fact that the cutoff function in linear condensation [Eq. (6.115)] is a power law itself at small z accounts for this difference.

An even more striking example is the universal molar mass distribution of hyperbranched polymers. This distribution [Eq. (6.31)] can also be written in the scaling ansatz form with $\tau = 2$:

$$n(p, N) = \frac{n_N(p)}{N_n} \approx \frac{N^{-3/2}}{N_n} \exp(-N/N^*) \approx \frac{N^{-3/2}}{(N^*)^{1/2}} \exp(-N/N^*)$$
$$\approx N^{-2}\left(\frac{N}{N^*}\right)^{1/2} \exp(-N/N^*). \tag{6.118}$$

The characteristic degree of polymerization N^* is related to N_n by Eqs (6.32) and (6.34):

$$N^* = N_n^2 = \frac{1}{(1 - p/p_c)^2}. \tag{6.119}$$

The cutoff function for hyperbranched polymers is

$$\hat{f}(z) = -z \exp(-z^2), \tag{6.120}$$

where the scaling parameter

$$z = -\left(\frac{N}{N^*}\right)^{1/2}. \tag{6.121}$$

Alternatively, the universal molar mass distribution [Eq. (6.111)] for hyperbranched polymers can be constructed:

$$n(p, N)(N^*)^2 \approx \left(\frac{N}{N^*}\right)^{-3/2} \exp(-N/N^*). \tag{6.122}$$

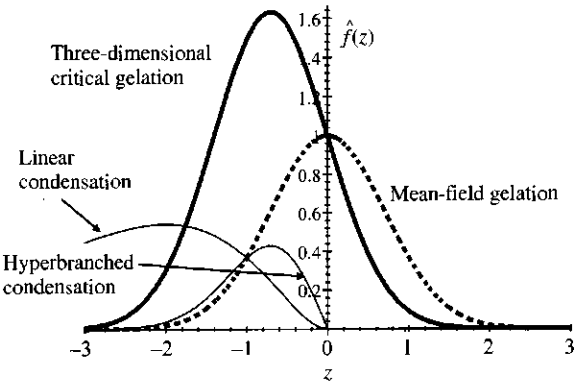

Fig. 6.28
Cutoff functions for critical gelation (thick curve), mean-field gelation (dotted curve), and linear and hyperbranched condensation (thin curves).

Using the proportionality between the characteristic degree of polymerization N^* and N_w, a universal distribution function for hyperbranched polymers can be constructed by plotting $n(p, N)N_w^2$ against N/N_w. The fact that the cutoff function contains the power law in z makes the apparent power law exponent 3/2 in the molar mass distribution different from $\tau = 2$. The cutoff function for gelation has no power law so the apparent exponent is equal to τ.

The cutoff functions are plotted in Fig. 6.28. For critical gelation in three dimensions (and in the more general case of $1 < d < 6$) the cutoff function is asymmetric with the maximum shifted to the negative values of z. In contrast, the cutoff function for mean-field gelation is perfectly symmetric. Linear and hyperbranched condensation are defined only for negative scaling parameter z (for $p < p_c$). The cutoff function for both of these reactions vanishes at $z = 0$ because there is only one macromolecule at complete reaction ($p = p_c = 1$). For small negative values of the parameter z, the cutoff function grows as a power law of z ($\sim -z$ for hyperbranched and $\sim z^2$ for linear condensation). Both of these cutoff functions have a maximum and decay at large negative values of z.

A very important caveat with the universal molar mass distributions and cutoff functions is that calculated molar mass distributions of linear condensation, hyperbranched condensation and mean-field percolation all assume no intramolecular reactions occur. Intramolecular reactions are hard to avoid in real polymerization experiments.

6.5.3 Size and overlap of randomly branched polymers

The correlation length ξ for percolation (and gelation) is the size of the characteristic branched polymer with N^* monomers. Randomly branched polymers are fractals, so the size R and the number of monomers N in a polymer are related by the fractal dimension $\mathcal{D}$:

$$N \sim R^{\mathcal{D}}. \tag{6.123}$$

The same relation is valid for the characteristic branched polymer:

$$N^* \sim \xi^{\mathcal{D}}. \tag{6.124}$$

Since N^* diverges at the gel point with exponent $1/\sigma$ [see Eq. (6.95)], the correlation length must also diverge:

$$\xi \sim (N^*)^{1/\mathcal{D}} \sim |\varepsilon|^{-\nu}. \tag{6.125}$$

The exponentt ν describing the divergence of the correlation length is related to σ and the fractal dimension $\mathcal{D}$ by combining Eqs (6.95) and (6.125):

$$\nu = \frac{1}{\mathcal{D}\sigma}. \tag{6.126}$$

In mean field, $\sigma = 1/2$ and $\mathcal{D} = 4$ (see Section 6.4) so $\nu = 1/2$. For three-dimensional percolation, this critical exponent is $\nu = 0.88$ and the fractal dimension of randomly branched polymers in the polymerization reactor is $\mathcal{D} = 2.53$.

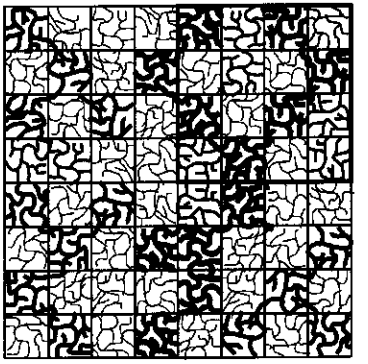

Fig. 6.29
Hyperscaling—polymers are at overlap with other chains of the same size and with similar sized parts of larger chains. Polymers of different size are denoted by lines of different thicknesses.

6.5.3.1 Hyperscaling

For critical percolation, the exponent ν and the fractal dimension $\mathcal{D}$ are related to the critical exponents discussed in Section 6.5.2 by the **hyperscaling** relation in dimensions $1 < d < 6$. The idea of hyperscaling is that polymers with a given number of monomers N are at the overlap concentration with themselves and with similar sized parts of larger polymers (see Fig. 6.29). Polymers of a given size cannot strongly overlap because they would have many contact points and would have already reacted to make a larger polymer. The pervaded volume for a randomly branched polymer with N monomers in d-dimensional space is proportional to $R^d \sim N^{d/\mathcal{D}}$ [see Eq. (6.123)]. Molecules with K monomers (for $K > N$) can be divided into K/N parts, each containing N monomers. Since the molecules are fractal, these smaller parts have the same size as individual molecules with N monomers. The number of molecules with K monomers is proportional to their number density $n(p, K)$. Therefore, the total volume pervaded by molecules with N monomers as well as smaller parts (containing N monomers) of larger molecules is proportional to

$$\int_N^\infty R^d \frac{K}{N} n(p, K)\, \mathrm{d}K \sim \frac{R^d}{N} \int_N^\infty K n(p, K)\, \mathrm{d}K. \tag{6.127}$$

The integral on the right-hand side of the above equation is the weight fraction of all molecules larger than N. This integral is dominated by the lower limit for critical exponent $\tau > 2$ and is proportional to $N^{2-\tau}$.

$$\int_N^\infty K n(p, K)\, \mathrm{d}K \sim N^{2-\tau}.$$

In order for the fragments of molecules containing N monomers to be at overlap (for all N), the combined pervaded volume has to be independent of N (and equal to the total volume of the system):

$$\int_N^\infty R^d \frac{K}{N} n(p, K)\, \mathrm{d}K \sim R^d N^{1-\tau} \sim N^{1-\tau+d/\mathcal{D}} \sim N^0. \tag{6.128}$$

This condition leads to the hyperscaling relation between critical exponents:

$$\frac{d}{\mathcal{D}} = \tau - 1. \tag{6.129}$$

Hyperscaling relates the fractal dimension of randomly branched molecules in the gelation reaction with the Fisher exponent and the space dimension (see Table 6.4):

$$\mathcal{D} = \frac{d}{\tau - 1} \quad \text{for } 1 \leq d \leq 6. \tag{6.130}$$

The mean-field value of the Fisher exponent is $\tau = 5/2$. The fractal dimension of ideal randomly branched polymers is $\mathcal{D} = 4$ [see Eq. (6.90)]. Equation (6.130) gives $\mathcal{D} = 4$ for $\tau = 5/2$ in dimension $d = 6$, which is the upper critical dimension for percolation. For dimensions larger than 6, the mean-field theory works and the hyperscaling relation does not (polymers strongly overlap). For three-dimensional percolation, $\tau \cong 2.18$ and $\mathcal{D} \cong 2.53$. Experimental measures of fractal dimension by Adam and coworkers using small-angle neutron scattering experiments report $\mathcal{D} = 2.50 \pm 0.06$.

6.5.3.2 Flory–de Gennes theory

The fractal dimension of randomly branched polymers in the polymerization reaction can be estimated using Flory theory (see Section 3.1.2). The free energy of the characteristic branched polymer consists of entropic and interaction parts:

$$F \approx kT\left[\frac{\xi^2}{[b(N^*)^{1/4}]^2} + \frac{\mathrm{v}}{N_\mathrm{w}}\frac{(N^*)^2}{\xi^d}\right]. \tag{6.131}$$

The first term is the entropic penalty for swelling the branched polymer from its ideal size $b(N^*)^{1/4}$ [Eq. (6.90)] to its size in the reactor ξ. The second term is the estimate of the excluded volume repulsion between $(N^*)^2$ pairs of monomers spread over the pervaded volume of the polymer ξ^d with excluded volume interactions screened by the polydisperse mix of smaller branched polymers inside the pervaded volume of this characteristic branched polymer. In Section 4.5.2, the screening of excluded volume interactions by overlapping chains was discussed for the case of a melt of linear chains [Eq. (4.73)]. Analogous screening occurs in the case of a polydisperse sample with the excluded volume reduced by the weight-average degree of polymerization of the polymers inside the pervaded volume of a given polymer (see Problem 4.19). In the case of the characteristic branched polymer, the excluded volume is reduced by the weight-average degree of polymerization of all finite-size branched polymers v/N_w.

The size of the characteristic branched polymer ξ is obtained by minimizing the free energy [Eq. (6.131)] with respect to its size:

$$\xi \approx b\left(\frac{v}{b^d}\frac{(N^*)^{5/2}}{N_w}\right)^{1/(d+2)}. \tag{6.132}$$

Substituting the mean-field relation between the weight-average and characteristic degrees of polymerization,

$$N_w \sim \varepsilon^{-\gamma} \sim (N^*)^{\gamma\sigma} \sim (N^*)^{1/2} \tag{6.133}$$

provides the de Gennes prediction for the correlation length in gelation based on Flory theory.

$$\xi \approx b\left(\frac{v}{b^d}\right)^{1/(d+2)}(N^*)^{2/(d+2)}. \tag{6.134}$$

Hence, the fractal dimension of the branched polymers is predicted in every dimension of space:

$$\mathcal{D} \cong \frac{d+2}{2} \quad \text{for } 2 \le d \le 6. \tag{6.135}$$

Note that this prediction is quite close to the values reported in Table 6.4.

6.5.4 Vulcanization universality class

Consider the crosslinking of long linear precursor chains with degree of polymerization N_0 and functionality f in the melt. This class of gelation is called vulcanization, named after Goodyear's famous process to crosslink natural rubber using sulphur. Vulcanization is one type of gelation for which the mean-field theory, described in Section 6.4, works well in a wide range of relative extents of reaction $\varepsilon = (p - p_c)/p_c$ [Eq. (6.25)]. The effective functionality of a long chain with N_0 crosslinkable monomers is $f \approx N_0$. The mean-field prediction for the gel point is [Eq. (6.47)]

$$p_c = \frac{1}{f-1} \approx \frac{1}{N_0} \quad \text{for } N_0 \gg 1 \tag{6.136}$$

and corresponds to an average of *one crosslink per chain*. The gel fraction is proportional to this relative extent of reaction [see Eq. (6.99) with mean-field value of exponent $\beta = 1$]:

$$P_{gel} \approx \varepsilon \quad \text{for } 0 < \varepsilon \ll 1. \tag{6.137}$$

At relative extent of reaction $\varepsilon = 1$, the gel fraction is of order unity $P_{gel} \approx 1$, and most of the chains are attached to the gel. The percolation transition is almost complete, with very small sol fraction left $P_{sol} \ll 1$ at extent of reaction $p \approx 2p_c$ (where $\varepsilon \approx 1$). Since the gel point corresponds to an average of one crosslink per chain, the end of the gelation regime corresponds to an

average of two crosslinks per chain. In some cases of vulcanization, the functionality is very large ($f \approx N_0 \gg 1$) leading to a small percolation threshold ($p_c \ll 1$). An example of such vulcanization is the Goodyear original process, where large values of the relative extent of reaction $\varepsilon \gg 1$ are possible. Such highly vulcanized networks (with many crosslinks per chain) are considered in the next chapter.

The correlation length ξ and the number of monomers in a characteristic branched polymer N^* have simple predictions for vulcanization. These predictions can be easily obtained from the mean-field percolation theory [Eqs (6.105) and (6.125) with exponents $\sigma = \nu = 1/2$] by replacing the monomer in the previous treatment by the precursor linear chain[5] of size $bN_0^{1/2}$ containing N_0 monomers.

$$\xi \approx bN_0^{1/2}|\varepsilon|^{-1/2}, \tag{6.138}$$

$$N^* \approx N_0\varepsilon^{-2}. \tag{6.139}$$

The number of monomers in the characteristic branched polymer N^* and its size ξ are symmetric around the gel point ($\varepsilon = 0$). The molar mass distribution is in fact similar for the same ε above and below the gel point (within the framework of mean-field scaling).

Beyond the gel point, the correlation length ξ also describes the size of the 'holes' in the network and N^* is the average number of monomers in a network strand. Each network strand is a branched polymer. The number of overlapping network strands P plays a vital role in our understanding of gelation. The volume fraction of a single network strand inside its pervaded volume is N^*b^3/ξ^3. The number of network strands with N^* monomers, sharing the same volume ξ^3 (which is the overlap parameter for the network strands) is given by the ratio of the volume fraction of all network strands (the gel fraction P_{gel}) and the volume fraction of a single strand:

$$P \approx \frac{P_{gel}}{N^*b^3/\xi^3} \approx \frac{P_{gel}}{N^*}\left(\frac{\xi}{b}\right)^3 \approx N_0^{1/2}|\varepsilon|^{3/2}. \tag{6.140}$$

The final result was obtained using Eqs (6.137)–(6.139). For long chains between branch points (large N_0), P can be large, meaning that network strands overlap each other extensively. This is hardly surprising, since we know that before any crosslinking takes place (at $\varepsilon = -1$) the long precursor chains will have $N_0^{1/2}$ other chains within their pervaded volume [see Eq. (5.11)]. The highly overlapping and interpenetrating precursor chains guarantee that there will be considerable overlap over most of the crosslinking reaction.

However, Eq. (6.140) shows that the overlap of the largest polymers diminishes as the gel point is approached. For any precursor chain length

[5] Although it decreases gradually as the reaction proceeds, the chain length between branch points *in the gelation regime* is of order N_0.

there is always a region very close to the gel point where the largest finite polymers (and network strands above the gel point) no longer overlap and the mean-field theory breaks down. As with other transitions that we have discussed, the mean-field theory only applies sufficiently far from the critical point. Closer to the critical point (near $\varepsilon = 0$) the mean-field theory must be replaced by the critical theory (discussed in detail in Section 6.5.1). The crossover point between the regions where each theory applies is given by the Ginzburg criterion. For percolation, the relative extent of reaction ε_G corresponding to the Ginzburg criterion is the point where the characteristic polymers (and network strands above the gel point) no longer overlap. Setting $P = 1$ in Eq. (6.140) determines the Ginzburg relative extent of reaction:

$$\varepsilon_G \approx N_0^{-1/3}. \tag{6.141}$$

For $|\varepsilon| > \varepsilon_G$, the mean-field theory describes the crosslinking reaction. For $|\varepsilon| < \varepsilon_G$, (sufficiently close to the gel point), critical percolation describes the actual transition. For very long precursor chains, ε_G is extremely small and the entire experimentally accessible region of crosslinking is described by mean-field percolation (in practice $N_0 \gtrsim 100$ is sufficient). The limit of $N_0 = 1$ is polymerization of monomers with functionality greater than 2, and all extents of reaction in the range $-1 < \varepsilon < 1$ are described by critical percolation.

The dependence of the overlap parameter on relative extent of reaction is sketched in Fig. 6.30. Equation (6.140) describes the decrease in overlap as the gel point is approached until $P = 1$ at the Ginzburg point. The characteristic polymers and the network strands above the gel point are just at their overlap concentration inside the critical region (where $P = 1$). Beyond the Ginzburg point on the gel side of the gel point, the overlap of network strands starts to increase again at ε_G and builds as the correlation length (and hence the network strand length) decreases. Notice that the overlap parameter is symmetric around the gel point.

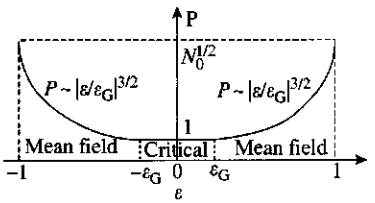

Fig. 6.30
Dependence of the overlap parameter P on relative extent of reaction ε.

Before the vulcanization reaction, long linear chains with degree of polymerization N_0 and size $bN_0^{1/2}$ overlap with each other strongly (recall from Problem 1.22 and Section 4.5.2 that there are $N_0^{1/2}$ other chains in the pervaded volume of any linear chain in the melt). Crosslinking these chains creates branched polymers with fractal dimension $\mathcal{D} = 4$ on scales larger than the linear chains. The size of these branched polymers with degree of polymerization N is

$$R_g \approx bN_0^{1/2}\left(\frac{N}{N_0}\right)^{1/4} \approx b(N_0 N)^{1/4}. \tag{6.142}$$

The intramolecular pair correlation function $g(r)$ is the number of monomers per unit volume of a section of chain with section size r inside its pervaded volume r^3, plotted in Fig. 6.31. The linear subsections of the randomly branched polymer have approximately N_0 monomers connected in a linear chain ($\mathcal{D} = 2$). The intramolecular pair correlation function $g(r)$

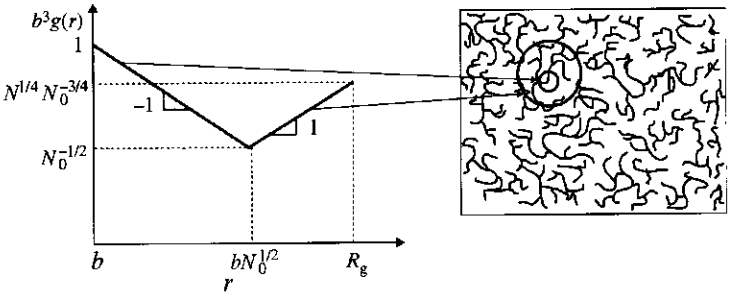

Fig. 6.31
Intramolecular pair correlation function $g(r)$ of directly connected monomers within a sphere of radius r of a given monomer, for randomly branched polymers with N monomers made from vulcanizing linear chains with degree of polymerization N_0. Both axes have logarithmic scales.

decreases for r smaller than $bN_0^{1/2}$ (the size of the linear chain sections), Eq. (2.121):

$$g(r) \approx \frac{n}{r^3} \approx \frac{1}{rb^2} \quad \text{for } r < bN_0^{1/2}. \tag{6.143}$$

This simple scaling results because a volume of size r contains $n = (r/b)^2$ monomers from that chain section. Equation (6.143) describes the minus one slope region of Fig. 6.31 on scales smaller than the size of the linear chains (with $r < bN_0^{1/2}$). When r reaches the size scale of the linear chain sections $bN_0^{1/2}$, Eq. (6.143) gives the expected result for the volume fraction of a linear chain inside its own pervaded volume in a melt, $\phi \approx N_0^{-1/2}$. On scales larger than the linear chains, the fractal dimension $\mathcal{D} = 4$ applies to chain sections of size r that are directly connected within the volume r^3 [see Eq. (6.142) and Fig. 6.31]:

$$r \approx b(N_0 n)^{1/4}. \tag{6.144}$$

The intramolecular pair correlation function grows with increasing r because the fractal dimension is larger than the space dimension:

$$g(r) \approx \frac{n}{r^3} \approx \frac{r}{b^4 N_0} \quad \text{for } bN_0^{1/2} < r < R_g. \tag{6.145}$$

The volume fraction of monomers inside the pervaded volume of the randomly branched polymer is $b^3 g(R_g) \approx N^{1/4} N_0^{-3/4}$, obtained by substituting R_g from Eq. (6.142) for r in Eq. (6.145). This approach is only valid in the vulcanization regime, with $\varepsilon > \varepsilon_G$. The number of monomers in a characteristic polymer at the Ginzburg point is $N^* \approx N_0 \varepsilon_G^{-2} \approx N_0^{5/3}$ [see Eqs (6.139) and (6.141)]. The volume fraction of monomers $b^3 g(R_g) \approx N_0^{-1/3} \ll 1$, so the polymers with fractal dimension $\mathcal{D} = 4$ fit in three-dimensional space.

The polymerization reactor contains a highly polydisperse distribution of molecules. The size of the characteristic polymer (with N^* monomers) defines the correlation length ξ [see Eq. (6.142)]:

$$\xi \approx b(N_0 N^*)^{1/4} \approx bN_0^{1/2} |\varepsilon|^{-1/2}. \tag{6.146}$$

This equation used Eq. (6.139) for the degree of polymerization of the characteristic polymer in the mean-field theory. The correlation length diverges as the gel point is approached for $|\varepsilon| > \varepsilon_G$ with mean-field exponent $\nu = 1/2$.

Below the gel point, the system is self-similar on length scales smaller than the correlation length ξ, with a power law distribution of molar masses with Fisher exponent $\tau = 5/2$ [Eq. (6.78)]. Each branched molecule is a self-similar fractal with fractal dimension $\mathcal{D} = 4$ for ideal branched molecules in the mean-field theory. The lower limit of this critical behaviour is the average distance between branch points ($\cong bN_0^{1/2}$). There are very few finite molecules larger than the characteristic branched polymer (with $N > N^*$) with size larger than the correlation length, because the distribution [Eq. (6.78)] has a sharp cutoff.

Above the gel point there is a macroscopic molecule (the gel). The structure of the gel is also self-similar (fractal) in the same range of length scales between the average distance between crosslinks (the linear chain size) and the correlation length:

$$bN_0^{1/2} < r < \xi. \tag{6.147}$$

The correlation length ξ is the average distance between branch points that are connected to several branches leading to 'infinity' (the boundary of the gel). At $p \approx 2p_c$ (at $\varepsilon \approx 1$) the gelation regime ends and most of the network strands are then simply linear chains. Chapter 7 shall discuss the properties of such well-developed networks.

6.6 Characterization of branching and gelation

Below the gel point, all species are soluble (in the appropriate solvent) allowing the standard dilute solution characterization methods to be utilized. Above the gel point, there is an insoluble gel fraction and a soluble sol fraction. When immersed in an excess of the appropriate solvent, the gel fraction will swell, and the sol fraction will slowly diffuse out of the swollen gel into the excess solvent. A convenient technique for such separation is **Soxhlet extraction**, shown in Fig. 6.32. Solvent is boiled in the bottom flask and condenses at the very top, dripping down onto the swollen gel. The gel is inside a carefully weighed glass thimble with a fritted filter at the bottom. As the thimble fills with solvent, the solvent flows through the filter, carrying with it the sol fraction. When the solvent outside the thimble reaches a certain level, it automatically siphons down into the lower boiling solvent. The Soxhlet extractor is designed to run continuously for many days virtually unattended. However, in practice a solvent with a very low boiling point is used to minimize degradation of the sol, and the high vapor pressure means that pure solvent must be added periodically. If the filter does not plug, the Soxhlet extractor eventually has all of the sol fraction in the boiling solvent and all of the gel fraction in the thimble. The gel fraction is characterized by its swelling (discussed in detail in Chapter 7). After allowing the excess solvent to flow through the filter, the thimble and swollen gel are weighed to determine the swollen mass. Then, the solvent is removed under vacuum and the thimble is weighed again to determine the gel fraction. The sol fraction can be characterized with the same dilute

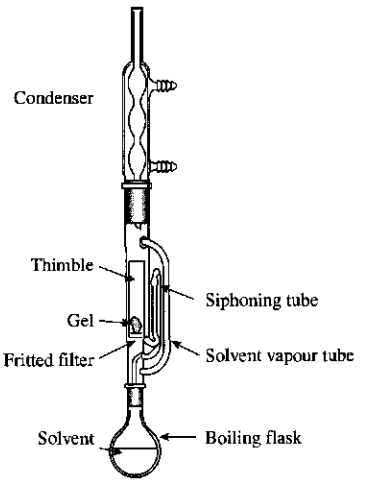

Fig. 6.32
Soxhlet extraction apparatus for separating sol and gel fractions.

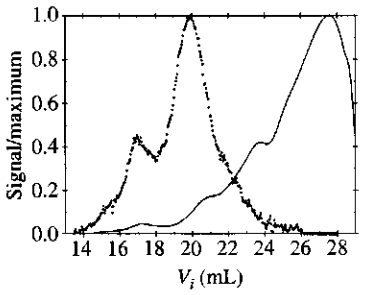

Fig. 6.33
Refractive index (line) and 15° light scattering (points) detector outputs as functions of elution volume for size exclusion chromatography on a randomly branched polyester sample dissolved in tetrahydrofuran. Data from C. P. Lusignan, Doctoral Dissertation, University of Rochester, 1996.

solution techniques used below the gel point. The fractal dimension of the swollen branched polymers is smaller than in their melt state.

Owing to the very broad molar mass distributions associated with random branching, the primary characterization tool is size exclusion chromatography, introduced in Section 1.7.4. For branched polymers, a low-angle light scattering detector is used together with a concentration-sensitive detector to determine the weight-average molar mass of each small volume of solution eluting from the columns. This experiment provides a wealth of information about the molecular characteristics of randomly branched polymers.

Depending on the chemical details of the polymer, a variety of concentration detectors can be used. The most common ones measure either refractive index or ultraviolet absorption. Figure 6.33 shows the measurements of refractive index and light scattering intensity at a scattering angle of 15° as functions of elution volume for a randomly branched polyester. Recall from Section 1.7.4 that the SEC separates polymers by size. The largest species access the smallest amount of column volume and thereby elute first (smaller elution volume V_i). Notice in Fig. 6.33 that there is a very small amount of the largest species, but they dominate the light scattering. This is because at low concentrations the intensity of scattered light is proportional to the product $c_i M_i$ [see Eq. (1.90)]. The scattering intensity has two local maxima. Experimentally, it is verified that the maximum intensity (at $V_i = 19.9$ mL in Fig. 6.33) corresponds to branched polymers with degree of polymerization proportional to N^*. The second peak at lower elution volume is an artefact of the exclusion limit of the columns. Close to the gel point, some branched polymers are so large that they do not fit into any of the pores in the columns. Such very large molecules are not separated by the SEC, and elute together (at $V_i \cong 17$ mL in Fig. 6.33). These imperfectly separated species must be removed before constructing universal molar mass distribution plots, such as Fig. 6.26.

Knowledge of the concentration c_i and weight-average molar mass M_{wi} of each elution volume enables calculation of the weight-average and z-average molar masses:

$$M_w = \frac{\sum_i c_i M_{wi}}{\sum_i c_i}, \tag{6.148}$$

$$M_z \cong \frac{\sum_i c_i (M_{wi})^2}{\sum_i c_i M_{wi}}. \tag{6.149}$$

Comparison with Eqs (1.31) and (1.32) shows that Eq. (6.148) is exact, but Eq. (6.149) is exact only if each elution volume i is monodisperse (see Problem 6.40). Particularly since this chromatography separates molecules by size and not mass, the different elution volumes are not truly monodisperse. In practice, however, Eq. (6.149) is used to calculate M_z.

The universality class of the randomly branched polymers can be determined by constructing a universal molar mass distribution plot, like the ones shown in Fig. 6.26. First, the number density distribution function $n(p, N)$ is determined from the concentration and weight-average molar mass of each elution volume. The concentration detector directly determines the weight fraction of polymer in each elution volume $w_N(V_i)$:

$$w_N(V_i) = \frac{c_i}{\sum_j c_j}. \tag{6.150}$$

This weight fraction must first be converted to a function of molar mass, using the calibration curve[6] for the columns used (Fig. 1.26). The two weight fraction distributions are related to each other as

$$w_N(M_i)\,\mathrm{d}M_i = -w_N(V_i)\,\mathrm{d}V_i \tag{6.151}$$

where the minus sign comes from the fact that larger molar masses elute at smaller elution volumes:

$$w_N(M_i) \doteq -w_N(V_i)\frac{\mathrm{d}V_i}{\mathrm{d}M_i} \cong \frac{-c_i}{2.303 M_i \sum_j c_j}\frac{\mathrm{d}V_i}{\mathrm{d}\log M_i}. \tag{6.152}$$

The final relation uses a derivative with respect to the base ten logarithm of molar mass, as is customary for the calibration curve (see Fig. 1.26). The number density distribution function $n(p, N)$ is related to w_N in a simple way:

$$n(p, N) = \frac{w_N}{N} \cong \frac{-M_0 c_i}{2.303 (M_i)^2 \sum_j c_j}\frac{\mathrm{d}V_i}{\mathrm{d}\log M_i}. \tag{6.153}$$

The characteristic degree of polymerization N^* is chosen for each sample so that the $n(p, N)$ data for that sample can be superimposed onto the universal curve. For both of the curves in Fig. 6.26, more than 10 samples with different extents of reaction were superimposed in this fashion. Although the Fisher exponent τ is not very different for the two classes of percolation, τ is sufficiently different not to allow the data from one class to be superimposed with the wrong exponent.

The system in Fig. 6.26 corresponding to critical percolation (with $\tau = 2.18$) has an average of $N_0 \cong 2$ monomers between branch points. The system corresponding to mean-field percolation (with $\tau = 5/2$) has long linear chains between branch points, with an average degree of polymerization of $N_0 \cong 900$. Most random branching reactions create chain lengths between branch points that are between these two clean limits. Such systems will exhibit the crossover anticipated by the Ginzburg criterion, between critical percolation close to the gel point and mean-field percolation further away. The critical and mean-field predictions can be simply

[6] With branched polymers the simplest procedure is to measure the concentration, intrinsic viscosity, and weight-average molar mass of each elution volume using appropriate detectors, see Section 1.7.4.

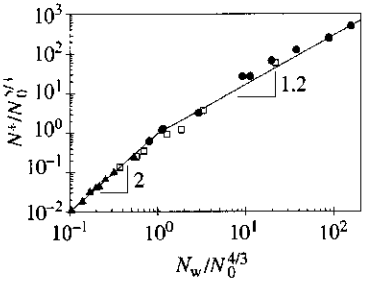

Fig. 6.34
Correlation of the characteristic degree of polymerization and the weight-average degree of polymerization for randomly branched polyesters below the gel point, using the scaling form suggested by Eqs (6.154) and (6.155) (lines with slope $1/(\sigma\gamma)$ for each class). Three different polyester chemistries are utilized, with average degree of polymerization between branch points of $N_0 = 2$ (filled circles), $N_0 = 20$ (open squares), and $N_0 = 900$ (filled triangles). $N_0 = 2$ data from C. P. Lusignan *et al.*, *Phys. Rev. E* **52**, 6271 (1995). $N_0 = 20$ data from E. V. Patton *et al.*, *Macromolecules* **22**, 1946 (1989). $N_0 = 900$ data from C. P. Lusignan *et al.*, *Phys. Rev. E* **60**, 5657 (1999).

matched at the Ginzburg extent of reaction ε_G.

$$N_w \approx N_0^{4/3} \begin{cases} (\varepsilon/\varepsilon_G)^{-\gamma} & \varepsilon < \varepsilon_G, \\ (\varepsilon/\varepsilon_G)^{-1} & \varepsilon > \varepsilon_G, \end{cases} \tag{6.154}$$

$$N^* \approx N_0^{5/3} \begin{cases} (\varepsilon/\varepsilon_G)^{-1/\sigma} & \varepsilon < \varepsilon_G, \\ (\varepsilon/\varepsilon_G)^{-2} & \varepsilon > \varepsilon_G. \end{cases} \tag{6.155}$$

This scaling-level matching expects a plot of $N^*/N_0^{5/3}$ against $N_w/N_0^{4/3}$ to be universal for all polymer gelation reactions. Such a plot is shown in Fig. 6.34 for three randomly branched polyester systems with $N_0 = 2$, 20, and 900. Figure 6.26 already showed that the system with $N_0 = 900$ corresponds to mean-field percolation and the triangles in Fig. 6.34 show that those samples have $N^*/N_0^{5/3} \approx (N_w/N_0^{4/3})^2$. Furthermore, all samples with $N_0 = 900$ have $N_w/N_0^{4/3} < 1$ and $N^*/N_0^{5/3} < 1$, which means that $\varepsilon > \varepsilon_G$, based on Eqs (6.154) and (6.155). Similarly, all samples with $N_0 = 2$ belong to the critical percolation universality class (circles in Fig. 6.26) and demonstrate the scaling expected from Eqs (6.154) and (6.155) in Fig. 6.34. The slope for $\varepsilon < \varepsilon_G$ ($N_w/N_0^{4/3} > 1$ and $N^*/N_0^{5/3} > 1$) in Fig. 6.34 is $1/(\sigma\gamma) \cong 1.2$. The $N_0 = 20$ system falls in the crossover between the two universality classes. For samples with $N_0 = 20$ that are far from the gel point, $\varepsilon > \varepsilon_G$ and the mean-field exponents apply, while for $N_0 = 20$ samples close to the gel point, $\varepsilon < \varepsilon_G$ and critical percolation exponents apply. However, it is important to notice that if the $N_0 = 20$ data in Fig. 6.34 were considered on their own, an apparent exponent intermediate between those of critical and mean-field theories would be observed. Figure 6.34 shows that such apparent exponents must not be used to extrapolate beyond the range of the data!

The extent of reaction p can, in principle, be measured by molecular spectroscopy methods such as FTIR and NMR. However, these methods always have some small relative error (typically of order a few percent). Since the same error has to apply to any determination of the extent of reaction at the gel point p_c, the relative error in the relative extent of reaction $\varepsilon = (p - p_c)/p_c$ *diverges* at the gel point. As a result, plots such as Fig. 6.34, where two quantities with finite relative errors (N_w and N^*) are plotted against each other, are more useful for determining exponent values and hence universality class. It is important to recognize that these plots always give information about combinations of exponents. For example, the slope in Fig. 6.34 is $1/(\sigma\gamma) = 1/(3 - \tau)$, as required by Eq. (6.104).

6.7 Summary of branching and gelation

A wide variety of linking processes can lead to the transformation from a liquid to a solid known as gelation. This transition occurs at a particular extent of reaction, p_c, called the gel point. A rough estimate of the gel point for linking precursor molecules (or monomers) with functionality f is

$p_c = 1/(f-1)$. As the reaction proceeds, a highly polydisperse mix of molecules is formed with a power law distribution of molar masses. The probability that a randomly chosen polymer at extent of reaction p will have molar mass M is

$$n(p, M) \sim M^{-\tau} f(M/M^*), \tag{6.156}$$

where τ is the Fisher exponent and the cutoff function $f(M/M^*)$ sharply truncates the distribution at the molar mass of the (largest) characteristic molecule M^*. This characteristic molar mass diverges as the gel point is approached.

$$M^* \sim \left| \frac{p - p_c}{p_c} \right|^{-1/\sigma}. \tag{6.157}$$

This molar mass distribution applies to all polymers below the gel point and above the gel point it applies to the sol fraction. The weight-average molar mass of this distribution also diverges as the gel point is approached from either side:

$$M_w \sim \left| \frac{p - p_c}{p_c} \right|^{-\gamma} \quad \text{with } \gamma = \frac{3 - \tau}{\sigma}. \tag{6.158}$$

The number-average molar mass stays finite at the gel point and therefore the polydispersity index of the sol diverges at the gel point proportional to M_w.

At the gel point, the distribution of molar masses is a power law, since M^* diverges. Above the gel point the system consists of a macroscopic gel, permeated by a polydisperse soup of microscopic molecules (the sol) described by the same self-similar distribution of molar masses. The distribution of molar masses in the sol gets progressively narrower as the reaction proceeds further beyond the gel point, since the characteristic molar mass M^* decreases. The fraction of the material that is a part of the gel, called the gel fraction P_{gel}, grows steadily above the gel point:

$$P_{gel} \sim \left(\frac{p - p_c}{p_c} \right)^{\beta} \quad \text{with } \beta = \frac{\tau - 2}{\sigma}. \tag{6.159}$$

Once the extent of reaction reaches approximately twice the gel point, nearly all monomers are attached to the gel and there is essentially no sol fraction remaining. Such well-developed networks are the subject of Chapter 7.

The numerical values of the critical exponents τ, σ, β, γ, ... and the functional form of the cutoff function $f(M/M^*)$ of gelation depend on the amount of overlap of the linking species. If the linking species have significant overlap, mean-field gelation theory provides a good description of the process with exponents $\tau = 5/2$ and $\sigma = 1/2$, and an exponential cutoff function $f(M/M^*) \sim \exp(-M/M^*)$ over a significant range of the relative extent of reaction. Sufficiently close to the gel point, *all* gelation transitions are believed to be described by the critical percolation model. The exponent

values and the cutoff function in critical percolation models depend on the dimension of space in which the linking process takes place. In three-dimensional critical percolation the exponents are $\tau \cong 2.18$ and $\sigma \cong 0.45$.

The precise point where critical percolation starts to apply is determined by the overlap parameter of the linking species. Long linear chains in a melt are strongly overlapping before any crosslinking occurs. Vulcanization of these linear chains creates branched structures with fractal dimension $\mathcal{D} = 4$, which makes the branched structures overlap each other less as they grow. Once the largest branched polymers are just at their overlap concentration, critical percolation begins to apply. In critical percolation, molecules of a given molar mass are just at overlap between themselves and with similar molar mass pieces of larger molecules. This condition is called hyperscaling and leads to a fractal dimension of $\mathcal{D} \cong 2.53$ in three-dimensional percolation.

In the polymerization of a melt of multifunctional monomers A_f with functionality f greater than two, the critical percolation model applies over the entire range of possible extents of reaction. However, such densely branched polymers are often not very useful because they are typically brittle, since the chain sections between branch points are not long enough to entangle. One interesting use of such materials is as electrophotographic toners. Electrophotography is the process by which copiers work. The toner is usually a polymer material that contains the appropriate dye for colour copiers or carbon black for black-and-white copiers. The image resolution in electrophotography is determined in part by how small the toner particles can be made. Hence, the brittle nature of densely branched gels near their gel point make them ideal toner materials, as they are easily broken down to a very small particle size.

Randomly branched polymers are of enormous importance for certain polymer processing operations, such as blow moulding and film blowing. The molar mass distribution of all randomly branched polymers is described by percolation models. For commercial randomly branched polymers, the critical percolation model applies only very close to the gel point. The branching chemistry used in commercial randomly branched polymers is usually stopped far short of the critical region. While critical percolation does not apply to these polymers, the mean-field percolation model does a superb job of describing the molar mass distribution of randomly branched commercial polymers.

Gelation processes, such as crosslinking linear chains or condensation of f-functional monomers A_f (where A reacts with A) with $f > 2$ are quite different from either linear condensation polymers or hyperbranched polymers. Linear condensation polymers (made from AB monomers, where A only reacts with B) and hyperbranched polymers (made from AB_{f-1} monomers, where A only reacts with B) have *both* their number-average and weight-average molar masses diverge as their reaction nears completion and they never make network polymers. The hyperbranching reaction makes the same structure of randomly branched polymers as gelation, but with a very different distribution of molar masses.

Problems

Section 6.1

6.1 Ergodicity refers to a system's ability to access all allowed states. Which of the following gels can access all possible states and are hence ergodic:

(i) weak physical gels;
(ii) strong physical gels;
(iii) condensation polymerized gels;
(iv) addition polymerized gels.

6.2 Prove that for any two-dimensional lattice that is constructed as a slice of a three-dimensional lattice, the percolation threshold is larger in two dimensions than in three dimensions.

6.3 Identify the class and dimension of percolation model that describes the following cases:

(i) addition polymerization in aqueous solution;
(ii) linear condensation polymerization at the air–water interface;
(iii) branched condensation polymerization at the air–water interface;
(iv) branched condensation polymerization in solution.

6.4 Calculate the number-average degree of polymerization N_n and weight-average degree of polymerization N_w for one-dimensional percolation with extent of reaction $p = 0.99$. What is the polydispersity index of the molecules at this extent of reaction?

6.5 In the process of developing a communication network, a start-up company CheepieCom decided to save money on cables and connected each new customer to the nearest existing one by a single cable.

(i) How many connecting cables did they run between N customers? What is the structure of the CheepieCom network?
(ii) What happens to this network if a storm breaks one cable? How can this network be made more robust against catastrophic failure?

6.6 Consider propagation of a forest fire in the presence of a strong wind.

(i) How would you modify the percolation model to take into account strong blowing in one direction.
(ii) Is the percolation threshold (critical probability of ignition of a neighbouring tree) the same, higher, or lower than in the absence of the wind?

Section 6.2

6.7 Prove that the number fraction distribution for hyperbranched polymers is properly normalized [i.e., show that Eq. (6.9) satisfies Eq. (6.12)].

6.8 Derive the following result for the z-average degree of polymerization of hyperbranched polymers assuming no intramolecular reactions:

$$N_z = \frac{[1-p^2(f-1)]^2 + 2p(f-1)(1-p)^2}{[1-p(f-1)]^2[1-p^2(f-1)]}. \tag{6.160}$$

Demonstrate that near complete reaction (for $p \to p_c$) the ratio N_z/N_w asymptotically approaches 3 for all functionalities f.

6.9 Calculate the radius of gyration for an ideal regular dendrimer of generation g with $n = f = 3$, where each generation has linear sections between branch points with one Kuhn monomer of length b. *Hint*: Use Kramers theorem.

6.10* Use Flory theory to determine the end-to-end distance of a linear strand that runs from the core to any end at generation g of the regular dendrimer in Problem 6.9 with excluded volume $v > 0$ (in good solvent).

Section 6.4

6.11 Calculate and plot sol and gel fractions for gelation of tetrafunctional monomers within mean-field theory, as functions of extent of reaction p.
Hint: Note that one of the solutions of Eq. (6.51) is $P_{sol} = 1$.

6.12 Demonstrate that the mean-field gelation prediction of the polydispersity index below the gel point is

$$\frac{N_w}{N_n} = \frac{(1+p)(1-fp/2)}{1-(f-1)p}. \tag{6.161}$$

How does this polydispersity index depend on functionality f at a given relative extent of reaction $\varepsilon = (p - p_c)/p_c$?

6.13 Draw all different possible structures of a trifunctional randomly branched 4-mer. Count and compare the number of unreacted groups in each 4-mer. Explain the significance of your results.

6.14 Evaluate the mean-field estimate of the gel point p_c for bond percolation on the following lattices:

(i) Honeycomb ($f = 3$).
(ii) Square ($f = 4$).
(iii) Triangular ($f = 6$).
(iv) Diamond ($f = 4$).
(v) Simple cubic ($f = 6$).
(vi) Compare your results with the values reported in Table 6.1. What is the origin of disagreement?
(vii) Compare your results with the values reported in Table 6.1 for lattices with the same functionalities but with different dimensions. Which dimensions ($d = 2$ or $d = 3$) are closer to your prediction? Explain why?

6.15* Demonstrate that the weight fraction w_{N_B,N_L} of randomly branched polymers of N_B f-functional and N_L bifunctional monomers ($N = N_B + N_L$) is

$$w_{N_B,N_L} = \left[\frac{(1-p)^2}{p} - (f-2)(1-p)\phi_B\right] N\left[p\phi_B(1-p)^{f-2}\right]^{N_B}[p(1-p)]^{N_L} \times \frac{[N_L + (f-1)N_B]!}{N_B![(f-2)N_L + 1]!},$$

where ϕ_B is the mole fraction of branched units.

The complexity of a molecule is defined as the number N_B of f-functional units in a molecule. The complexity distribution is therefore $\sum_{N_L} w_{N_B,N_L}$. Show that the complexity distribution is similar to the simple f-functional case in the absence of bifunctional units (derived in Section 6.4).

6.16* Calculate the distribution function for $\phi_{A_1}, \phi_{A_2}, \ldots, \phi_{A_i}$ moles of reactants with functionalities $f_1, f_2, \ldots, f_i$ of A groups which are allowed to react with $\phi_{B_1}, \phi_{B_2}, \ldots, \phi_{B_j}$ moles of reactants with functionalities $g_1, g_2, \ldots, g_j$ of B groups where condensation occurs only between A and B groups.

6.17 Calculate the weight-average degree of polymerization N_w above the gel point in the mean-field theory for functionality $f=3$ using the recurrence relation approach.

6.18 Calculate the number-average degree of polymerization N_n and the number of finite molecules per site n_{tot} above the gel point in the mean-field theory for functionality $f=3$.

6.19 Compare the asymptotic distribution function for mean-field gelation of tetrafunctional monomers [Eq. (6.77) with $f=4$] with the exact result [Eq. (6.63)] at the gel point. How large does N need to be for the two distributions to agree within 1% for $p=0.330$?

6.20 (i) Derive the general relation between the fraction of monomers that are crosslinked p and the gel fraction P_{gel} for random crosslinking of long linear chains of N monomers:

$$1 - P_{gel} = (1 - pP_{gel})^N. \tag{6.162}$$

Hint: $p(1 - P_{gel})$ is the probability that a given monomer is crosslinked but not part of the gel.

(ii) Show that in the large N limit, this equation becomes the relation known in the literature as the gel curve:

$$1 - P_{gel} \cong \exp(-NpP_{gel}). \tag{6.163}$$

Section 6.5

6.21 Power law distribution of molar masses.
Consider a polymer system (with either linear or branched polymers) with a power law number density of molecules:

$$n(N) \approx N^{-\tau}.$$

(i) For what values of the Fisher exponent τ is the number-average degree of polymerization finite for all extents of reaction?

(ii) For what values of τ is the polydispersity index of these polymers finite for all extents of reaction?

(iii) For what values of τ is the z-average degree of polymerization finite for all extents of reaction?

6.22 Size of randomly branched polymers.
Consider a gelation process stopped at relative extent of reaction

$$\varepsilon = \frac{p - p_c}{p_c} = -0.01.$$

(i) What is the characteristic degree of polymerization N^* at this extent of reaction, assuming that starting molecules were monomers ($N_0 = 1$)?

(ii) What is the ideal size of the characteristic randomly branched molecule, if the monomer size is $b = 3$ Å?

(iii) What is the size of the characteristic molecule in the polymerization reactor?

(iv) What is the size of the characteristic molecule in dilute solution in an athermal solvent?

Hint: Use Flory theory to estimate the swelling of a randomly branched polymer in an athermal solvent.

6.23 Ginzburg criterion

(i) Estimate the size of the critical zone ε_G for vulcanization of precursor chains with degree of polymerization $N_0 = 1000$.
(ii) What is the characteristic degree of polymerization N_G of the branched polymers at the crossover extent of reaction ε_G?
(iii) What is the size ξ of the characteristic branched polymer at ε_G if the monomer size is $b = 3$ Å?
(iv) What is the volume fraction of the characteristic branched polymer inside its pervaded volume at ε_G?
(v) What is the gel fraction at ε_G above gel point?
(vi) Compare the answers to (iv) and (v).

6.24 The number density of molecules in the mean-field theory for a general functionality is given by Eq. (6.63). Use Stirling's approximation to estimate this distribution near the gel point in the form

$$n(p, N) = N^{-\tau} f_{\pm}(N/N^*).$$

Show that $\tau = 5/2$, find N^* and evaluate the cutoff function $f_{\pm}(N/N^*)$ for a general functionality f.

6.25 What is the analogue of the scaling form of molar mass distribution

$$n(p, N) = N^{-\tau} f_{-}(N/N^*)$$

for one-dimensional percolation?

How do the number- and weight-average molar masses diverge as the extent of reaction approaches unity (complete reaction)?

6.26 Show that Eq. (6.99) is consistent with Eq. (6.53).

6.27 Consider random crosslinking of monodisperse primary molecules with degree of polymerization N_0. Let $\hat{p}$ be the number of crosslinking units per primary molecule. Show that the weight fraction of molecules containing N/N_0 primary molecules is

$$w_N(\hat{p}) = \frac{(\hat{p}N/N_0)^{N/N_0-1}}{(N/N_0)!} \exp(-\hat{p}N/N_0). \tag{6.164}$$

If the extent of reaction is defined as the number of bonds per monomer $p = \hat{p}/N_0$ show that the gel point corresponds to $p = 1/N_0$ or $(\hat{p} = 1)$.

6.28 Calculate the size of an ideal randomly branched polymer with precursor chains made of N_0 Kuhn monomers with Kuhn length $b = 5$ Å and total number $N = 10^4$ monomers. Estimate this size for

(i) $N_0 = 100$.
(ii) $N_0 = 10$.
(iii) Estimate the volume fraction of Kuhn monomers belonging to this molecule inside its pervaded volume for cases (i) and (ii). Explain your results.

6.29 State whether the following combinations of parameters are constants of order unity, or diverge, or vanish at the gel point for

(i) mean-field percolation,
(ii) critical percolation,

$$\frac{N_w}{N^*} \quad \frac{N_w^2}{N^*} \quad \frac{N_w}{P_{gel}N^*} \quad N_w P_{gel}.$$

Which combinations provide information about universality class and thereby can determine the Ginzburg extent of reaction ε_G?
Which combinations are independent of universality class and hence useful for checking consistency of measurements?

6.30 Consider the total number of monomers per site in a sol (the first moment of the number density distribution function):

$$\int Nn(p,N)\,\mathrm{d}N = \int N^{1-\tau}\hat{f}(z)\,\mathrm{d}N$$

(i) Show that for negative values of z

$$\int N^{1-\tau}[\hat{f}(z)-\hat{f}(0)]\,\mathrm{d}N = 0.$$

(ii) Use the relation between the scaling variable z and N to show that

$$\int |z|^{[(2-\tau)/\sigma]-1}[\hat{f}(z)-\hat{f}(0)]\,\mathrm{d}z = 0.$$

(iii) Can $\hat{f}(z)$ be a monotonic function for negative values of z? What is the shape of the simplest cutoff function that satisfies this equation.

6.31 Plot the cutoff function $N^{\tau}n(p,N)$ as a function of N/N^* for mean-field gelation using the exact expression Eq. (6.63) for $f=3$ and extents of reaction $p=0.45$, 0.49, and 0.499. What happens with the maximum of the cutoff function in mean field as $p \to p_c$?

6.32 Calculate the prefactors for critical percolation predictions of gel fraction, correlation length, and characteristic degree of polymerization for crosslinking short chains with degree of polymerization N_0. *Hint*: These predictions are required to match the mean-field predictions at the Ginzburg point.

6.33 Use hyperscaling to derive the following relation for the correlation length exponent ν in terms of β, γ and the dimension of space d:

$$\nu = \frac{2\beta+\gamma}{d}. \tag{6.164}$$

6.34 Use hyperscaling and the Flory–de Gennes calculation of fractal dimension to derive the following approximate relation for the Fisher exponent τ in any space dimension and compare with the results in Table 6.4 for $d=2,3,4,5$ and 6:

$$\tau = \frac{3d+2}{d+2}. \tag{6.165}$$

6.35 Derive equations for the exponents τ and σ in terms of the exponents β and γ.

6.36 What is the largest possible volume fraction $b^3g(r)$ of a randomly branched polymer inside its own pervaded volume in the vulcanization of precursor N_0-mers below the gel point?
Hint: Use Eq. (6.145).

6.37 What distinguishes a hyperbranched polymer at complete reaction from a gel formed by random branching?

6.38 Compare random crosslinking of linear precursor N_0-mers (with $f \approx N_0$) and end-linking of linear precursor N_0-mers with tetrafunctional crosslinkers.

(i) What is the qualitative difference between gel points of these two gelation processes?

(ii) How different are the resulting networks at the completion of all possible reactions?
(iii) Do they have Ginzburg zones of similar size $\varepsilon_G \approx N_0^{-1/3}$? Explain your answer.

6.39* How can symmetric amplitude ratios below and above the gel point in the mean-field zone outside the critical gelation regime $|\varepsilon| \gg \varepsilon_G$ match with asymmetric amplitude ratios in the critical region? Here, $\varepsilon = (p - p_c)/p_c$ is the relative extent of the reaction and ε_G is its value at the Ginzburg point (the boundary of the critical regime). Consider, for example, the weight-average number of monomers in the branched molecules:

$$N_w \approx A\left|\frac{\varepsilon}{\varepsilon_G}\right|^{-\gamma}.$$

The amplitude A is the same below and above the gel point in the mean-field regime $|\varepsilon| \gg |\varepsilon_G|$, while the values below and above gel point are quite different in the critical gelation regime. Propose a way of matching these differences at the Ginzburg point ε_G.

Section 6.6

6.40 Equations (6.148) and (6.149) provide a way of obtaining weight- and z-average molar masses from size exclusion chromatography. Are they approximate or exact methods? If the concentration c_i and weight-average molar mass M_{wi} of each elution volume are accurately measured, would the correct M_w and M_z of the whole sample be known?

Bibliography

Burchard, W. Solution properties of branched macromolecules, *Adv. Polym. Sci.* **143**, 113 (1999).
Flory, P. J. *Principles of Polymer Chemistry* (Cornell University Press, Ithaca, New York, 1953).
de Gennes, P. G. *Scaling Concepts in Polymer Physics* (Cornell University, Ithaca, New York, 1979).
Hawker, C. J. Dendritic and hyperbranched macromolecules: precisely controlled macromolecular architectures, *Adv. Polym. Sci.* **147**, 113 (1999).
Stauffer, D. and Aharony, A. *Introduction to Percolation Theory*, 2nd edn (Taylor and Francis, 1992).
Stauffer, D., Coniglio, A., and Adam, M. Gelation and critical phenomena, *Adv. Polym. Sci.* **44**, 103 (1982).

Networks and gels

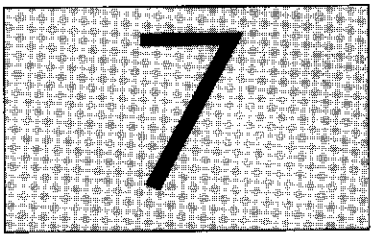

When the crosslinking reactions of Chapter 6 are driven far beyond the gel point, nearly all species are attached to the gel in a single macroscopic network polymer. Such networks, with either chemical or strong physical bonds, are important soft solids. If the glass transition and melting temperatures are below room temperature, the material is a **rubber**. Rubbers are an important class of materials with many practical uses. Common examples are rubber bands, gaskets, adhesives, and automobile tires. Rubber bands can be stretched enormous amounts without breaking or even losing their elasticity. In this chapter, the physics that allow for such marvellous properties will be considered in detail. The entropic nature of elasticity in rubbers is the origin of their remarkable mechanical properties.

7.1 Thermodynamics of rubbers

The first law of thermodynamics states that the change in internal energy of a system, such as a polymeric network, is the sum of all the energy changes: heat added to the system $T\,\mathrm{d}S$, work done to change the network volume $-p\,\mathrm{d}V$ and work done upon network deformation $f\,\mathrm{d}L$:

$$\mathrm{d}U = T\,\mathrm{d}S - p\,\mathrm{d}V + f\,\mathrm{d}L. \tag{7.1}$$

The differential $\mathrm{d}U$ represents the change in internal energy that arises if there is an entropy change $\mathrm{d}S$, a volume change $\mathrm{d}V$, or sample length change $\mathrm{d}L$. The internal energy U is a thermodynamic state function of variables S, V, and L. The Helmholtz free energy F is defined as internal energy minus the product of temperature and entropy:

$$F = U - TS. \tag{7.2}$$

The change in the Helmholtz free energy is written in differential form:

$$\begin{aligned}\mathrm{d}F &= \mathrm{d}U - \mathrm{d}(TS) = \mathrm{d}U - T\,\mathrm{d}S - S\,\mathrm{d}T \\ &= -S\,\mathrm{d}T - p\,\mathrm{d}V + f\,\mathrm{d}L.\end{aligned} \tag{7.3}$$

The Helmholtz free energy is a thermodynamic state function of variables T, V, and L. The change in the Helmholtz free energy can be written as a

complete differential:

$$dF = \left(\frac{\partial F}{\partial T}\right)_{V,L} dT + \left(\frac{\partial F}{\partial V}\right)_{T,L} dV + \left(\frac{\partial F}{\partial L}\right)_{T,V} dL. \tag{7.4}$$

Comparing Eqs (7.3) and (7.4), we identify the partial derivatives of the Helmholtz free energy:

$$\left(\frac{\partial F}{\partial T}\right)_{V,L} = -S, \tag{7.5}$$

$$\left(\frac{\partial F}{\partial V}\right)_{T,L} = -p, \tag{7.6}$$

$$\left(\frac{\partial F}{\partial L}\right)_{T,V} = f. \tag{7.7}$$

A second derivative of the Helmholtz free energy does not depend on the order of differentiation:

$$\frac{\partial^2 F}{\partial T \partial L} = \frac{\partial^2 F}{\partial L \partial T}. \tag{7.8}$$

Using Eqs (7.5) and (7.7), Eq. (7.8) can be rewritten as one of the **Maxwell relations**:

$$-\left(\frac{\partial S}{\partial L}\right)_{T,V} = \left(\frac{\partial f}{\partial T}\right)_{V,L}. \tag{7.9}$$

The force f, applied to deform a network, consists of two contributions:

$$f = \left(\frac{\partial F}{\partial L}\right)_{T,V} = \left[\frac{\partial (U - TS)}{\partial L}\right]_{T,V} = \left(\frac{\partial U}{\partial L}\right)_{T,V} - T\left(\frac{\partial S}{\partial L}\right)_{T,V}. \tag{7.10}$$

The first term describes how the internal energy changes with the sample length and the second contribution is the product of absolute temperature and the rate of change of entropy with sample length. The second term can be rewritten using the Maxwell relation above [Eq. (7.9)]:

$$f = \left(\frac{\partial U}{\partial L}\right)_{T,V} + T\left(\frac{\partial f}{\partial T}\right)_{V,L} = f_E + f_S. \tag{7.11}$$

The two contributions to the force are an energetic term that is the change of internal energy with sample length

$$f_E = \left(\frac{\partial U}{\partial L}\right)_{T,V}, \tag{7.12}$$

and an entropic term that is the product of temperature and the change of entropy with sample length:

$$f_S = T\left(\frac{\partial f}{\partial T}\right)_{V,L} = -T\left(\frac{\partial S}{\partial L}\right)_{T,V}. \tag{7.13}$$

In typical crystalline solids, such as metals, the energetic contribution dominates the force because the internal energy increases when the crystalline lattice spacings are distorted from their equilibrium positions. In rubbers, the entropic contribution to the force is more important than the energetic one. In 'ideal networks' there is no energetic contribution to elasticity, so $f_E = 0$.

The dominance of the entropic part of Eq. (7.11) bestows a peculiar temperature dependence to the force at constant extension. While crystalline solids have the force decrease weakly with increasing temperature, rubbers show the opposite behaviour. The network strands lose conformational entropy when stretched (see Section 2.6) making $\partial S/\partial L < 0$ and the force *increases* with increasing temperature [Eq. (7.13)].

7.1.1 Flory construction

A simple way to separate energetic from entropic contributions to the elastic force was developed by Flory. Consider a typical temperature dependence of a retraction force f for a network of constant volume V at constant elongation L, as shown in Fig. 7.1. The slope of the curve at temperature T is

$$\text{slope} = \left(\frac{\partial f}{\partial T}\right)_{V,L}, \tag{7.14}$$

and the change in the ordinate from the point on the curve to the intercept of the tangent with the f axis is the entropic contribution to the force [Eq. (7.13)]. Therefore, the value at the intercept of the tangent to the curve with the f axis is the energetic contribution to the force [Eq. (7.12)]. Figure 7.1 is schematic, but shows the typical relative importance of the energetic f_E and entropic f_S parts of the force in a stretched polymer network. Note that the entropic component f_S accounts for more than 90% of total force in the rubbery state. **Rubber elasticity** has primarily *entropic* origins. In the rest of this chapter, we ignore the energetic contribution and concentrate exclusively on the entropic one.

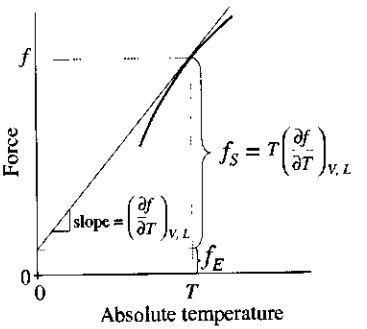

Fig. 7.1
A schematic representation of the Flory construction for a polymer network,

7.2 Unentangled rubber elasticity

7.2.1 Affine network model

Polymer networks are unique in their ability to reversibly deform to several times their size. The enormous deformability of networks arises from the entropic elasticity of the polymer chains that make up the network

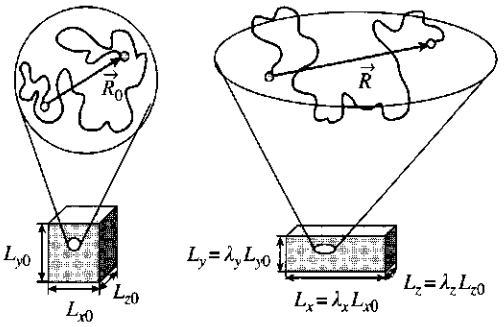

Fig. 7.2
Affine deformation requires each network strand to adopt the relative deformation of the macroscopic network.

(the network strands). The simplest model that captures this idea of rubber elasticity is the **affine network model** originally proposed by Kuhn. The main assumption of the affine network model is an **affine deformation**: the relative deformation of each network strand is the same as the macroscopic relative deformation imposed on the whole network.

Consider a rubber network with undeformed dimensions L_{x0}, L_{y0}, and L_{z0} (Fig. 7.2). If the network experiences relative deformations in the x, y, and z directions by the factors λ_x, λ_y, and λ_z, then the dimensions of the deformed network are

$$L_x = \lambda_x L_{x0}, \quad L_y = \lambda_y L_{y0} \quad \text{and} \quad L_z = \lambda_z L_{z0}. \tag{7.15}$$

Assume that each network strand has N monomers. One network strand, shown in Fig. 7.2, has end-to-end vector $\vec{R}_0$ with projections along the x, y, and z directions of R_{x0}, R_{y0}, and R_{z0} in the undeformed state. In the affine network model, the positions of the junction points (the ends of the strands) are always fixed at particular points in space by the deformation and not allowed to fluctuate. For affine deformation, the end-to-end vector of the same chain in the deformed state is $\vec{R}$ (see Fig. 7.2) with projections along the x, y, and z directions of

$$R_x = \lambda_x R_{x0}, \quad R_y = \lambda_y R_{y0} \quad \text{and} \quad R_z = \lambda_z R_{z0}. \tag{7.16}$$

Recall the entropy of a chain of N Kuhn monomers of length b with end-to-end vector $\vec{R}$ [Eq. (2.92)]:

$$S(N, \vec{R}) = -\frac{3}{2}k\frac{\vec{R}^2}{Nb^2} + S(N, 0) = -\frac{3}{2}k\frac{R_x^2 + R_y^2 + R_z^2}{Nb^2} + S(N, 0). \tag{7.17}$$

The entropy change of this chain upon deformation is the difference in entropy of the final and initial states:

$$\begin{aligned} S(N, \vec{R}) - S(N, \vec{R}_0) &= -\frac{3}{2}k\frac{R_x^2 + R_y^2 + R_z^2}{Nb^2} + \frac{3}{2}k\frac{R_{x0}^2 + R_{y0}^2 + R_{z0}^2}{Nb^2} \\ &= -\frac{3}{2}k\frac{(\lambda_x^2 - 1)R_{x0}^2 + (\lambda_y^2 - 1)R_{y0}^2 + (\lambda_z^2 - 1)R_{z0}^2}{Nb^2}. \end{aligned} \tag{7.18}$$

The entropy change of the whole network is the sum of all the entropy changes of the network's n strands:

$$\Delta S_{\text{net}} = -\frac{3}{2}\frac{k}{Nb^2}\left[(\lambda_x^2 - 1)\sum_{i=1}^{n}(R_{x0})_i^2 + (\lambda_y^2 - 1)\sum_{i=1}^{n}(R_{y0})_i^2 + (\lambda_z^2 - 1)\sum_{i=1}^{n}(R_{z0})_i^2\right]. \tag{7.19}$$

If the network is formed by crosslinking chains in their ideal state (in a melt) the components of the mean-square end-to-end distance in the undeformed state are given by Eq. (2.83):

$$\langle R_{x0}^2\rangle = \frac{1}{n}\sum_{i=1}^{n}(R_{x0})_i^2 = \frac{Nb^2}{3} = \langle R_{y0}^2\rangle = \langle R_{z0}^2\rangle. \tag{7.20}$$

Therefore, the sums of the squares of the components of the end-to-end vectors of all n strands can be written quite simply:

$$\sum_{i=1}^{n}(R_{x0})_i^2 = \sum_{i=1}^{n}(R_{y0})_i^2 = \sum_{i=1}^{n}(R_{z0})_i^2 = \frac{n}{3}Nb^2. \tag{7.21}$$

The entropy change upon deformation of the network is the central feature of rubber elasticity:

$$\begin{aligned}\Delta S_{\text{net}} &= -\frac{3}{2}k\frac{(\lambda_x^2 - 1)(n/3)Nb^2 + (\lambda_y^2 - 1)(n/3)Nb^2 + (\lambda_z^2 - 1)(n/3)Nb^2}{Nb^2} \\ &= -\frac{nk}{2}(\lambda_x^2 + \lambda_y^2 + \lambda_z^2 - 3).\end{aligned} \tag{7.22}$$

The main contribution to the free energy of the network comes from the changes in entropy, as discussed in Section 7.1.1. Ignoring any enthalpic contribution, the free energy required to deform a network is minus temperature times the entropy change:

$$\Delta F_{\text{net}} = -T\Delta S_{\text{net}} = \frac{nkT}{2}(\lambda_x^2 + \lambda_y^2 + \lambda_z^2 - 3). \tag{7.23}$$

Dry networks are typically incompressible, which means that their volume does not change appreciably when they are deformed:

$$V = L_{x0}L_{y0}L_{z0} = L_xL_yL_z = \lambda_xL_{x0}\lambda_yL_{y0}\lambda_zL_{z0} = \lambda_x\lambda_y\lambda_zV. \tag{7.24}$$

If the volume of the network remains constant, the product of the deformation factors is unity:

$$\lambda_x\lambda_y\lambda_z = 1. \tag{7.25}$$

In practice, the volume change that occurs when a network is deformed is measurable, but extremely small (see Problem 7.7).

7.2.1.1 Uniaxial deformation

If the network is either stretched or compressed in a single direction (along the x axis), the deformation is termed uniaxial. For uniaxial deformations at constant volume, the other two dimensions of the network adjust to keep the volume constant:

$$\lambda_x = \lambda \quad \lambda_y = \lambda_z = \frac{1}{\sqrt{\lambda}}. \tag{7.26}$$

The free energy change for a uniaxial deformation at constant volume is obtained by simply substituting the deformation factors [Eq. (7.26)] into Eq. (7.23):

$$\Delta F_{\text{net}} = \frac{nkT}{2}\left(\lambda^2 + \frac{2}{\lambda} - 3\right) \quad \text{for uniaxial deformation.} \tag{7.27}$$

The force required to deform a network is the rate of change of its free energy with respect to its size along the axis of deformation. For example, the x component of the force is the derivative of the free energy with respect to length along the x axis [see Eq. (7.7)]:

$$f_x = \frac{\partial \Delta F_{\text{net}}}{\partial L_x} = \frac{\partial \Delta F_{\text{net}}}{\partial(\lambda L_{x0})} = \frac{1}{L_{x0}}\frac{\partial \Delta F_{\text{net}}}{\partial \lambda}$$
$$= \frac{nkT}{L_{x0}}\left(\lambda - \frac{1}{\lambda^2}\right) \quad \text{for uniaxial deformation.} \tag{7.28}$$

If the cross-sectional area L_yL_z of the macroscopic network is doubled, then twice as large a force is required to obtain the same deformation. This leads naturally to a definition of **stress** as the ratio of force and cross-sectional area. Both the force and the cross-sectional area have direction and magnitude (the direction of the cross-sectional area being described by the unit vector normal to its surface), making the stress a tensor. The ij-component of the **stress tensor** is the force applied in the i direction per unit cross-sectional area of a network perpendicular to the j axis. For example, the xx-component σ_{xx} is the force applied in the x direction f_x divided by the area L_yL_z perpendicular to the x axis:

$$\sigma_{xx} = \frac{f_x}{L_yL_z} = \frac{nkT}{L_{x0}L_yL_z}\left(\lambda - \frac{1}{\lambda^2}\right) = \frac{nkT}{L_{x0}L_{y0}L_{z0}}\lambda\left(\lambda - \frac{1}{\lambda^2}\right)$$
$$= \frac{nkT}{V}\left(\lambda^2 - \frac{1}{\lambda}\right) \equiv \sigma_{\text{true}} \quad \text{for uniaxial deformation in } x. \tag{7.29}$$

This is the **true stress** in the network and it is therefore denoted by σ_{true}. Since it is often not easy to measure the cross-sectional area of the deformed network, an engineering stress is also defined. In the **engineering stress** the original cross-sectional area $L_{y0}L_{z0}$ is used instead of the

deformed cross-sectional area $L_y L_z$:

$$\sigma_{\text{eng}} = \frac{f_x}{L_{y0} L_{z0}} = \frac{nkT}{L_{x0} L_{y0} L_{z0}} \left(\lambda - \frac{1}{\lambda^2}\right) = \frac{nkT}{V} \left(\lambda - \frac{1}{\lambda^2}\right) = \frac{\sigma_{\text{true}}}{\lambda}. \quad (7.30)$$

The coefficient relating the stress and the deformation is the shear modulus G, as will be shown in Problem 7.43:

$$G = \frac{nkT}{V} = \nu kT = \frac{\rho \mathcal{R} T}{M_s}. \quad (7.31)$$

The number of network strands per unit volume (number density of strands) is $\nu = n/V$. In the last equality, ρ is the network density (mass per unit volume), M_s is the number-average molar mass of a network strand, and $\mathcal{R}$ is the gas constant. The network modulus increases with temperature because its origin is entropic, analogous to the pressure of an ideal gas $p = nkT/V$. The modulus also increases linearly with the number density of network strands $\nu = n/V = \rho \mathcal{N}_{\text{Av}}/M_s$. Equation (7.31) states that the modulus of any network polymer is kT per strand.

The affine predictions for both true and engineering stresses in uniaxial deformation at constant network volume can be rewritten using the shear modulus:

$$\sigma_{\text{true}} = G\left(\lambda^2 - \frac{1}{\lambda}\right), \quad (7.32)$$

$$\sigma_{\text{eng}} = G\left(\lambda - \frac{1}{\lambda^2}\right). \quad (7.33)$$

By writing these equations in terms of the shear modulus, the form of the stress–elongation relation becomes quite general. Many other network elasticity models also predict stress–elongation relations of this form, with different predictions for the shear modulus. For this reason, we refer to Eqs (7.32) and (7.33) as the *classical* stress–elongation forms. As demonstrated in Fig. 7.3, this classical form describes the small deformation uniaxial data on polymer networks quite well. The main physics behind such classical models is the *entropic elasticity of polymer chains*.

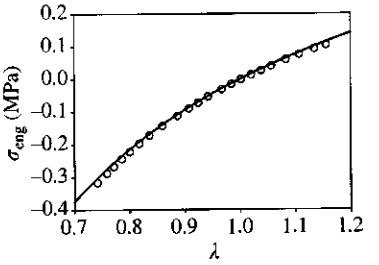

Fig. 7.3
Engineering stress in uniaxial compression ($\lambda < 1$ and $\sigma_{\text{eng}} < 0$) and tension ($\lambda > 1$ and $\sigma_{\text{eng}} > 0$) for a poly(dimethyl siloxane) network prepared by end-linking chains with $M_n = 18\,400\ \text{g mol}^{-1}$. The curve is the classical prediction of Eq. (7.33), with $G = 0.28$ MPa. Data are from W. Oppermann and N. Rennar, *Prog. Colloid Polym. Sci.* **75**, 49 (1987).

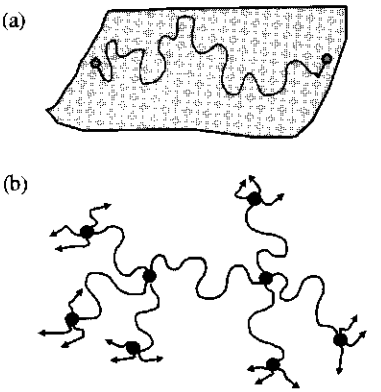

Fig. 7.4
(a) In the affine network model, the ends of each network strand are pinned to an elastic background. (b) In the phantom network model, the ends of network strands are joined at crosslink junctions that can fluctuate. Circles are crosslink junctions and arrows denote attachments to the rest of the macroscopic network.

7.2.2 Phantom network model

The main assumption of the affine network model is that the ends of network strands (the crosslink junctions) are fixed in space and are displaced affinely with the whole network, as if they were permanently attached to some elastic background [see Fig. 7.4(a)]. In real networks, the ends of network strands are attached to other strands at crosslinks [see Fig. 7.4(b)]. These crosslinks are not fixed in space—they can fluctuate around their average positions. These fluctuations lead to a net lowering of the free energy of the system by reducing the cumulative stretching of the network

strands. The simplest model that incorporates these fluctuations is called the **phantom network model**. In a phantom network, the strands are ideal chains with ends joined at crosslinks. The ends of the strands at the surface of the network are attached to the elastic non-fluctuating boundary of the network. This attachment fixes the volume of the phantom network and prevents its collapse that would have been inevitable because such simple models ignore excluded volume interactions between monomers.

Recall from Problem 2.38 that the fluctuations of a single monomer in an ideal chain with fixed ends are identical to the fluctuations of an end monomer of a single **effective chain** of K monomers. For the particular case of the center monomer of an ideal chain with $2N$ monomers, the effective chain has $K = N/2$ monomers. Hence, the constraining effect of the two strands of N monomers is identical to the constraining effect of a single effective chain of $K = N/2$ monomers. More generally, if there are f chains of N monomers connected to a given monomer (such as in the case of the branch point of an f-arm star polymer) the fluctuations of this branch point are the same as the fluctuations of an effective chain of $K = N/f$ monomers.

The fluctuations of junction points in a network are quite similar to those of the branch point of an f-arm star polymer. In order to calculate the amplitude of these fluctuations, start with $f-1$ strands that are attached at one end to the surface of the network and joined at the other end by a junction point connecting them to a single strand [see the left-most part of Fig. 7.5(a)]. The strands attached to the elastic non-fluctuating network surface are called seniority-zero strands. Each of these $f-1$ seniority-zero strands are attached to a single seniority-one strand by a f-functional crosslink [see the left-most part of Fig. 7.5(a)]. The seniority of a particular strand is defined by the number of other network strands along the shortest path between it and the network surface. The $f-1$ seniority-zero strands

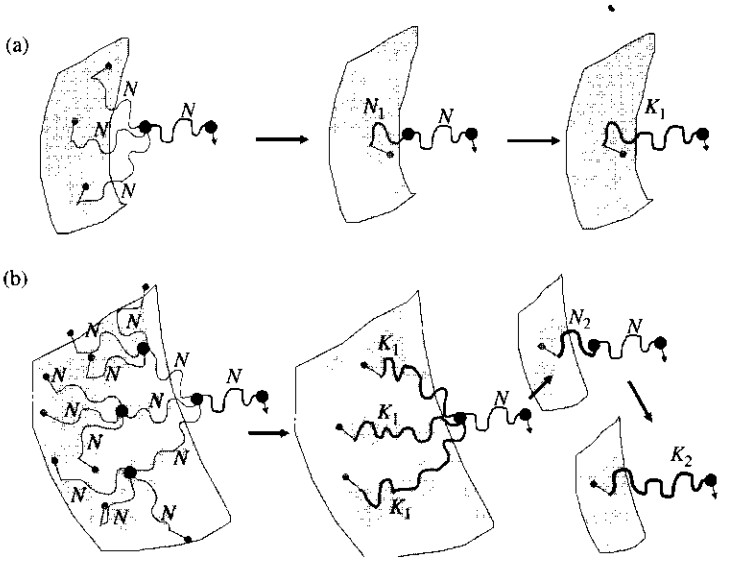

Fig. 7.5
Recurrence relation diagrams for the effective chains of phantom networks, shown here for tetrafunctional networks ($f = 4$). In each sketch the leftmost ends of the effective chains are pinned to the macroscopic boundary of the network.

are connected in parallel and can be replaced by a single effective chain containing N_1 monomers with the same constraining effect as the $f-1$ original chains together [see Fig. 7.5(a)]:

$$N_1 = \frac{N}{f-1}. \tag{7.34}$$

This single effective chain containing N_1 monomers is connected in series with a single seniority-one N-mer and together with it can be described by an effective chain of $K_1 = N + N_1$ monomers. In this way, Fig. 7.5(a) sketches how $f-1$ zero-seniority strands together with one seniority-one network strand can be replaced by an effective strand with K_1 monomers:

$$K_1 = N + N_1 = N + \frac{N}{f-1} = N\left(1 + \frac{1}{f-1}\right). \tag{7.35}$$

As can be seen from the left-most part of Fig. 7.5(b), $f-1$ of the seniority-one network strands are connected at a single crosslink junction to one seniority-two strand. Each of these seniority-one strands together with the corresponding $f-1$ seniority-zero strands can be replaced by one effective chain with K_1 monomers [central part of Fig. 7.5(b)]. A parallel combination of $f-1$ of these effective chains can be replaced by one effective chain with N_2 monomers:

$$N_2 = \frac{K_1}{f-1} = \frac{N}{f-1}\left(1 + \frac{1}{f-1}\right). \tag{7.36}$$

Combining this effective chain with the real seniority-two chain connected to it in series, gives an effective chain representing the combined effect of a tree of strands from seniority-zero through seniority-two [Fig. 7.5(b)]:

$$K_2 = N + N_2 = N\left(1 + \frac{1}{f-1} + \frac{1}{(f-1)^2}\right). \tag{7.37}$$

Continuing this procedure gives a geometric series for the number of monomers in an effective chain representing a combined effect of a tree of strands from seniority-zero through an arbitrarily large seniority. This series rapidly converges and each junction point in the bulk of a phantom network can be thought of as connected to the elastic non-fluctuating surface of the network through f effective chains with K monomers in each.

$$\begin{aligned} K &= N\left(1 + \frac{1}{f-1} + \frac{1}{(f-1)^2} + \frac{1}{(f-1)^3} + \cdots\right) \\ &= \frac{N}{1 - 1/(f-1)} = \frac{f-1}{f-2}N. \end{aligned} \tag{7.38}$$

This means that each of the original $f-1$ chains, connecting any network strand to the macroscopic network through a very long tree-like

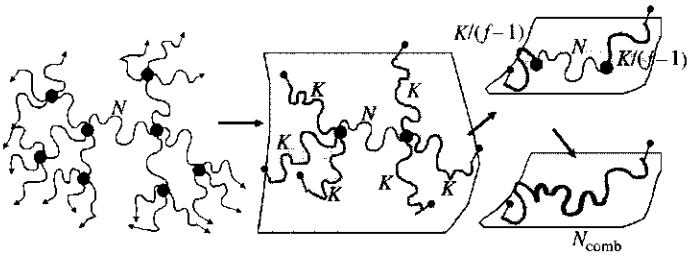

Fig. 7.6
The combined chain of a phantom network.

sequence of junction points, can be replaced by an effective chain with K monomers. That effective chain connects one end of each network strand to the elastic background. There are $f-1$ of these effective chains at each end of every network strand and they can be replaced by another effective chain with

$$\frac{K}{f-1} = \frac{N}{f-2} \tag{7.39}$$

monomers (see Fig. 7.6). Every network strand has one of these effective chains at each of its ends. Effective chains represent the way elasticity is transmitted from macroscopic scales down to individual chains. The network strand with N monomers together with the two effective chains with $N/(f-2)$ monomers each, can be considered as one **combined chain** with

$$N_{\text{comb}} = N + 2\frac{N}{f-2} = \frac{f}{f-2}N \tag{7.40}$$

monomers (Fig. 7.6). The ends of this combined chain are not fluctuating and can be assumed to be attached to an elastic non-fluctuating background just as the ends of the network strand in the affine network model. Thus, a phantom network model with fluctuating junction points is equivalent to an affine network model with a combined chain containing N_{comb} monomers.

The shear modulus of the phantom network is obtained from the modulus of the affine network [Eq. (7.31)] by replacing N with $Nf/(f-2)$:

$$G = \nu kT\frac{f-2}{f} = \frac{\rho \mathcal{R}T}{M_s}\left(1-\frac{2}{f}\right). \tag{7.41}$$

For any functionality f, the phantom network modulus is lower than the affine network modulus [Eq. (7.31)] because allowing the crosslinks to fluctuate in space makes the network softer. The phantom network has the same number density of strands as the affine network but only the fraction $(f-2)/f$ of the combined chain is the real strand [Eq. (7.40)] and only this fraction supports stress. The phantom network modulus approaches the affine prediction in the limit of high functionality of crosslinks. Crosslinks in phantom networks with high functionality f do not fluctuate much and are almost fixed in space as in the affine network model. Networks typically

have functionalities of 3 or 4. For $f = 3$, the phantom prediction is one third of the affine network modulus and for $f = 4$, the phantom modulus is half of the affine prediction.

These predictions need to be modified because real networks have defects. As shown in Fig. 7.7, some of the network strands are only attached to the network at one end. These dangling ends cannot bear stress and hence do not contribute to the modulus. Similarly, other structures in the network (such as dangling loops) are also not elastically effective. The phantom network prediction can be recast in terms of the number density of elastically effective strands ν and the number density of elastically effective crosslinks μ. For a perfect network without defects, the phantom network modulus is proportional to the difference of the number densities of network strands ν and crosslinks $\mu = 2\nu/f$, since there are $f/2$ network strands per crosslink:

$$G = kT(\nu - \mu). \tag{7.42}$$

This equation applies to networks with defects as well, and hence is more general than Eq. (7.41), but care must be taken to only include elastically effective strands and crosslinks. Elastically effective strands are the ones that deform and store elastic energy upon network deformation. Elastically effective crosslinks are those that connect at least two elastically effective strands.

Experimental estimates of ν and μ usually must rely on a model for the crosslinking chemistry, making quantitative tests of the phantom model difficult. Network defects preclude the use of Eqs (7.31) and (7.41), written in terms of the molar mass of a network strand M_s. Indeed, since M_s is not known for real networks and the affine and phantom models predict the same classical form of the stress–elongation curve [Eqs (7.32) and (7.33)] there is no practical means of determining which (if either) model is correct for small deformations of unentangled networks. For these reasons, we henceforth describe the modulus of all classical models G_x as a network of strands with apparent molar mass M_x:

$$G_x = \frac{\rho \mathcal{R} T}{M_x}. \tag{7.43}$$

For the affine network model, M_x is the actual strand molar mass ($M_x = M_s$) whereas the phantom network model requires a longer combined strand length $M_x = fM_s/(f-2)$ [Eq. (7.40)].

Fig. 7.7
Defects in a randomly crosslinked network are dangling ends and loops, denoted by thin lines. Circles are crosslink junctions and arrows denote attachments to the macroscopic network.

7.2.3 Finite extensibility

Both the affine and phantom network models predict the same (classical) dependence of stress on deformation [Eqs (7.32) and (7.33)]. Detailed quantitative comparison of the classical form with experiments indicates two major disagreements (see Fig. 7.8). Experiments demonstrate softening at intermediate deformations and hardening at higher deformations. In

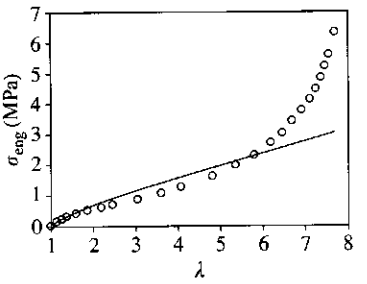

Fig. 7.8
Engineering stress in tension for a crosslinked rubber (data from L. R. G. Treloar, *The Physics of Rubber Elasticity*, 3rd edition, Clarendon Press, Oxford, 1975). The solid curve is the classical form [Eq. (7.33)] fit to the small deformation data.

order to understand the origins of these disagreements, the assumptions made in the classical theories must be re-examined. Here the strain hardening is discussed and in Section 7.3.3 the softening at intermediate deformations will be treated.

Strain hardening at high deformations λ can be explained by the non-Gaussian statistics of strongly deformed chains. Recall that the Gaussian approximation for a freely jointed chain model is valid for end-to-end distances much shorter than that for a fully stretched state $R \ll R_{max} = bN$. In Section 2.6.2, the Langevin functional dependence of normalized end-to-end distance R/Nb on the normalized force $fb/(kT)$ for a freely jointed chain [Eq. (2.112)] was derived:

$$\frac{R}{Nb} = \mathcal{L}\left(\frac{fb}{kT}\right) = \coth\left(\frac{fb}{kT}\right) - \frac{kT}{fb}. \tag{7.44}$$

The force f required to stretch a single chain to an end-to-end distance R can be expressed through the inverse Langevin function:

$$f = \frac{kT}{b}\mathcal{L}^{-1}\left(\frac{R}{Nb}\right). \tag{7.45}$$

This dependence of the force f on chain elongation R deviates from the Gaussian approximation (Hooke's law) at large elongations, as shown in Fig. 2.15. Owing to the finite extensibility of chains, the force diverges at the maximum end-to-end distance $R_{max} = bN$ [Eq. (2.116)]. A different relation with an even stronger divergence [Eq. (2.117)] has been used for the worm-like chain model.

Finite chain extensibility is the major reason for strain hardening at high elongations (Fig. 7.8). Another source of hardening in some networks is stress-induced crystallization. For example, vulcanized natural rubber (*cis*-polyisoprene) does not crystallize in the unstretched state at room temperature, but crystallizes rapidly when stretched by a factor of 3 or more. The extent of crystallization increases as the network is stretched more. The amorphous state is fully recovered when the stress is removed. Since the crystals invariably have larger modulus than the surrounding amorphous network, the effective modulus increases with crystallization, which makes the stress increase more rapidly with elongation.

7.3 Entangled rubber elasticity

7.3.1 Chain entanglements and the Edwards tube model

In the 1940s, it was recognized that the classical predictions of network modulus were bounded. A real network could certainly not be expected to have lower modulus than the phantom prediction, since it is based on unrestricted fluctuations of ideal strands that are allowed to pass through each other. At the other extreme, the classical models have no means to attain a higher modulus than the affine prediction, based on junctions that

are not allowed to fluctuate at all. However, the modulus of many real networks is considerably larger than the predictions of either classical model!

In both the affine and phantom network models, chains are only aware that they are strands of a network because their ends are constrained by crosslinks. Strand ends are either fixed in space, as in the affine network model, or allowed to fluctuate by a certain amplitude around some fixed position in space, as in the phantom network model. Monomers other than chain ends do not 'feel' any constraining potential in these simple network models.

In real networks made of long linear polymers, network chains impose topological constraints on each other because they cannot cross (see Fig. 7.9). The importance of these topological constraints, called **entanglements**, in polymer networks was discussed by Treloar as early as 1940. Since then a great many models of *entanglement effects* in polymers have been proposed. Indeed, the focus of Chapter 9 is the consequences of entanglement in polymer liquids. However, a clearer picture of what an entanglement really is remains elusive and the sketch in Fig. 7.9 is a very crude representation of an entanglement[1] between two chains.

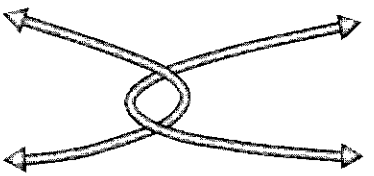

Fig. 7.9
The fact that two chains cannot pass through one another creates topological interactions known as entanglements that raise the network modulus.

Despite this rather vague notion of individual entanglements, Edwards showed that the essence of entanglements can be treated using a tube model. The collective effect of all surrounding chains on a given strand is represented in the Edwards tube model by a quadratic constraining potential acting on every monomer of each network strand. The minima of these constraining potentials lie along the dashed line of Fig. 7.10, called the **primitive path**. Every network strand is effectively confined by constraining potentials to a tube-like region with the primitive path at its centre (see Fig. 7.10).

Each monomer is constrained to stay fairly close to the primitive path, but fluctuations driven by the thermal energy kT are allowed. Strand excursions in the quadratic potential are not likely to have free energies much more than kT above the minimum. Strand excursions that have free energy kT above the minimum at the primitive path define the width of the **confining tube**, called the **tube diameter** a (Fig. 7.10). In the classical affine and phantom network models, the amplitude of the fluctuations of a typical network monomer, that is not adjacent to the crosslinks, is of the order of the unperturbed strand size. In entangled polymer networks, the topological interactions of neighbouring chains restrict the transverse fluctuations of a network strand to the confining tube of diameter a.

This tube diameter can be interpreted as the end-to-end distance of an **entanglement strand** of N_e monomers:

$$a \approx bN_e^{1/2}. \tag{7.46}$$

[1] Entanglement appears to be caused by a collective topological restriction of many neighbouring chains (see Section 9.1).

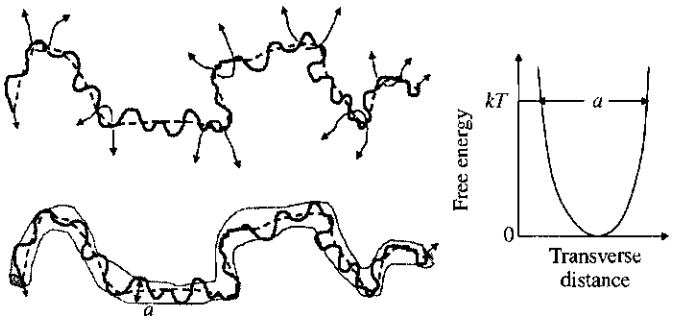

Fig. 7.10
A chain or network strand (thick curve) is topologically constrained to a tube-like region by surrounding chains. The primitive path is shown as the dashed curve. The roughly quadratic potential defining the tube is also sketched.

The entanglement strand has **entanglement molar mass** $M_e = N_e M_0$. The entanglement strand effectively replaces the network strand in the determination of the modulus for networks made from long strands, and also determines the rubbery plateau modulus of high molar mass polymer melts:

$$G_e = \frac{\rho \mathcal{R} T}{M_e}. \tag{7.47}$$

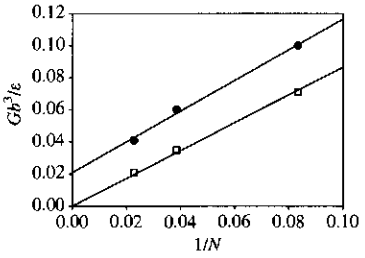

Fig. 7.11
Computer simulations of network modulus for networks with three different strand lengths (filled circles with number of monomers per strand $N = 12$, 26, and 44). The open squares are the same networks but the modulus is measured when the strands are allowed to pass through each other as in a true phantom network. Data from R. Everaers, *New J. Phys.* 1, 12.1–12.54 (1999), see http://www.njp.org. ε is the energy scale in the Lennard–Jones potential [Eq. (3.96)].

The importance of entanglements in network elasticity is proven beyond any doubt by three experimental observations.

(1) Computer simulations of polymer networks demonstrate that allowing chains to pass through each other (forming a true phantom network with no entanglements possible) lowers the shear modulus greatly, as demonstrated in Fig. 7.11. Computer simulations have the enormous advantage of knowing the number of monomers in a strand *N a priori*. The modulus of three such networks was measured at constant monomer density and plotted against $1/N$ (filled circles in Fig. 7.11). Since $1/N$ is proportional to the number density of strands, both the affine and phantom models predict a straight line going through the origin. However, in contrast to the prediction of either classical model, the straight line has a non-zero intercept! Another advantage of computer simulations, is that the rules of the simulation can be changed to be quite unrealistic. By allowing the chains to artificially pass through each other in the simulation, the open squares in Fig. 7.11 are obtained for the modulus. The straight line describing these phantom networks has an intercept of zero within numerical uncertainties, and agrees with the predictions of the phantom network model. Figure 7.11 proves that *topological interactions between network strands raise the network modulus*. The simplest idea that accounts for interactions of these strands is the notion of entanglements embodied in the Edwards tube model.

(2) Instantaneously deformed high molar mass polymer melts (long polymer chains in their liquid state) behave at intermediate times as networks with well-defined values of shear modulus, called the plateau modulus G_e, which is independent of molar mass for long-chain polymers. This rubbery plateau is seen for all polymer melts with

molar mass significantly above the molar mass of an entanglement strand M_e, as will be discussed in detail in Chapter 9. Experiments on polymer melts suggest that chains form some sort of temporary entanglement network due to the topological constraints they impose on each other. Only on very long time scales do they 'find out' that they are not permanently crosslinked and the melt begins to flow as a liquid. When such long chains are crosslinked to form a network, there is *no reason to expect these entanglements to disappear*!

(3) The modulus of well-developed networks (having sol fraction near zero) with molar mass of network strands considerably larger than the molar mass of an entanglement strand ($M_s > M_e$) is always significantly larger than either of the classical predictions. Figure 7.12 shows experimental data for networks prepared by end-linking linear poly (dimethyl siloxane) (PDMS) telechelic chains (meaning that there is a reactive group at each end of the chain, but none along the chains). Both of the classical models expect a zero intercept, and hence would allow for fully reacted networks of arbitrarily low modulus, provided that the molar mass of the starting chains is sufficiently large. However, the data suggest instead a non-zero intercept, that is consistent with the plateau modulus of high molar mass linear PDMS melts ($G_e/\mathcal{R}T \cong 80\,\text{mol}\,\text{m}^{-3}$).

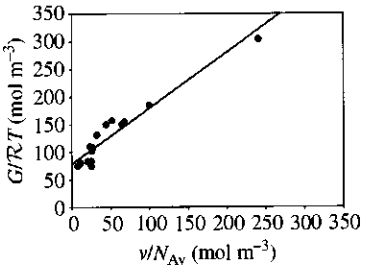

Fig. 7.12
Modulus of end-linked PDMS networks with $f = 4$ at 30 °C from S. K. Patel *et al.*, *Macromolecules* **25**, 5241 (1992). The line has an intercept determined by the plateau modulus of a melt of high molar mass PDMS linear polymers $G_e = 2.0 \times 10^5$ Pa.

Therefore, it is well established that topological entanglements dominate and control the modulus of polymer networks with long network strands. The Edwards tube model explains the non-zero intercept in plots of network modulus against number density of strands (see Figs 7.11 and 7.12). The modulus of networks with very long strands between crosslinks approaches the plateau modulus of the linear polymer melt. The modulus of the entangled polymer network can be approximated as a simple sum.

$$G \cong G_x + G_e \approx \rho\mathcal{R}T\left(\frac{1}{M_x} + \frac{1}{M_e}\right) \tag{7.48}$$

The modulus is controlled by crosslinks for low molar mass strands between crosslinks ($G \cong G_x$ for $M_x < M_e$) and by entanglements for high molar mass strands between crosslinks ($G \cong G_e$ for $M_x > M_e$). The modulus becomes nearly independent of the molar mass of the network strands between crosslinks in the limit of very long strands. The straight lines with non-zero intercept in Figs 7.11 and 7.12 are Eq. (7.48).

Equation (7.48) is applicable to well-developed networks with essentially no sol fraction. The effective modulus is of order kT per network strand without entanglements and kT per entanglement strand when entanglements dominate. Equation (7.48) allows no possibility of making a fully developed network with a modulus smaller than the plateau modulus of the corresponding melt of linear chains. However, networks with smaller modulus can of course be made if the crosslinking reaction is kept close to the gel point. The modulus of gels in the gelation regime is discussed in

Section 7.5. Networks with modulus lower than the plateau modulus can also be prepared by crosslinking chains in solution and then removing the solvent, because fewer entanglements are trapped by crosslinking in solution.

The deformation dependence of the stress in the Edwards tube model is the same as in the classical models [Eqs (7.32) and (7.33)] because each entanglement effectively acts as another crosslink junction in the network. Therefore, the Edwards tube model is unable to explain the stress softening at intermediate deformations, demonstrated in Fig. 7.8. The reason for the classical functional form of the stress–strain dependence is that the confining potential is assumed to be independent of deformation.

7.3.2 The Mooney–Rivlin model

As an alternative to the molecular approach of the three models described above, a phenomenological model of elasticity may be used. In such a model, a general expression for the free energy is written without asking any questions about the molecular interpretation of the terms of this free energy.

The model developed by Mooney and Rivlin starts from three **strain invariants**:[2]

$$I_1 = \lambda_x^2 + \lambda_y^2 + \lambda_z^2, \tag{7.49}$$

$$I_2 = \lambda_x^2\lambda_y^2 + \lambda_y^2\lambda_z^2 + \lambda_z^2\lambda_x^2, \tag{7.50}$$

$$I_3 = \lambda_x^2\lambda_y^2\lambda_z^2. \tag{7.51}$$

The free energy density of the network F/V is written as a power series in the difference of these invariants from their values in the undeformed network ($\lambda_x = \lambda_y = \lambda_z = 1$):

$$\frac{F}{V} = C_0 + C_1(I_1 - 3) + C_2(I_2 - 3) + C_3(I_3 - 1) + \cdots \tag{7.52}$$

The second term in this series is analogous to the free energy of the classical models [Eq. (7.23)]

$$C_1(I_1 - 3) = C_1(\lambda_x^2 + \lambda_y^2 + \lambda_z^2 - 3) \tag{7.53}$$

with the identification $C_1 = G_x/2$. The third term in Eq. (7.52) describes the deviations from the classical dependence. For incompressible networks, the third invariant does not change with deformation,

$$I_3 = \lambda_x^2\lambda_y^2\lambda_z^2 = \left(\frac{V}{V_0}\right)^2 = 1, \tag{7.54}$$

making the fourth term of Eq. (7.52) zero.

[2] They are called invariants because they are independent of the choice of coordinate system.

For uniaxial deformation of an incompressible network,

$$\lambda_x = \lambda \quad \lambda_y = \lambda_z = \frac{1}{\sqrt{\lambda}}, \tag{7.55}$$

the Mooney–Rivlin free energy density is written in terms of the stretching factor λ:

$$\frac{F}{V} = C_0 + C_1\left(\lambda^2 + \frac{2}{\lambda} - 3\right) + C_2\left(2\lambda + \frac{1}{\lambda^2} - 3\right) + \cdots \tag{7.56}$$

The true stress in the Mooney–Rivlin model can be obtained from the free energy density:

$$\begin{aligned}\sigma_{\text{true}} &= \frac{1}{L_y L_z}\frac{\partial F}{\partial L_x} = \lambda\frac{\partial (F/V)}{\partial \lambda} = 2C_1\left(\lambda^2 - \frac{1}{\lambda}\right) + 2C_2\left(\lambda - \frac{1}{\lambda^2}\right) + \cdots \\ &= \left(2C_1 + \frac{2C_2}{\lambda}\right)\left(\lambda^2 - \frac{1}{\lambda}\right) + \cdots \end{aligned} \tag{7.57}$$

The engineering stress can be calculated from the true stress [Eq. (7.30)]:

$$\sigma_{\text{eng}} = \frac{\sigma_{\text{true}}}{\lambda} = \left(2C_1 + \frac{2C_2}{\lambda}\right)\left(\lambda - \frac{1}{\lambda^2}\right). \tag{7.58}$$

This leads to the famous **Mooney–Rivlin equation**:

$$\frac{\sigma_{\text{true}}}{\lambda^2 - 1/\lambda} = \frac{\sigma_{\text{eng}}}{\lambda - 1/\lambda^2} = 2C_1 + \frac{2C_2}{\lambda}. \tag{7.59}$$

For classical models, the Mooney–Rivlin coefficients are $2C_1 = G$ and $C_2 = 0$. However, experimental data plotted in Fig. 7.13, in the form suggested by Eq. (7.59), show that $C_2 > 0$. In this Mooney–Rivlin plot, the stress divided by the prediction of the classical models is plotted as a function of the reciprocal deformation $1/\lambda$. The predictions of the affine, phantom, and Edwards tube network models correspond to horizontal lines on the Mooney–Rivlin plot ($C_2 = 0$). Experimental data on uniaxial extension of networks are described well by the Mooney–Rivlin equation with $C_2 > 0$, indicating strain softening as deformation increases (as $1/\lambda$ decreases). Molecular interpretation of this phenomenological result is considered next.

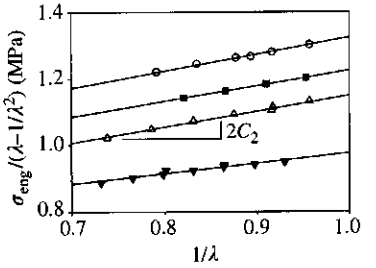

Fig. 7.13
Mooney–Rivlin plots for uniaxial tension data on three networks prepared from radiation-crosslinking a linear polybutadiene melt with $M_w = 344\,000\ \text{g mol}^{-1}$, with four different doses, making four different crosslink densities. The lines are fits of Eq. (7.59) to each data set. Data of L. M. Dossin and W. W. Graessley, *Macromolecules* **12**, 123 (1979).

7.3.3 Constrained fluctuations models

The phantom network model assumes there are no interactions between network strands other than their connectivity at the junction points. It has long been recognized that this is an oversimplification. Chains surrounding a given strand restrict its fluctuations, raising the network modulus. This is a very complicated effect involving interactions of many polymer chains, and hence, is most easily accounted for using a mean-field theory. In the

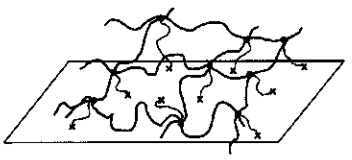

Fig. 7.14
The constrained junction model has virtual chains (thin lines) connecting each network junction (circles) to the elastic background (at the crosses).

mean-field theory, the constraining effect of many surrounding chains is replaced by an effective constraining field acting on a given network strand. The mean-field approximation is reasonable as long as the overlap parameter (the number of chains overlapping with a given chain) is large. Mean-field models of constrained fluctuations are now briefly reviewed.

In the 1970s Ronca, Allegra, Flory, and Erman proposed to take into account the additional interaction between chains by constraining junctions of network strands. The **constrained-junction model** can be represented by a phantom network with an additional harmonic constraining potential acting on network junctions (see Fig. 7.14). This constraining potential can be represented by 'virtual' chains[3] connecting junction points to the elastic non-fluctuating background. The points of attachment of the virtual chains to the elastic background are chosen in such a way to maintain the Gaussian statistics of network strands in their preparation condition.

The constraining potential represented by virtual chains must be set up so that the fluctuations of junction points are restricted, but the virtual chains must not store any stress. If the number of monomers in each virtual chain is independent of network deformation, these virtual chains would act as real chains and would store elastic energy when the network is deformed. A principal assumption of the constrained-junction model is that the constraining potential acting on junction points changes with network deformation. In the virtual chain representation of this constraining potential, this important assumption means that the number of monomers in the virtual chains changes with deformation. In the case of anisotropic deformation, the constraining potential becomes anisotropic and can be represented by virtual chains with different number of monomers n_i constraining fluctuations of junction points in the direction i ($i = x, y,$ or z)

$$n_i = \lambda_i^2 n_0, \tag{7.60}$$

where n_0 is the number of monomers in virtual chains constraining junction fluctuations in a given direction in an undeformed network and λ_i is the deformation parameter in the direction i. In Problem 7.21, it is demonstrated that Eq. (7.60) is the only possible assumption leading to no contribution to stress from virtual chains and all elastic energy being stored only in real chains. The physical reason for the deformation dependence of the constraining potential is that strands move further apart from each other in the elongation direction ($\lambda > 1$) and have a weaker constraining effect on strand fluctuations in that direction. In contrast, the strands move closer together in the compressing direction ($\lambda < 1$) where the constraining effect is strengthened. The decrease of constraining potential upon network elongation leads to increased fluctuations and to a non-classical dependence of stress on elongation with strain softening qualitatively similar to that observed in experiments (see Fig. 7.8).

[3] Virtual chains represent topological interactions between strands, as opposed to effective chains that model the effects of strand connections.

The constrained-junction model relies on an additional parameter that determines the strength of the constraining potential, and can be thought of as the ratio of the number of monomers in real network strands and in virtual chains N/n_0. If this ratio is small, the virtual chain is relatively long ($n_0 \gg N$), and surrounding chains have very little effect on the fluctuations of the junction points. If the ratio N/n_0 is large, the virtual chain is relatively short ($n_0 \ll N$) and fluctuations of the junction points are strongly suppressed, practically pinning them to the elastic non-fluctuating background. Hence, the constrained-junction model continuously crosses over from the phantom network model to the affine network model with increasing strength of the constraining potential (as N/n_0 increases from 0 to ∞).

The interactions between long overlapping network strands suppress fluctuations not only of the network junctions, but of all monomers in every network strand. In an attempt to capture this effect, Kloczkowski, Mark, and Erman proposed a **diffused-constraints model**. Instead of the constraining potential acting on network junctions, a constraining potential was applied to a single monomer on each network strand. The location along the strand of this constrained monomer is different in different network strands. The constraining potential of this diffused-constraints model can also be represented by a virtual chain with its number of monomers changing with deformation, as given by Eq. (7.60). This constraint reduces fluctuations of the particular monomer the virtual chain is attached to and its immediate neighbours, but it does not have a significant effect on fluctuations of monomers of the network strand that are far from the virtual chain. Constraining only one monomer per network strand is not enough to represent the extent of topological constraints imposed on a given strand by the surrounding network chains. In the limit of very strong confining potential ($N/n_0 \to \infty$) the diffused-constraints model also reduces to the affine network model.

7.3.3.1 Tube models of constrained fluctuations

Topological entanglements imposed by surrounding chains upon a given network strand reduce fluctuations of all monomers of this strand. Therefore, the constraining potential providing a mean-field representation of these topological interactions should be applied to *all* monomers of the chain. This is the basic assumption of the Edwards tube model, discussed in Section 7.3.1. The parabolic constraining potential acting on all monomers reduces their fluctuations to the confining tube of width a [Eq. (7.46)]. This constraining potential can be described by virtual chains that connect each monomer of the network strand to the elastic non-fluctuating background. The collective effect of these virtual chains is to restrict the fluctuations of each network strand to a confining tube (Fig. 7.10).

The same confinement of monomer fluctuations can be achieved by attaching shorter virtual chains with $n(p)$ 'virtual' monomers to every pth monomer of the network strand as long as the product $pn(p)$ is the same

and $p < n(p)$. In Problem 7.22, it is shown that for a comb polymer with side branches containing n monomers attached to every pth monomer of backbone at one end and to the elastic non-fluctuating background at the other end, the mean-square fluctuations of backbone monomers are

$$a^2 \approx b^2\sqrt{pn(p)}, \tag{7.61}$$

as long as $p \lesssim n$. Thus, virtual chains with $n \approx N_e^2$ can be attached to every monomer on the network strand (with $p = 1$) or shorter virtual chains with $n \approx N_e$ can be attached to monomers separated by $p \approx N_e$ monomers along the strand (one per entanglement strand). In both cases the fluctuations of network monomers will be constrained to the same confining tube with diameter $a \approx bN_e^{1/2}$. The condition $p \lesssim n$ assures that all monomers of the network strand have similar amplitude of fluctuations independent of how far they are from the points of attachment to virtual chains. This avoids the problem of inhomogeneous fluctuations of monomers seen in the diffused-constraints model.

One of the main assumptions of the Edwards tube model is that the number n of monomers in the virtual chains (the strength of the constraining potential) is independent of network deformation. This assumption implies that the amplitude of monomer fluctuations (the tube diameter a) does not change upon network deformation [Eq. (7.61)]. As mentioned in Section 7.3.1, this assumption of deformation-independent confining potential in the Edwards tube model leads to the classical dependence of stress on deformation.

Non-affine tube model. Rubinstein and Panyukov combined the main ideas of the constrained junction model and the Edwards tube model into a **non-affine tube model**. As in the Edwards tube model, the constraining effect of surrounding network strands on a given strand is represented by a confining potential, modelled by virtual chains. The virtual chain attachments to the elastic non-fluctuating background are not forced to be located along the primitive path line as in the Edwards tube model, but rather are placed randomly in space in such a way to make the primitive path a random walk in the preparation state. This random placement of attachment points represents the randomness of the network crosslinking process and assures that the tube has random walk statistics.

The number of monomers in virtual chains is assumed to change with deformation according to Eq. (7.60), similar to the constrained-junction and diffused-constraints models. If one virtual chain is attached to every entanglement strand of N_e monomers, it contains of order N_e virtual monomers in the undeformed state of the network. The number of monomers in each virtual chain changes as the network is deformed [see Eq. (7.60)].

$$n_i \approx \lambda_i^2 N_e. \tag{7.62}$$

For anisotropic deformation, it is important to realize that the virtual chains in component directions $i = x, y, z$ have different numbers of

monomers because the λ_i are different. As with the constrained-junction model, the constraining potential in the non-affine tube model is chosen so that no stress will be supported by virtual chains when the network is deformed, to be consistent with the microscopic definition of the stress tensor. Combining Eqs (7.61) and (7.62), we discover that the tube diameter changes non-affinely with network deformation:

$$a_i \approx bN_e^{1/2}\lambda_i^{1/2} \approx a\lambda_i^{1/2}, \tag{7.63}$$

where a is the tube diameter of the network in the undeformed state. This means that fluctuations of monomers increase along the elongation direction and decrease along the compression direction. The physical picture of the confining tube is that entanglements suppress fluctuations of monomers. As the distance between entanglements changes upon network deformation, so should the amplitude of monomer fluctuations. In fact, the amplitude of these fluctuations in the non-affine tube model coincides with the distance between entanglements in the corresponding direction, which is equal to the size of an entanglement strand of N_e monomers (see Problem 7.20).

The deformation dependence of the confining potential [Eq. (7.62)] results in a non-classical stress–strain dependence of the non-affine tube model. The prediction of this model for the stress–elongation relation in tension is qualitatively similar to the Mooney–Rivlin equation [Eq. (7.59)] and is also in excellent agreement with experiments on uniaxial deformation of networks in tension:

$$\frac{\sigma_{true}}{\lambda^2 - 1/\lambda} = \frac{\sigma_{eng}}{\lambda - 1/\lambda^2} = G_x + \frac{G_e}{\lambda - \lambda^{-1/2} + 1} \tag{7.64}$$

However, this form still overpredicts the stress required to compress a network.

Non-affine slip-tube model. In the non-affine slip-tube model, the stored length of network chains is allowed to redistribute along the contour of the tube (Fig. 7.15). Upon asymmetric (uniaxial or biaxial) deformation, the network is stretched in some directions and compressed in others. Stored length from compressed directions of the tube can redistribute itself into the stretched directions, balancing the tension in all directions and lowering the free energy and the stress in the network. The resulting dependence of stress on the deformation in the non-affine slip-tube model does not have a simple analytical form. However, the model has been solved numerically and its solution in the experimentally relevant range of $0.1 < \lambda < 10$ can be approximated in a form similar to Eq. (7.64):

$$\frac{\sigma_{true}}{\lambda^2 - 1/\lambda} = \frac{\sigma_{eng}}{\lambda - 1/\lambda^2} = G_x + \frac{G_e}{0.74\lambda + 0.61\lambda^{-1/2} - 0.35}. \tag{7.65}$$

Both Eqs (7.64) and (7.65) reduce to Eq. (7.48) in the small deformation limit ($\lambda \to 1$). This simple additivity separates the crosslink and entanglement contributions to the stress and hence allows them to be determined

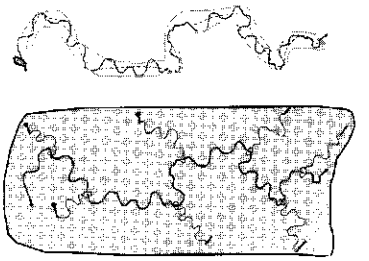

Fig. 7.15
In the non-affine slip-tube model, entanglements are represented by slip-rings that are attached to the elastic background through virtual chains that represent the potential of the confining tube.

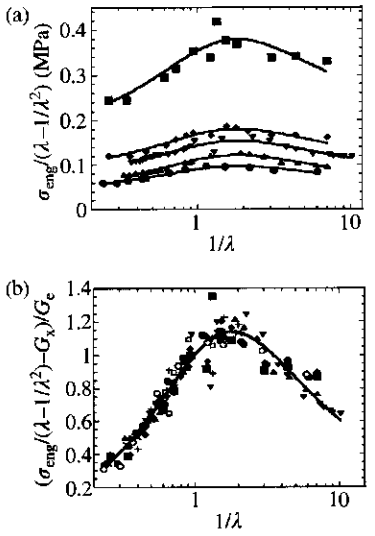

Fig. 7.16
Comparison of the non-affine slip-tube model [Eq. (7.65) using G_x and G_e as adjustable parameters] with experiments, see M. Rubinstein and S. Panyukov, *Macromolecules* **35**, 6670 (2002). Filled squares and diamonds are data on vulcanized natural rubber from R. S. Rivlin and D. W. Saunders, *Philos. Trans. R. Soc. London A* **243**, 251 (1951). Filled and open circles are PDMS network data of H. Pak and P. J. Flory, *J. Polym. Sci., Polym. Phys.* **17**, 1845 (1979). Triangles and inverted triangles are PDMS network data of P. Xu and J. E. Mark, *Rubber Chem. Technol.* **63**, 276 (1990). Part (b) demonstrates the universal form of Eq. (7.65) and also includes simulation data on end-linked networks with $N_s = 35$ (open squares), $N_s = 100$ (+) and $N_s = 350$ (×) from G. S. Grest *et al.*, *J. Non-Cryst. Solids* **274**, 139 (2000).

from experiment. Experimental data for different networks are plotted in the Mooney–Rivlin form in Fig. 7.16(a). Using G_x and G_e as fitting parameters, Eq. (7.65) provides a reasonable description of the data. Note the maximum on the Mooney–Rivlin plot for uniaxially compressed networks. The simple Mooney–Rivlin expression [Eq. (7.59)] predicts a straight line and does not agree with network compression data. Figure 7.16(b) reduces all data from both experiments and simulations to a common curve in the form suggested by Eq. (7.65).

7.4 Swelling of polymer gels

Another amazing property of polymer networks is their ability to change volume manyfold when exposed to an appropriate solvent. When a network polymer is swollen in a solvent it is called a gel. In this section, the swelling of unentangled gels is treated. At the level of the Edwards tube model, swelling of entangled gels is identical, with the number of monomers in a strand N replaced by the number of monomers in an entanglement strand N_e in the preparation state. However, as the previous section indicates, deformation of entangled networks (including swelling) is more complicated than the affine treatment of the Edwards tube model, with the topological confinement significantly diminished upon swelling.

The volume fraction ϕ of polymer in a swollen (or partly swollen) state can be easily determined experimentally by measuring the volume V of the gel (including the solvent within it) and its volume in the dry state V_{dry}:

$$\phi = \frac{V_{dry}}{V}. \tag{7.66}$$

Let ϕ_0 be the polymer volume fraction in the preparation state where crosslinking was performed, with the gel volume V_0. The total amount of polymer in a well-developed gel (with no sol fraction) does not change upon swelling or deswelling. The change of the volume is due entirely to the change in the amount of solvent within the gel:

$$V_0\phi_0 = V\phi = V_{dry}. \tag{7.67}$$

When an unconstrained macroscopic network polymer is swollen in a solvent, it undergoes uniform swelling by the same amount in all directions. In this case, the linear deformation λ in each direction is simply the 1/3 power of the ratio of final and initial volumes V/V_0, or the 1/3 power of the initial and final volume fractions ϕ_0/ϕ:

$$\lambda = \left(\frac{V}{V_0}\right)^{1/3} = \left(\frac{\phi_0}{\phi}\right)^{1/3}. \tag{7.68}$$

On swelling, each network strand is stretched as the crosslink junctions move further apart. The stretching of an ideal chain was treated in

Section 2.6.1. The free energy required to stretch the ideal chain is quadratic in its end-to-end distance R [see Eqs (2.94) and (2.101)]:

$$F_{el} \approx kT\frac{R^2}{Nb^2}. \tag{7.69}$$

This equation is the Flory form of the elastic part of the free energy of a network. The mean-square end-to-end distance of network strands in their preparation state is R_0^2. Assuming affine deformation on the length scales of a network strand, the mean-square end-to-end distance in the final state is $R^2 = (\lambda R_0)^2$. Modern treatments of network swelling and elasticity utilize a more general form of Eq. (7.69) for the elastic energy of a swollen or deformed network strand, known as the Panyukov form

$$F_{el} \approx kT\frac{(\lambda R_0)^2}{R_{ref}^2}, \tag{7.70}$$

where R_{ref}^2 is the mean-square fluctuation of the end-to-end distance of the network strand. In many cases, R_{ref}^2 is equal to the mean-square end-to-end distance of a free chain with the same number of monomers as the strand in the same solution. As the network swells (or the quality of the solvent is changed) the strand elasticity changes because R_{ref}^2 changes. The modulus $G(\phi)$ of the gel in the swollen (or partly swollen) state is proportional to the chain number density $\nu = \phi/(Nb^3)$ times the elastic free energy per chain [Eq. (7.70)] (see Problem 7.29):

$$G(\phi) \approx \nu kT\frac{(\lambda R_0)^2}{R_{ref}^2} \approx \frac{kT}{b^3}\frac{\phi}{N}\frac{(\lambda R_0)^2}{R_{ref}^2}. \tag{7.71}$$

At swelling equilibrium, the elasticity is balanced by the osmotic pressure Π of a semidilute solution of uncrosslinked chains at the same concentration.[4] Since the modulus is proportional to the elastic free energy per unit volume, any gel swells until the modulus and osmotic pressure are balanced. The **equilibrium swelling ratio** Q is the ratio of the volume in the fully swollen state V_{eq} and the volume in the dry state V_{dry}:

$$Q \equiv \frac{V_{eq}}{V_{dry}} \quad \text{when } G \approx \Pi. \tag{7.72}$$

It is important to emphasize the fact that the osmotic pressure in Eq. (7.72) is the osmotic pressure of a semidilute solution of linear chains at the same volume fraction as the gel. This is not to be confused with the osmotic pressure of the gel calculated from its definition in Eq. (4.62), which includes effects from the elasticity of the gel.

[4] Equilibrium is really attained by minimizing the free energy ($\partial F/\partial V = 0$) but if both dominant terms of the free energy are power laws in concentration, then the scaling method used here is correct up to a numerical prefactor.

7.4.1 Swelling in θ-solvents

The mean-square end-to-end distance of a free chain in a θ-solvent is independent of concentration, with $R_0^2 \approx b^2 N$. The fluctuations of a network strand that control its elasticity are also independent of concentration:

$$R_{\text{ref}}^2 \approx R_0^2 \approx b^2 N. \tag{7.73}$$

Hence, the more general Panyukov form [Eq. (7.70)] reduces to the Flory form [Eq. (7.69)] for swelling in θ-solvents. The gel modulus in a θ-solvent is then proportional to the 1/3 power of concentration:

$$G(\phi) \approx \frac{kT}{b^3}\frac{\phi}{N}\lambda^2 \approx \frac{kT}{b^3}\frac{\phi}{N}\left(\frac{\phi_0}{\phi}\right)^{2/3} \approx \frac{kT}{Nb^3}\phi_0^{2/3}\phi^{1/3}. \tag{7.74}$$

Originally derived by James and Guth, this weak concentration dependence of the network modulus comes from two competing effects. As concentration is lowered, the number density of strands naturally decreases. However, the strands also stretch as concentration is lowered, and this stretching raises the modulus somewhat through the proportionality to λ^2 (see Problem 7.29). The net effect is the weak decrease of the gel modulus upon swelling, given by Eq. (7.74).

The osmotic pressure of a semidilute solution in a θ-solvent was discussed in Section 5.4.2 [Eq. (5.57)]:

$$\Pi \approx \frac{kT}{b^3}\phi^3. \tag{7.75}$$

From the condition of swelling equilibrium [Eq. (7.72)] using Eqs (7.74) and (7.75) for θ-solvents, the equilibrium swelling ratio is obtained:

$$Q \approx \frac{N^{3/8}}{\phi_0^{1/4}}. \tag{7.76}$$

If the network was prepared in the dry state $\phi_0 = 1$, the volume fraction of polymer in the equilibrium swollen state in a θ-solvent provides a direct measure of the average number of monomers N in a network strand:

$$N \approx Q^{8/3}. \tag{7.77}$$

For networks prepared at other preparation concentrations (at the θ-temperature) Eq. (7.76) can be solved for N to estimate the average number of monomers in a network strand from the volume fraction of polymer in the preparation state ϕ_0 and the equilibrium swelling Q. However, extreme caution must be used in estimating N from Eq. (7.77) because of trapped entanglements. For densely crosslinked networks with $N \ll N_e$, entanglements are not important and Eq. (7.77) will provide an excellent estimate of N. On the other hand, for entangled networks with $N \gg N_e$,

Eq. (7.77) would only serve to estimate the entanglement strand in the preparation state assuming the Edwards tube model is correct ($N_e \approx Q^{8/3}$).

The modulus of the network in the dry state is obtained from Eq. (7.74) with $\phi = 1$:

$$G(1) \approx \frac{kT}{Nb^3}\phi_0^{2/3} \approx \frac{kT}{b^3}Q^{-8/3}. \tag{7.78}$$

The last relation is valid for any preparation concentration, and was obtained using Eq. (7.76). Such *universal* relations that are independent of the details of the preparation state are useful for predicting the equilibrium swelling in a θ-solvent from a measurement of the modulus of the network in the dry state (and vice versa). Equation (7.78) has not been tested in a θ-solvent, but it does describe swelling in concentrated solution, where ideal chain statistics apply (see the small swelling part of Fig. 7.17).

7.4.2 Swelling in athermal solvents

The end-to-end distance of a network strand in the preparation state at initial concentration ϕ_0 in an athermal solvent is given by Eq. (5.26) with $v \approx b^3$.

$$R_0 \approx bN^{1/2}\phi_0^{-(\nu-1/2)/(3\nu-1)}. \tag{7.79}$$

As shown in Section 5.3.1, the size of semidilute polymer chains in an athermal solvent decreases weakly with concentration as $R \sim \phi^{-0.12}$, since the exponent $\nu \cong 0.588$. The end-to-end distance of a free chain at concentration ϕ in an athermal solvent is also the fluctuation of the strand that determines its elasticity in the swollen (or partly swollen) state:

$$R_{\text{ref}} \approx bN^{1/2}\phi^{-(\nu-1/2)/(3\nu-1)}. \tag{7.80}$$

In contrast, the Flory form [Eq. (7.69)] underestimates the fluctuation size by assuming that R_{ref} is the ideal size $bN^{1/2}$.

The gel modulus in an athermal solvent has a stronger concentration dependence than in a θ-solvent:

$$\begin{aligned} G(\phi) &\approx \frac{kT}{b^3}\frac{\phi}{N}\left(\frac{\lambda R_0}{R_{\text{ref}}}\right)^2 \approx \frac{kT}{b^3}\frac{\phi}{N}\left(\frac{\phi_0}{\phi}\right)^{2/3}\left(\frac{\phi}{\phi_0}\right)^{(2\nu-1)/(3\nu-1)} \\ &\approx \frac{kT}{Nb^3}\phi_0^{1/[3(3\nu-1)]}\phi^{(9\nu-4)/[3(3\nu-1)]}. \end{aligned} \tag{7.81}$$

Since $\nu \cong 0.588$, the modulus of a gel swollen in an athermal solvent is predicted to decrease as solvent is added as $G(\phi) \sim \phi_0^{0.44}\phi^{0.56}$.

The osmotic pressure in an athermal solvent was considered in Section 5.3.2 [Eq. (5.48) with $v \approx b^3$]:

$$\Pi \approx \frac{kT}{b^3}\phi^{3\nu/(3\nu-1)}. \tag{7.82}$$

The prediction of $\Pi \sim \phi^{2.3}$ [Eq. (7.82) with $\nu \cong 0.588$] was shown to be consistent with experiments in Fig. 5.7. The equilibrium swelling ratio is determined using Eqs (7.81) and (7.82) in Eq. (7.72):

$$Q \approx \frac{N^{3(3\nu-1)/4}}{\phi_0^{1/4}}. \tag{7.83}$$

Comparing Eqs (7.76) and (7.83) shows the expected result that any network swells much more in an athermal solvent than in a θ-solvent.

If the network was prepared in the dry state ($\phi_0 = 1$) the average number of monomers in a network strand can be determined by measurement of the equilibrium swelling in an athermal solvent (with $\nu \cong 0.588$).

$$N \approx Q^{1.75}. \tag{7.84}$$

However, in practice Eq. (7.84) is not as useful as Eq. (7.77). Most good solvents are not in the athermal limit (with $v \approx b^3$) meaning that the exact value of the excluded volume (or χ) must be known to calculate N from equilibrium swelling measurements in a good solvent, as discussed in the next section. As in a θ-solvent, the modulus in the dry state $G(1)$ is universally related to the equilibrium swelling ratio Q in an athermal solvent:

$$G(1) \approx \frac{kT}{Nb^3}\phi_0^{1/[3(3\nu-1)]} \approx \frac{kT}{b^3}Q^{-4/[3(3\nu-1)]}. \tag{7.85}$$

Since $\nu \cong 0.588$, the dry modulus is related to the equilibrium swelling in an athermal solvent as $G(1) \sim Q^{-1.75}$. This dependence is considerably weaker than in a θ-solvent, simply because the same network will not swell nearly as much in a θ-solvent. Equation (7.85) applies to networks that are swollen into the semidilute regime in a good solvent, as shown in the large swelling part of Fig. 7.17.

7.4.3 Swelling in good solvents

In a good solvent that is not in the athermal limit ($0 < v < b^3$), Eq. (5.48) must be used for the osmotic pressure:

$$\Pi \approx \frac{kT}{b^3}\left(\frac{v}{b^3}\right)^{3(2\nu-1)/(3\nu-1)}\phi^{3\nu/(3\nu-1)} \quad \text{for } \phi < \phi^{**} \approx \frac{v}{b^3}. \tag{7.86}$$

Recall from Chapter 5 that the crossover concentration $\phi^{**} \approx v/b^3$ [Eq. (5.36)] denotes the boundary between semidilute and concentrated solutions. For $\phi > \phi^{**}$ chains are nearly ideal in concentrated solutions, whereas for $\phi < \phi^{**}$ chains are swollen on intermediate scales. Network modulus and equilibrium swelling depend on the relative value of preparation and fully swollen concentrations (ϕ_0 and $1/Q$) with respect to the crossover concentration ϕ^{**}. Since the swollen concentration is always lower than the preparation concentration ($1/Q < \phi_0$) there are three

possible cases:

(i) good solvent regime with $1/Q < \phi_0 < \phi^{**}$;
(ii) intermediate regime with $1/Q < \phi^{**} < \phi_0$;
(iii) θ-regime with $\phi^{**} < 1/Q < \phi_0$.

In the good solvent regime (i), the lower excluded volume [see Eq. (5.37)] reduces R_0 and R_{ref} relative to the athermal case [Eqs (7.79) and (7.80)]. However, the modulus in the good solvent regime (with $\phi < \phi_0 < \phi^{**}$) predicted by Eq. (7.81) is independent of the excluded volume, since R_0 and R_{ref} only enter into Eq. (7.81) as the ratio R_0/R_{ref}. Using Eqs (7.81) and (7.86) in equating modulus and osmotic pressure, gives the equilibrium swelling ratio for $\phi_0 < \phi^{**}$:

$$Q \approx \frac{N^{3(3\nu-1)/4}}{\phi_0^{1/4}} \left(\frac{\mathrm{v}}{b^3}\right)^{9(2\nu-1)/4} \quad \text{for } 1/Q < \phi_0 < \phi^{**}. \tag{7.87}$$

In the intermediate regime (ii), the chain is ideal in the preparation state $R_0 \approx bN^{1/2}$, but is swollen in the final state [Eq. (5.37)]. The modulus of the swollen gel is calculated from Eq. (7.71):

$$\begin{aligned} G(\phi) &\approx \frac{kT}{b^3}\frac{\phi}{N}\left(\frac{\lambda R_0}{R_{ref}}\right)^2 \approx \frac{kT}{b^3}\frac{\phi}{N}\left(\frac{\phi_0}{\phi}\right)^{2/3}\left(\frac{\phi}{\phi^{**}}\right)^{(2\nu-1)/(3\nu-1)} \\ &\approx \frac{kT}{Nb^3}\left(\frac{b^3}{\mathrm{v}}\right)^{(2\nu-1)/(3\nu-1)} \phi_0^{2/3}\phi^{(9\nu-4)/[3(3\nu-1)]} \quad \text{for } \phi < \phi^{**} < \phi_0. \end{aligned} \tag{7.88}$$

Since $\nu \cong 0.588$, the modulus of a gel in the intermediate regime decreases as good solvent is added as $G(\phi) \sim \mathrm{v}^{-0.23}\phi_0^{2/3}\phi^{0.56}$. Increasing the excluded volume at constant ϕ, ϕ_0 and T, *lowers* the modulus because the larger excluded volume only increases R_{ref}.

Balancing this network elastic modulus in the intermediate regime [Eq. (7.88)] with the osmotic pressure [Eq. (7.86)] produces the expression for equilibrium swelling in the intermediate regime:

$$Q \approx \frac{N^{3(3\nu-1)/4}}{\phi_0^{(3\nu-1)/2}} \left(\frac{\mathrm{v}}{b^3}\right)^{3(2\nu-1)} \quad \text{for } 1/Q < \phi^{**} < \phi_0. \tag{7.89}$$

The general relation for the equilibrium swelling in any solvent has three branches that correspond to the good solvent case [Eq. (7.87)], the intermediate case [Eq. (7.89)], and the θ-solvent case [Eq. (7.76)].

$$Q \approx \begin{cases} (\mathrm{v}/b^3)^{0.40} N^{0.57} \phi_0^{-1/4} & 1/Q < \phi_0 < \phi^{**} \\ (\mathrm{v}/b^3)^{0.53} N^{0.57} \phi_0^{-0.38} & 1/Q < \phi^{**} < \phi_0 \\ N^{3/8}\phi_0^{-1/4} & \phi^{**} < 1/Q < \phi_0. \end{cases} \tag{7.90}$$

The swelling increases steadily as the excluded volume increases. If the network is prepared in the bulk ($\phi_0 = 1$), the general relation between the dry network modulus and the equilibrium swelling depends upon whether

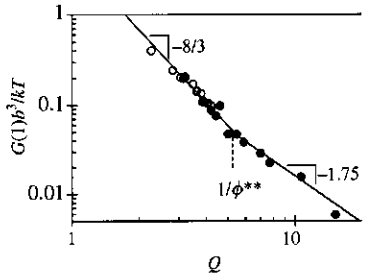

Fig. 7.17
Dry nework modulus $G(1)$ correlated with equilibrium swelling Q in toluene for PDMS networks. The open circles are for model networks made from end-linking linear chains with two reactive ends. The filled symbols are networks with dangling end defects made by end-linking mixtures of chains with one and two reactive ends. Data from S. K. Patel *et al.*, *Macromolecules* **25**, 5241 (1992).

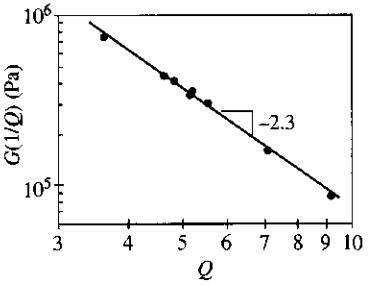

Fig. 7.18
Fully swollen modulus of end-linked PDMS networks swollen to equilibrium in toluene at 25 °C. The starting telechelic chains had $M_n = 4400\ \mathrm{g\,mol^{-1}}$ and they were crosslinked at various preparation concentrations in the range $0.3 \le \phi_0 \le 1$. The line is the prediction of Eq. (7.92) with $Q > 1/\phi^{**}$. Data from K. Urayama *et al.*, *J. Chem. Phys.* **105**, 4833 (1996).

the concentration of the swollen state $1/Q$ is above or below the crossover concentration ϕ^{**}:

$$G(1) \approx \frac{kT}{b^3} \begin{cases} Q^{-1.75}(\phi^{**})^{0.69} & Q > 1/\phi^{**} \\ Q^{-8/3} & Q < 1/\phi^{**}. \end{cases} \tag{7.91}$$

In Fig. 7.17, the dry modulus of various PDMS networks is plotted as a function of their equilibrium swelling in toluene. A single curve results for both 'model' networks (open symbols) made by end-linking linear chains with two reactive ends and networks with intentionally introduced defects in the form of dangling ends (filled symbols) made by end-linking mixtures of chains with one and two reactive ends. The data are fit to Eq. (7.91) as the solid lines in Fig. 7.17 and their intersection determines the crossover concentration $\phi^{**} \cong 0.2$, which is typical for good solvents.

A similar 'universal' relation exists (for networks prepared in either melt or concentrated solution with $\phi_0 > \phi^{**}$) between the modulus of the equilibrium fully swollen state $G(1/Q)$ and the equilibrium swelling:

$$G(1/Q) \approx \frac{kT}{b^3} \begin{cases} Q^{-2.3}(\phi^{**})^{0.69} & Q > 1/\phi^{**} \\ Q^{-3} & Q < 1/\phi^{**}. \end{cases} \tag{7.92}$$

This relation is of particular importance for estimating the modulus of a fully swollen gel (which can be challenging to measure) from the equilibrium swelling. Figure 7.18 demonstrates that Eq. (7.92) describes experimental data quite well.

The results in this section were all derived for unentangled networks. The Edwards tube model for entangled networks gives identical results with N replaced by N_e, the number of Kuhn monomers in an entanglement strand in the preparation state, because both entanglement strands and network strands are assumed to deform affinely in the Edwards tube model. If the Edwards tube model were correct, the universal relations [Eqs (7.91) and (7.92)] would still apply for entangled networks, since they are independent of N. However, the non-affine tube models predict that entangled networks will swell considerably more than the Edwards tube model predicts.

7.5 Networks in the gelation regime

For the gels in the gelation regime of Chapter 6, percolation theory predicts the modulus of unentangled gels in their preparation state using the same physics as presented in Section 7.2 (either the phantom or affine network models predict that modulus is proportional to kT per strand). The number density of network strands is determined from the correlation volume ξ^3 (the pervaded volume of a network strand in the gelation regime) and the overlap parameter P [Eq. (6.140), the number of overlapping strands per correlation volume]. The number density of strands inside the correlation volume (P/ξ^3) is the same as the overall number density of strands:

$$G \approx \nu kT \approx \frac{P}{\xi^3} kT \approx \frac{kT}{b^3} \frac{P_{gel}}{N^*}. \tag{7.93}$$

The final relation was obtained using Eq. (6.140), where P_{gel} is the gel fraction and N^* is the number of monomers in each highly branched network strand in the gelation regime.

The Soxhlet extraction method discussed in Section 6.6 can be used to separate the sol and gel fractions of a gel in the gelation regime, allowing direct determination of the gel fraction P_{gel}. Percolation theory expects the molar mass of a network strand M^* to be the same as the characteristic molar mass in the sol fraction. Hence, M^* can be determined by the size exclusion chromatography methods of Section 6.6, applied to the sol fraction. Equation (7.93) is tested in Fig. 7.19, where the shear modulus is shown to be proportional to P_{gel}/M^*.

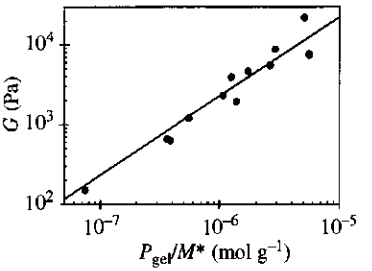

Fig. 7.19
Shear modulus of polyester gels in the gelation regime as a function of the ratio of gel fraction and the characteristic molar mass of the sol. The line has the slope of unity expected by Eq. (7.93). Data of R. H. Colby *et al.*, *Phys. Rev. E* **48**, 3712 (1993).

Recall from Chapter 6, the relative extent of reaction ε, which describes the proximity to the gel point for gels in the gelation regime. At the gel point $\varepsilon = 0$ and the gelation regime ends at $\varepsilon \approx 1$, where the gel fraction is approximately unity. The gel fraction grows above the gel point with exponent β [$P_{gel} \sim \varepsilon^{\beta}$ see Eq. (6.99)]. The number of monomers in the characteristic branched polymer decreases beyond the gel point with exponent $-1/\sigma$ [$N^* \sim \varepsilon^{-1/\sigma}$ see Eq. (6.95)]. Hence, Eq. (7.93) expects the modulus in their preparation state to grow beyond the gel point with exponent $\beta + 1/\sigma$:

$$G \sim \varepsilon^{\beta+1/\sigma}. \tag{7.94}$$

For critical percolation, $\beta = 0.41$ and $\sigma = 0.45$ (see Table 6.4), so Eq. (7.94) predicts $G \sim \varepsilon^{2.6}$ close to the gel point. Mean-field percolation has $\beta = 1$ and $\sigma = 1/2$, and predicts $G \sim \varepsilon^3$ may apply further from the gel point. These predictions are in reasonable agreement with data on gels in the gelation regime that do not have entanglement effects.

A simple way to think about the effect of entanglements is written in the spirit of Eq. (7.48):

$$G \approx \frac{\rho RT}{M_x} + T_e G_e. \tag{7.95}$$

The **entanglement trapping factor** T_e changes from zero at the gel point to unity for fully developed networks that have very few defects (formed by end-linking telechelic chains). If long entangled chains are randomly crosslinked in the melt, a fraction T_e of the entanglements will be permanently trapped in the network, and hence, have a similar effect on the modulus as an actual network junction would have. This trapping of entanglements starts in the gelation regime, but since there are many dangling ends and loops in randomly crosslinked networks, they often have many entanglements that are not trapped. Entanglements that involve dangling ends are only temporary and do not contribute to the equilibrium modulus of the network. The details of how T_e grows beyond the gel point are not yet fully established, although some simple ideas exist (see Problem 7.33). Equation (7.95) clearly indicates how to make networks with lower modulus than the plateau modulus of the polymer melt G_e. Either crosslinking chains just barely beyond the gel point or crosslinking

in solution and removing the solvent can keep T_e small and result in low modulus networks.

7.6 Linear viscoelasticity

Linear mechanical properties of the networks and gels discussed in this chapter are measured with the same methods of linear viscoelasticity as the polymer liquids (melts and solutions) discussed in Chapters 8 and 9. The various methods are described here, with examples pertaining to each class of materials.

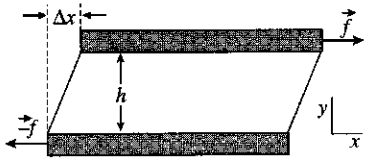

Fig. 7.20
Deformation in simple shear requires application of equal and opposite forces to the two plates. The shear strain is $\gamma = \Delta x/h$. The figure is a two-dimensional representation.

Consider the deformation geometry of simple shear, sketched in Fig. 7.20. The material being sheared is between two flat rigid surfaces. The adhesion between the material and the surfaces is assumed to be strong enough that there is no slippage at either surface. The bottom surface is held so that it does not move, and the upper surface is free to move, apart from the fact that the material between the surfaces may resist that motion. If a force f is applied to the top surface in the x direction, the force will be transmitted through the material to the bottom surface (even if the material is a liquid!). Since the bottom surface is held so that it does not move, this 'holding' must be done so as to apply an equal-and-opposite force $-f$ to the bottom surface. Otherwise, the entire assembly would need to accelerate in the x direction in response to force f. The **shear stress** σ_{xy} (called here σ for short) in this simple shear is defined as the ratio of the applied force and the cross-sectional area of the surfaces A, which is also the area of any plane perpendicular to the y direction within the material being sheared:

$$\sigma \equiv \frac{f}{A}. \tag{7.96}$$

The **shear strain** is defined as the displacement of the top plate Δx relative to the thickness of the sample h (see Fig. 7.20):

$$\gamma \equiv \frac{\Delta x}{h}. \tag{7.97}$$

By defining the stress and strain in this fashion, each part of the entire sample being sheared has identical shear stress σ and shear strain γ in simple shear, *as long as the material shears uniformly*.

If the material between the surfaces is a perfectly elastic solid, the shear stress σ and shear strain γ are proportional, with the constant of proportionality defining the **shear modulus** G:

$$G \equiv \frac{\sigma}{\gamma}. \tag{7.98}$$

Since the stress has units of force/area and the strain is dimensionless, the modulus has units of force/area. Equation (7.98) is **Hooke's law of elasticity** and it is valid for all solids at sufficiently small strains.

On the other hand, if the material between the surfaces is a simple liquid, the stress is identically zero at any constant strain γ. In liquids, the stress is determined by deformation *rate*. The rate of change of shear strain with time is called the **shear rate**:

$$\dot{\gamma} \equiv \frac{d\gamma}{dt} \tag{7.99}$$

If the top plate moves with a constant velocity v, the shear rate is $\dot{\gamma} = v/h$. For simple liquids, the shear stress σ is linearly proportional to shear rate $\dot{\gamma}$, with the constant of proportionality defining the **shear viscosity** η:

$$\eta \equiv \frac{\sigma}{\dot{\gamma}}. \tag{7.100}$$

This relation is **Newton's law of viscosity** and liquids that obey it are referred to as Newtonian liquids. Since the stress has units of force/area and the shear rate has units of reciprocal time, the viscosity has units of force · time/area. The SI unit of stress is the Pascal ($\text{Pa} \equiv \text{kg m}^{-1}\text{ s}^{-2}$) and the SI viscosity unit is $\text{Pa s} = \text{kg m}^{-1}\text{ s}^{-1}$.

Polymers are viscoelastic, meaning that they have intermediate properties between Newtonian liquids and Hookean solids. The simplest model of viscoelasticity is the **Maxwell model**, which combines a perfectly elastic element with a perfectly viscous element in series, as shown in Fig. 7.21. Since the elements are in series, the total shear strain γ is the sum of the shear strains in each element:

$$\gamma = \gamma_e + \gamma_v. \tag{7.101}$$

The shear strain in the elastic element is γ_e and the shear strain in the viscous element is γ_v (see Fig. 7.21). Since the elements are in series, they must each bear the same stress:

$$\sigma = G_M \gamma_e = \eta_M \frac{d\gamma_v}{dt} \tag{7.102}$$

The ratio of the viscosity η_M of the viscous element and the modulus G_M of the elastic element defines a time scale with special significance, called the **relaxation time**:

$$\tau_M \equiv \frac{\eta_M}{G_M}. \tag{7.103}$$

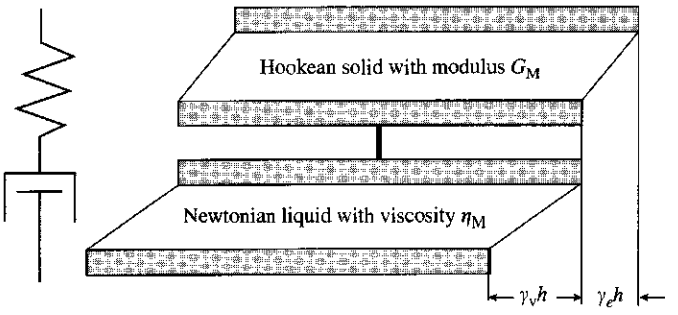

Fig. 7.21
The Maxwell model is a Hookean solid and a Newtonian liquid in series. The shear stress is identical at all points in both the solid and the liquid. The total shear strain is the sum of the strains in the solid and liquid elements. Each element must have the same vertical gap h between the rigid plates that the real sample has.

In the next few sections, we will see that the Maxwell model responds like a solid on time scales that are short compared with the relaxation time. In contrast, on time scales that are longer than the relaxation time, the Maxwell model flows like a liquid.

7.6.1 Stress relaxation after a step strain

Consider imposing a step strain of magnitude γ at time $t = 0$ (see Fig. 7.20). If the material between the plates is a perfectly elastic solid, the stress will jump up to its equilibrium value $G\gamma$ given by Hooke's law [Eq. (7.98)] and stay there as long as the strain is applied. On the other hand, if the material is a Newtonian liquid, the transient stress response from the jump in strain will be a spike that instantaneously decays to zero. For viscoelastic materials, the stress after such a step strain can have some general time dependence $\sigma(t)$. The **stress relaxation modulus** $G(t)$ is defined as the ratio of the stress remaining at time t (after a step strain was applied at time $t = 0$) and the magnitude of this step strain γ:

$$G(t) \equiv \frac{\sigma(t)}{\gamma}. \tag{7.104}$$

Notice that the above equation is simply a time-dependent generalization of Hooke's law [Eq. (7.98)]. For viscoelastic solids, $G(t)$ relaxes to a finite value, called the **equilibrium shear modulus** G_{eq} (see Fig. 7.22, top curve):

$$G_{eq} = \lim_{t\to\infty} G(t). \tag{7.105}$$

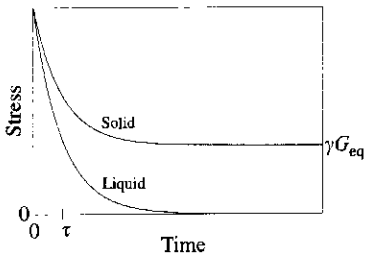

Fig. 7.22
Stress relaxation in step strain experiments on a viscoelastic solid (upper curve) and a viscoelastic liquid (lower curve). The dashed lines show the value of the stress at the relaxation time τ of the liquid. The solid has the same relaxation time.

For viscoelastic liquids, the Maxwell model can be used to qualitatively understand the stress relaxation modulus. In the step strain experiment, the total strain γ is constant and Eqs (7.101)–(7.103) can be combined to give a first order differential equation for the time-dependent strain in the viscous element:

$$\tau_M \frac{d\gamma_v(t)}{dt} = \gamma - \gamma_v(t). \tag{7.106}$$

Combined with the initial condition of no strain in the viscous element when the strain is first applied [$\gamma_v(0) = 0$] allows integration of this differential equation:

$$\frac{d\gamma_v(t)}{\gamma - \gamma_v(t)} = \frac{dt}{\tau_M}, \tag{7.107}$$

$$\ln[\gamma - \gamma_v(t)] = \frac{-t}{\tau_M} + C. \tag{7.108}$$

The constant of integration in evaluated from the initial condition, giving $C = \ln\gamma$:

$$\gamma_e(t) = \gamma - \gamma_v(t) = \gamma \exp(-t/\tau_M). \tag{7.109}$$

The stress relaxes exponentially towards zero on the time scale τ_M, evaluated using Eq. (7.102):

$$\sigma(t) = G_M \gamma_e(t) = G_M \gamma \exp(-t/\tau_M). \tag{7.110}$$

In the Maxwell model, the stress relaxation modulus has a simple exponential decay.

$$G(t) \equiv \frac{\sigma(t)}{\gamma} = G_M \exp(-t/\tau_M). \tag{7.111}$$

Beyond their relaxation time, the stress or the relaxation modulus of most viscoelastic liquids has a nearly exponential time decay to zero, sketched as the bottom curve in Fig. 7.22:

$$G(t) \equiv \frac{\sigma(t)}{\gamma} \approx G(\tau) \exp(-t/\tau) \quad \text{for } t > \tau. \tag{7.112}$$

The relaxation time τ is a fundamental dynamic property of all viscoelastic liquids. Polymer liquids have multiple relaxation modes, each with its own relaxation time. Any stress relaxation modulus can be described by a series combination of Maxwell elements.

All materials have a region of **linear response** at sufficiently small values of applied strain, where the relaxation modulus is independent of strain. Thus, doubling the strain in the linear response regime merely doubles the value of the stress at all times, making the stress relaxation modulus $G(t)$ independent of strain at small values of the applied strain.

7.6.2 The Boltzmann superposition principle

Another manifestation of linear response is the **Boltzmann superposition principle**. The stress from any combination of small step strains is simply the linear combination of the stresses resulting from each individual step $\delta\gamma_i$ applied at time t_i:

$$\sigma(t) = \sum_i G(t - t_i)\delta\gamma_i. \tag{7.113}$$

This equation simply states that, for linear response, the stress resulting from each step is independent of all the other steps. The system remembers the deformations that were imposed on it earlier, and continues to relax from each earlier deformation as new ones are applied. The stress relaxation modulus tells how much stress remains at time t from each past deformation $\delta\gamma_i$ through the elapsed time $t - t_i$ that has passed since that deformation was applied at time t_i.

Using the definition of the shear rate [Eq. (7.99)] the summation increment can be transformed into time, since $\delta\gamma_i = \dot{\gamma}_i \delta t_i$.

$$\sigma(t) = \sum_i G(t - t_i)\dot{\gamma}_i \delta t_i. \tag{7.114}$$

The stress from any smooth strain history can be written as an integral over the strain history, by replacing the above summation with an integration:

$$\sigma(t) = \int_{-\infty}^{t} G(t-t')\dot{\gamma}(t')\,\mathrm{d}t'. \tag{7.115}$$

The lower integration limit is $t = -\infty$ because we must integrate over *all* past times (not just those starting at some arbitrarily defined zero point) to ensure that all past deformations are accounted for. Equation (7.115) can be used to relate many different linear response experiments.

The stress in any material is the result of all past deformations. The memory of each past deformation only decays as the relaxation modulus decays over the *elapsed* time $t - t'$ from the application of that deformation.

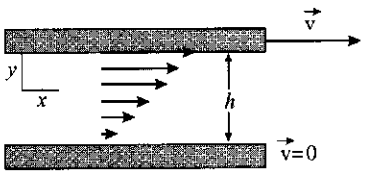

Fig. 7.23
Steady simple shear of a liquid is accomplished by confining the liquid between a moving top plate and a stationary bottom plate. The velocity in the liquid is in the x direction and changes linearly in the y direction, making the shear rate the same everywhere.

7.6.3 Steady shear

In steady simple shear, the top plate in Fig. 7.23 is moved at a constant velocity $\vec{v}$. The shear rate $\dot{\gamma} = |\vec{v}|/h$ is a time-independent constant that can be pulled out of the Boltzmann superposition integral:

$$\sigma(t) = \dot{\gamma}\int_{-\infty}^{t} G(t-t')\,\mathrm{d}t' = \dot{\gamma}\int_{0}^{\infty} G(s)\,\mathrm{d}s. \tag{7.116}$$

The last relation was obtained using the variable transformation $s \equiv t - t'$, which implies $\mathrm{d}s = -\mathrm{d}t'$. The integration limits change with this transformation because when $t' = -\infty$, $s = \infty$, and at $t' = t$, $s = 0$. For any liquid, the relaxation modulus $G(t)$ eventually decays to zero fast enough that the integral in the above equation is simply a number with units of stress · time. Thus, the stress at long times in the steady simple shear experiment is constant, and proportional to the shear rate $\dot{\gamma}$. Newton's law of viscosity [Eq. (7.100)] already defined the viscosity in steady shear as the ratio of shear stress and shear rate. Therefore, the viscosity of any liquid is the time integral of its stress relaxation modulus:

$$\eta = \int_{0}^{\infty} G(t)\,\mathrm{d}t. \tag{7.117}$$

The Maxwell model [Eq. (7.111)] has a particularly simple viscosity:

$$\eta = G_{\mathrm{M}}\int_{0}^{\infty} \exp(-t/\tau_{\mathrm{M}})\mathrm{d}t = G_{\mathrm{M}}\tau_{\mathrm{M}} = \eta_{\mathrm{M}}. \tag{7.118}$$

For viscoelastic solids (Fig. 7.22, top curve) the modulus does not decay to zero, meaning that the viscosity of any solid is infinite. For most viscoelastic liquids (Fig. 7.22, bottom curve) the stress decays to zero in a nearly

exponential fashion on time scales longer than their longest relaxation time [Eq. (7.112)]:

$$\eta \approx G(\tau) \int_0^\infty \exp(-t/\tau)\, \mathrm{d}t = G(\tau)\tau \int_0^\infty \exp(-s)\, \mathrm{d}s = G(\tau)\tau. \quad (7.119)$$

The second integral is simply a number (in this case unity) because it is written in terms of the *dimensionless* integration variable $s \equiv t/\tau$, so $\mathrm{d}s = \mathrm{d}t/\tau$. The viscosity is proportional to the product of the relaxation time and the value of the modulus at that relaxation time:

$$\eta \approx G(\tau)\tau. \quad (7.120)$$

This relation will be used many times in the remainder of this book to estimate the viscosity from scaling models. It is essentially stating that the area under the bottom curve in Fig. 7.22 is proportional to the area of the rectangle defined by the dashed lines.

In practice, it is more precise to evaluate the viscosity from a step strain experiment by transforming the integration of Eq. (7.117) to a logarithmic time scale using the identity $t\, \mathrm{d} \ln t = \mathrm{d}t$, and the lower limit of integration changes because when $t = 0$, $\ln t = -\infty$:

$$\eta = \int_{-\infty}^{\infty} tG(t)\, \mathrm{d} \ln t. \quad (7.121)$$

The improved precision of Eq. (7.121) as compared to Eq. (7.117), for determining the viscosity from the step strain experiment, arises from the fact that $tG(t)$ is a function with a well-defined peak, and the relaxation modulus can decay over many decades of time for viscoelastic materials, such as polymers.

If the applied shear rate is too large for linear response, Boltzmann superposition no longer holds in steady shear. An apparent viscosity is still operationally defined as the ratio of shear stress and shear rate, but that apparent viscosity should not be confused with the zero shear rate viscosity η of the liquid. Most polymeric liquids exhibit **shear thinning** of the apparent viscosity at large shear rates, meaning that the viscosity progressively decreases as shear rate is raised. The apparent viscosity has also been observed to increase with shear rate for some materials and such response is called **shear thickening**. The zero shear rate viscosity of the liquid is only measured at low shear rates where $\dot{\gamma} \ll 1/\tau$. In this book we will only consider the linear response of viscoelastic liquids, and hence our use of the term 'viscosity' always signifies the zero shear rate viscosity.

On some time scale, all liquids display viscoelasticity. Newtonian liquids like water have viscosity independent of shear rate over ordinary ranges of measurement ($10^{-5}\,\mathrm{s}^{-1} < \dot{\gamma} < 10^{5}\,\mathrm{s}^{-1}$). Dielectric spectroscopy reveals that water molecules respond to an oscillating electric field at a frequency of 17 GHz at room temperature. Hence, at shear rates of order $10^{10}\,\mathrm{s}^{-1}$, water would be expected to be viscoelastic, and have a shear thinning apparent viscosity.

7.6.4 Creep and creep recovery

Thus far we have imposed a constant strain (the step strain experiment) and constant shear rate (the steady shear experiment). Another simple viscoelastic experiment is accomplished by applying a constant shear stress to the sample. In a creep (step stress) experiment, a constant stress σ is applied to an initially relaxed sample, and the strain is monitored as a function of time $\gamma(t)$. The shear **creep compliance** $J(t)$ is defined as the ratio of the time dependent strain and the applied stress:

$$J(t) \equiv \frac{\gamma(t)}{\sigma}. \tag{7.122}$$

The Maxwell model has a particularly simple response in creep, because for constant stress, Eq. (7.102) requires the strain in the elastic element to be constant

$$\gamma_e = \frac{\sigma}{G_M}, \tag{7.123}$$

and the strain in the viscous element is simply linear in time:

$$\frac{d\gamma_v(t)}{dt} = \frac{\sigma}{\eta_M} \quad \Rightarrow \quad \gamma_v(t) = \frac{\sigma}{\eta_M} t. \tag{7.124}$$

The creep compliance of the Maxwell model is linear in time,

$$J(t) = \frac{\gamma_e + \gamma_v(t)}{\sigma} = \frac{1}{G_M} + \frac{t}{\eta_M}, \tag{7.125}$$

with the value at $t = 0$ determining the elastic response (G_M) and the slope determining the viscosity (η_M).

The strain of a viscoelastic liquid in creep is shown as the top curve in Fig. 7.24. The slope in Fig. 7.24 at long times is the shear rate $\dot{\gamma}$ and the viscosity is therefore determined using Newton's law of viscosity [Eq. (7.100)]. For liquids, the long-time creep compliance is linear in time and its form is reminiscent of the Maxwell model [Eq. (7.125)]:

$$J(t) = J_{eq} + \frac{t}{\eta} \quad \text{for } t \gg \tau. \tag{7.126}$$

The $t = 0$ intercept of the long-time creep compliance is a measure of the stored elastic energy in flow, and is called the **steady state compliance** J_{eq}.

The time-dependent strain of a viscoelastic solid in creep is sketched as the bottom curve in Fig. 7.24. The long-time creep compliance of any solid is simply a time-independent compliance J_{eq} that is the reciprocal of its equilibrium modulus G_{eq}.

$$J_{eq} = \lim_{t\to\infty} J(t) = \frac{1}{\sigma} \lim_{t\to\infty} \gamma(t) = \frac{1}{G_{eq}}. \tag{7.127}$$

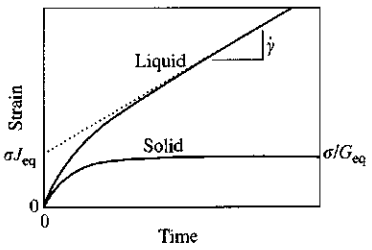

Fig. 7.24
Strain from a creep experiment with constant applied stress σ for a viscoelastic solid (lower curve) and a viscoelastic liquid (upper curve). The slope at long times is the steady shear rate $\dot{\gamma}$, from which the viscosity is calculated as $\eta = \sigma/\dot{\gamma}$ (the viscosity of any solid is infinite, corresponding to zero slope). The extrapolation of this straight line to zero time (dotted line) gives the elastic part of the strain, from which the recoverable compliance J_{eq} is determined.

The final result was obtained using Hooke's law [Eq. (7.98)], which does not discriminate between application of stress with measurement of strain (creep) or application of strain and measurement of stress (step strain).

The Boltzmann superposition principle can be used to relate the steady state compliance to the stress relaxation modulus (see Problem 7.44):

$$J_{eq} = \frac{1}{\eta^2}\int_0^\infty tG(t)\,dt. \tag{7.128}$$

This integral is dominated by the long-time behaviour of $tG(t)$, given by Eq. (7.112):

$$J_{eq} \approx \frac{G(\tau)}{\eta^2}\int_0^\infty t\exp(-t/\tau)\,dt. \tag{7.129}$$

This integral is evaluated via integration by parts: $u = t$, making $du = dt$, and $dv = \exp(-t/\tau)\,dt$, making $v = -\tau\exp(-t/\tau)$:

$$J_{eq} \approx \frac{G(\tau)}{\eta^2}\left([-t\tau\exp(-t/\tau)]_0^\infty + \tau\int_0^\infty \exp(-t/\tau)\,dt\right). \tag{7.130}$$

The term in square brackets is zero and the integral is evaluated by making the variable transformation $s \equiv t/\tau$, so $ds = dt/\tau$:

$$J_{eq} \approx \frac{G(\tau)\tau^2}{\eta^2}\int_0^\infty \exp(-s)\,ds = \frac{G(\tau)\tau^2}{\eta^2}. \tag{7.131}$$

Combining with Eq. (7.120) provides a very important relation for the relaxation time:

$$\tau \approx \eta J_{eq}. \tag{7.132}$$

Furthermore, substitution of this relaxation time into Eq. (7.131) shows the significance of the steady state compliance:

$$J_{eq} \approx \frac{1}{G(\tau)}. \tag{7.133}$$

Using Eq. (7.132) for the relaxation time, the long-time behaviour of a liquid in creep can be rewritten:

$$J(t) = J_{eq} + \frac{t}{\eta} \approx \frac{\tau + t}{\eta} \quad \text{for } t \gg \tau. \tag{7.134}$$

Creep has special intuitive appeal for understanding viscoelasticity because the elastic part $J_{eq} = \tau/\eta$ and the viscous part t/η are simply *additive* in creep.

To evaluate the steady state compliance from a step strain experiment, it is useful to transform the integration of Eq. (7.128) to a logarithmic time

scale using the identity $t\,d\ln t = dt$, and the lower limit of integration changes because when $t = 0$, $\ln t = -\infty$:

$$J_{eq} = \frac{1}{\eta^2}\int_{-\infty}^{\infty} t^2 G(t)\, d\ln t. \tag{7.135}$$

Combining Eqs (7.117), (7.128), and (7.132) allows us to recognize that the relaxation time is a number average on a linear time scale and a weight average on a log time scale, with the distribution in both cases being the stress relaxation modulus $G(t)$:

$$\tau = \frac{\int_0^{\infty} tG(t)\,dt}{\int_0^{\infty} G(t)\,dt} = \frac{\int_{-\infty}^{\infty} t^2 G(t)\,d\ln t}{\int_{-\infty}^{\infty} tG(t)\,d\ln t}. \tag{7.136}$$

Two steady states are recognized for the long-time creep compliance of materials. Either the sample is a solid and the compliance becomes time independent or the sample is a liquid and the compliance becomes linear in time. Once steady state has been achieved in creep, the stress can be removed ($\sigma = 0$) and the elastic recoil, called creep recovery, can be measured. Recovery strain is defined as $\gamma_R(t) \equiv \gamma(0) - \gamma(t)$ for $t > 0$, where t is defined to be zero at the start of recovery. The **recoverable compliance** is defined as the ratio of the time-dependent recovery strain $\gamma_R(t)$ and the initially applied stress σ, where both γ_R and t are now defined to be zero at the start of recovery:

$$J_R(t) \equiv \frac{\gamma_R(t)}{\sigma}. \tag{7.137}$$

Boltzmann superposition relates the recoverable compliance after steady state has been achieved in creep to the creep compliance:[5]

$$J_R(t) = J(t) - \frac{t}{\eta}. \tag{7.138}$$

For a solid, the viscosity is infinite, and $J_R(t) = J(t)$, so all deformation in creep is subsequently recovered in creep recovery, with precisely the same time dependence, as shown in the lower curves in Fig. 7.25. In contrast, only the elastic part of the compliance of a liquid is recovered, as shown in the upper curves of Fig. 7.25:

$$\lim_{t\to\infty} J_R(t) = \lim_{t\to\infty}\left[J(t) - \frac{t}{\eta}\right] = J_{eq}. \tag{7.139}$$

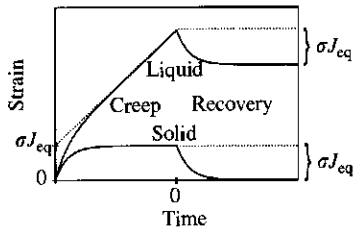

Fig. 7.25
Strain from a creep experiment with constant applied stress σ followed by a creep recovery experiment (starting at $t = 0$) with zero applied stress, for a viscoelastic solid (lower curves) and a viscoelastic liquid (upper curves). The recoverable compliance can be determined from either creep or recovery. All deformation is recovered for solids but only the elastic part of the deformation is recovered for liquids.

7.6.5 Oscillatory shear

A simple linear viscoelastic measurement that has become very easy to implement with the advent of modern electronics is oscillatory shear. A sinusoidal strain with angular frequency ω is applied to a sample in simple shear:

$$\gamma(t) = \gamma_0 \sin(\omega t). \tag{7.140}$$

[5] Note that $t = 0$ in the left hand side of Eq. (7.138) corresponds to the start of recovery, while $t = 0$ on the right hand side corresponds to the start of creep.

The principal advantage of this technique is that the viscoelastic response of any material can be probed directly on different time scales ($1/\omega$) of interest by simply varying the angular frequency ω. If the material studied is a perfectly elastic solid, then the stress in the sample will be related to the strain through Hooke's law [Eq. (7.98)]:

$$\sigma(t) = G\gamma(t) = G\gamma_0 \sin(\omega t). \tag{7.141}$$

The stress is perfectly in-phase with the strain for a Hookean solid, as shown in Fig. 7.26. At times $t = \pi/(2\omega), 5\pi/(2\omega), 9\pi/(2\omega), \ldots$ the strain has a maximum and the stress also has a maximum. Similarly, at times $t = 0, \pi/\omega, 2\pi/\omega, \ldots$ both the strain and the stress are simultaneously zero.

On the other hand, if the material being studied is a Newtonian liquid, the stress in the liquid will be related to the *shear rate* through Newton's law [Eq. (7.100)]:

$$\sigma(t) = \eta \frac{\mathrm{d}\gamma(t)}{\mathrm{d}t} = \eta\gamma_0\omega\cos(\omega t) = \eta\gamma_0\omega\sin\left(\omega t + \frac{\pi}{2}\right). \tag{7.142}$$

The stress in a Newtonian liquid still oscillates with the same angular frequency ω, but is out-of-phase with the strain by $\pi/2$, as shown in Fig. 7.27. At times $t = \pi/(2\omega), 5\pi/(2\omega), 9\pi/(2\omega), \ldots$ the strain has a maximum, but both the shear rate and the stress are zero at these points. Conversely, at times $t = 0, \pi/\omega, 2\pi/\omega, \ldots$ the strain is zero, but both the shear rate and the stress are either at their maximum or minimum values.

More generally, the linear response of a viscoelastic material always has the stress oscillate at the same frequency as the applied strain, but the stress leads the strain by a **phase angle** δ.

$$\sigma(t) = \sigma_0 \sin(\omega t + \delta). \tag{7.143}$$

In general, δ can be frequency dependent, with any value in the range $0 \leq \delta \leq \pi/2$. The two simple cases already treated correspond to the limits allowed for the phase angle. Solids that obey Hooke's law have $\delta = 0$ at all frequencies, while liquids that obey Newton's law have $\delta = \pi/2$ at all frequencies. Since the stress is always a sinusoidal function with the same frequency as the strain, we can separate the stress into two orthogonal functions that oscillate with the same frequency, one in-phase with the strain and the other out-of-phase with the strain by $\pi/2$:

$$\sigma(t) = \gamma_0[G'(\omega)\sin(\omega t) + G''(\omega)\cos(\omega t)]. \tag{7.144}$$

Equation (7.144) defines $G'(\omega)$ as the **storage modulus** and $G''(\omega)$ as the **loss modulus**. Equation (7.144) can be related to the previous equation for the stress in oscillatory shear using the trigonometric identity for the sine of a sum:

$$\sin(\omega t + \delta) = \cos\delta\sin(\omega t) + \sin\delta\cos(\omega t). \tag{7.145}$$

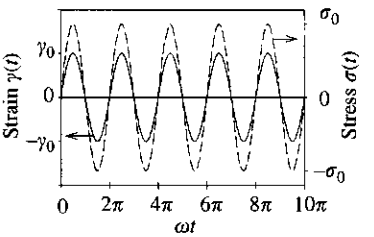

Fig. 7.26
Oscillatory strain (solid curve and left axis) and oscillatory stress (dashed curve and right axis) are in-phase for a Hookean solid.

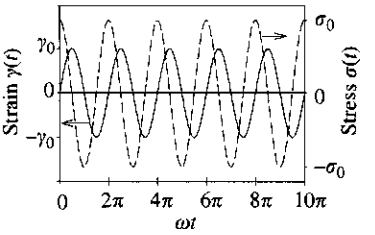

Fig. 7.27
Oscillatory strain (solid curve and left axis) and oscillatory stress (dashed curve and right axis) are out-of-phase for a Newtonian liquid. The stress leads the strain by phase angle $\delta = \pi/2$.

This suggests that the storage and loss moduli can be related to the phase angle and the modulus amplitude σ_0/γ_0 at each frequency ω:

$$G' = \frac{\sigma_0}{\gamma_0}\cos\delta, \tag{7.146}$$

$$G'' = \frac{\sigma_0}{\gamma_0}\sin\delta. \tag{7.147}$$

The ratio of loss and storage moduli is the tangent of the phase angle, called the **loss tangent**:

$$\tan\delta = \frac{G''}{G'}.$$

The storage and loss moduli are the real and imaginary parts of the **complex modulus** $G^*(\omega)$:

$$G^*(\omega) = G'(\omega) + iG''(\omega). \tag{7.148}$$

The Boltzmann superposition principle can be used to show that the storage modulus is related to the sine transform of $G(t)$,

$$G'(\omega) = G_{eq} + \omega\int_0^\infty [G(t) - G_{eq}]\sin(\omega t)\,dt, \tag{7.149}$$

and the loss modulus is obtained from the cosine transform (see Problem 7.41):

$$G''(\omega) = \omega\int_0^\infty [G(t) - G_{eq}]\cos(\omega t)\,dt. \tag{7.150}$$

In these equations, G_{eq} is the equilibrium modulus of the solid at long times (or low frequencies). For a liquid, $G_{eq} \equiv 0$.

Figure 7.22 showed that the relaxation modulus distinguishes viscoelastic solids from viscoelastic liquids via the long-time behaviour of $G(t)$. Since low frequencies correspond to long times, the oscillatory shear experiment makes this distinction in the low frequency response of the material. The terminal (low frequency) response of any solid is dominated by the storage modulus because the stress is very nearly in-phase with the strain. The viscoelastic solid has $G' \gg G''$ at low frequencies, and G' becomes independent of frequency in the low frequency limit, with a value equal to the equilibrium modulus G_{eq}:

$$G_{eq} = \lim_{\omega\to 0} G'(\omega). \tag{7.151}$$

The viscoelastic response of a liquid in oscillatory shear is markedly different. The terminal response (at low frequency) of any liquid is dominated by the loss modulus because the stress is very nearly in-phase with the shear rate. The viscoelastic liquid has $G'' \gg G'$ at low frequencies. G'' is

proportional to frequency in the low-frequency limit, and the proportionality constant is the viscosity [compare Eqs (7.142) and (7.144)]:

$$\eta = \lim_{\omega \to 0} \frac{G''(\omega)}{\omega}. \tag{7.152}$$

The storage modulus of a viscoelastic liquid is not zero, but instead is proportional to the square of frequency, and provides a measure of the stored elastic energy. Traditionally, this is written in terms of the steady state compliance J_{eq}:

$$J_{eq} = \frac{1}{\eta^2} \lim_{\omega \to 0} \frac{G'(\omega)}{\omega^2} = \lim_{\omega \to 0} \frac{G'(\omega)}{[G''(\omega)]^2}. \tag{7.153}$$

An example of the linear viscoelastic response in oscillatory shear for a nearly monodisperse linear polybutadiene melt is shown in Fig. 7.28. Extrapolation of the limiting power laws of $G' \sim \omega^2$ and $G'' \sim \omega$ (the dashed lines in Fig. 7.28) to the point where they cross has special significance. The intersection of the power laws $G' = J_{eq}\eta^2\omega^2$ and $G'' = \eta\omega$ using the above two equations allows us to solve for the frequency where they cross $\omega = 1/(\eta J_{eq})$, which is the reciprocal of the relaxation time[5] τ [Eq. (7.132)]. The modulus level where the two extrapolations cross, obtained by setting $\omega = 1/\tau = 1/(\eta J_{eq})$ in either equation, is simply the reciprocal of the steady state recoverable compliance $1/J_{eq}$.

The viscoelastic responses of two polymer networks are shown in Fig. 7.29. One is a nearly perfect network (circles) made by end-linking linear chains with two reactive ends. The storage modulus for this network (filled circles) is independent of frequency and much larger than the loss modulus (open circles). For comparison, an imperfect network made by linking a mixture of chains with one and two reactive ends is also shown. While $G' > G''$ for the imperfect network, the storage modulus (filled squares) has a weak frequency dependence and the loss modulus (open squares) is significantly larger than for the perfect network. Both of these observations are caused by the gradual relaxation of dangling structures in the imperfect network (see Problem 9.43). The loss tangent $\tan\delta = G''/G'$ is much larger for the imperfect network than for the nearly perfect one.

The various experimental methods of linear viscoelasticity are summarized in Table 7.1. All information for linear viscoelastic response can, in principle, be obtained from each method. The oscillatory methods are particularly useful because they directly probe the response of the system on the time scale of the imposed frequency of oscillation $1/\omega$. Commercial rheometers can accomplish this with either applied stress or applied strain, and the two methods are both listed in Table 7.1.

[5] This relaxation time for the Maxwell model is an average relaxation time [see Eq. 7.136] whenever a material has multiple relaxation modes.

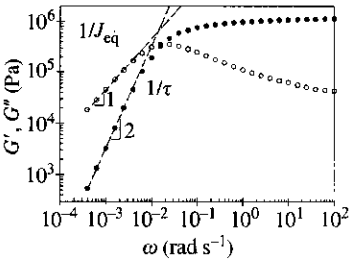

Fig. 7.28
Oscillatory shear response of a linear polybutadiene at 25 °C, with $M_w = 925\,000$ g mol^{-1} and $M_w/M_n < 1.1$. Filled symbols are the storage modulus G' and open symbols are the loss modulus G''. The crossing of the terminal slopes of 1 and 2 (dashed lines) determines the relaxation time and the steady state recoverable compliance.

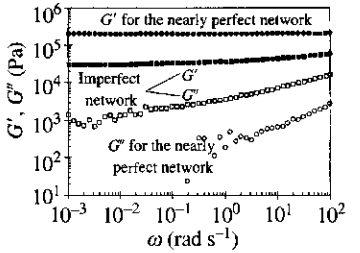

Fig. 7.29
Oscillatory shear response of two PDMS networks at 30 °C. Filled symbols are the storage modulus G' and open symbols are the loss modulus G''. The circles are nearly perfect networks made by end-linking linear chains of $M_n = 20\,000$ g mol^{-1} with two reactive ends. The squares are imperfect networks made by reacting 48 mol% linear chains of $M_n = 71\,000$ g mol^{-1} with one reactive end and 52 mol% linear chains of $M_n = 58\,000$ g mol^{-1} with two reactive ends. Notice that the storage modulus is lower and the loss modulus is higher for the imperfect networks. The increased noise in G'' at low frequencies is caused by the difficulty in precise determination of a phase angle very close to zero.

Table 7.1 Comparison of linear viscoelastic experimental methods

Technique	Apply	Measure	Determine
Step strain	Constant strain γ	Stress $\sigma(t)$	Relaxation modulus $G(t)=\sigma(t)/\gamma$
Steady shear	Constant shear rate $\dot{\gamma}$	Steady stress σ	Viscosity $\eta=\sigma/\dot{\gamma}$
Step stress (creep)	Constant stress σ	Strain $\gamma(t)$	Compliance $J(t)=\gamma(t)/\sigma$
Oscillatory strain	$\gamma(t)=\gamma_0\sin\omega t$	$\sigma(t)=\sigma_0\sin(\omega t+\delta)$	$G'(\omega)=(\sigma_0/\gamma_0)\cos\delta$; $G''(\omega)=(\sigma_0/\gamma_0)\sin\delta$
Oscillatory stress	$\sigma(t)=\sigma_0\sin\omega t$	$\gamma(t)=\gamma_0\sin(\omega t-\delta)$	$G'(\omega)=(\sigma_0/\gamma_0)\cos\delta$; $G''(\omega)=(\sigma_0/\gamma_0)\sin\delta$

7.7 Summary of networks and gels

Polymer networks are very important soft solids. As such, they find applications ranging from adhesives to automobile tires. The mechanical properties of network polymers arise primarily from the changes in entropy of the network strands when the network is macroscopically deformed. One direct consequence of entropic elasticity is that the modulus increases as temperature is raised (whereas conventional solids get softer). Network polymers are thus quite different from other solids, such as crystalline metals, where mechanical properties have energetic origins, coming from the change in internal energy when lattice spacings are distorted from their equilibrium values. The modulus G of network polymers in their preparation state is proportional to kT per elastically effective network strand, plus any contribution from trapped entanglements:

$$G \cong G_x + G_e \tag{7.154}$$

The number density of network strands determines G_x and the plateau modulus caused by inter-chain entanglements is G_e. This plateau modulus is understood on a molecular level by imagining surrounding chains confining each network strand to an effective tube.

Many models lead to a classical form for the variation of the true stress with uniaxial elongation:

$$\sigma_{true} = G\left(\lambda^2 - \frac{1}{\lambda}\right). \tag{7.155}$$

For large stretching ratios, finite extensibility of the network strands becomes important and this strong stretching is better described by finite extensibility models such as the inverse Langevin function for freely jointed chains. Classical theory [Eq. (7.155)] is not applicable for entangled networks because entanglements are qualitatively different than crosslinks, when the network is deformed. This qualitative difference leads to non-affine deformation of the confining tube and a non-classical stress–strain relation [Eq. (7.65)].

Polymer gels are diluted polymer networks. The diluent can be other polymer chains or solvent. The modulus of gels decreases on dilution, in ways that depend on the details of the polymer–solvent interaction. When immersed in an excess of an appropriate solvent, polymer networks can often swell considerably. The swelling is driven by the favorable free energy

of mixing with solvent (osmotic pressure) and is resisted by the energy required to stretch network strands (modulus). The swelling reaches an equilibrium state when the osmotic and elastic parts of the free energy balance. The equilibrium swelling of an unentangled network in a θ-solvent can be used to estimate the average number of monomers in a network strand:

$$N \approx Q^{8/3}. \tag{7.156}$$

However, such relations only apply to networks that do not have entanglements. Real networks usually have important effects from entanglements and their swelling is not yet quantitatively understood. However, some qualitative features apply to both entangled and unentangled swollen networks. At a constant extent of crosslinking, the modulus always increases with both the preparation state concentration and the concentration of use. Furthermore, fewer entanglements exist in networks prepared at lower concentrations and deswelling such networks to the melt state can make networks with a modulus *below* the plateau modulus of the melt.

Dynamics in polymer networks and also in polymer liquids can be studied by a variety of viscoelasticity experiments. For networks and gels, these methods determine the modulus from the long time (or low frequency) viscoelastic response and directly measure the relaxation of dangling structures and sol fraction at higher frequencies. For polymer liquids in solution or melt states, the viscosity and relaxation time are determined from the long time (or low frequency) viscoelastic response, with higher frequencies providing information about other relaxation modes. The linear viscoelastic response of polymer liquids will be discussed in Chapters 8 and 9.

Problems

Section 7.1

7.1 Equation (7.9) is an example of a Maxwell relation. Derive the other two Maxwell relations associated with the Helmholtz free energy of a rubber.

7.2 Estimate the fraction of the tensile force at 300 K that has energetic origins by using a Flory construction on the following data for the temperature dependence of tensile force for a crosslinked rubber with 1 cm^2 cross-sectional area held at constant elongation.

T (K)	219	253	293	335
Force (N)	1.13×10^4	1.28×10^4	1.45×10^4	1.64×10^4

7.3 If a crosslinked rubber is rapidly stretched at constant volume, does it get warmer or cooler? Explain your answer.

Section 7.2

7.4 Consider an affine model of an incompressible network with polydisperse strands between crosslinks. Prove that the stress σ in this network due to

uniaxial extension still follows the classical dependence on deformation λ [Eqs (7.32) and (7.33)]. Which average molar mass of network strands enters into Eq. (7.31) for the network modulus?

7.5 What would be the size of a phantom network, made from strands with N monomers of size b and with functionality f of crosslinks, if it were not attached to the macroscopic boundaries of the network?

7.6 For any isotropic solid stretched in the x direction, the longitudinal tensile strain ε_{xx} is the change in length divided by the initial length. Similarly, the transverse tensile strains ε_{yy} and ε_{zz} are the changes in width and height divided by the initial values.

(i) Write the longitudinal and transverse strains in terms of the deformation factor λ.

Poisson's ratio ν is defined from the ratio of transverse and longitudinal strains in tension:

$$\nu \equiv \frac{-\varepsilon_{yy}}{\varepsilon_{xx}}. \tag{7.157}$$

(ii) Write Poisson's ratio in terms of λ, and show that for small deformations ($\lambda \to 1$) at constant volume, Poisson's ratio is 1/2. What happens to Poisson's ratio at larger deformations?

7.7 The **bulk modulus** K is defined as the reciprocal of the isothermal compressibility, and Young's modulus E is defined as the ratio of longitudinal tensile stress and longitudinal tensile strain:

$$K \equiv -V\left.\frac{\partial P}{\partial V}\right|_T \qquad E \equiv \frac{\sigma_{xx}}{\varepsilon_{xx}} \tag{7.158}$$

Poisson's ratio relates Young's modulus to either the shear modulus G or the bulk modulus K:

$$E = 2(1+\nu)G = 3(1-2\nu)K. \tag{7.159}$$

A vulcanized natural rubber (*cis*-polyisoprene) has bulk modulus $K = 2 \times 10^9$ Pa and Young's modulus $E = 1.3 \times 10^6$ Pa.

(i) What is Poisson's ratio for this vulcanized natural rubber?
(ii) What is the shear modulus of this vulcanized natural rubber?
(iii) Show that in the limit where the bulk modulus is much larger than the shear modulus, Poisson's ratio is 1/2. This limit is also achieved for most liquids (including polymer melts and solutions) which is why they are termed incompressible.
(iv) Relate the deviation of Poisson's ratio from its incompressible limit ($\nu = 1/2$) to the ratio of moduli E/K.

7.8 Heating up a strip of natural rubber from $T_1 = 300$ K to $T_2 = 350$ K increases the stress at constant elongation $\lambda = 2$ from $\sigma_1 = 4.3 \times 10^5$ Pa to $\sigma_2 = 5 \times 10^5$ Pa. Assuming a linear dependence of stress on temperature at constant elongation, estimate the energetic σ_E and entropic σ_S contributions to the stress at $T_1 = 300$ K.

7.9 A crosslinked polybutadiene ball of mass 100 g is dropped at 300 K from a height of 1 m and bounces back 92 cm.

(i) Assuming that the floor does not deform and all energy lost in this collision goes into heating up the ball, how much did the ball's temperature increase? The heat capacity of polybutadiene at 300 K is $C_p = 2.2\,\mathrm{kJ\,kg^{-1}\,K^{-1}}$.
(ii) By how much does this temperature change alter the elastic modulus of the ball?

7.10 The rubber in an inflated balloon is stretched biaxially, with initial diameter d_0 and initial thickness of its walls t_0. This incompressible rubber contains ν elastic strands per unit volume.

(i) Derive the tensile stress σ in either of the two stretching directions in the rubber in terms of the relative change of balloon size $\lambda = d/d_0$ during subsequent inflation or deflation. Assume that the rubber obeys the affine network model.
(ii) Relate the internal pressure (p) and the degree of expansion ($\lambda = d/d_0$). Assume that the ideal gas law ($pV = n\mathcal{R}T$) is valid for the helium inside the balloon.
(iii) At what value of λ is the helium pressure maximum?

This problem was adapted from U. W. Gedde, *Polymer Physics*, Chapman and Hall, London (1995).

7.11 A steel ball is attached to a rubber band of size $0.2\,\text{cm} \times 0.2\,\text{cm} \times 10\,\text{cm}$ and stretches it in the z direction to a 40 cm length, developing an engineering stress $2 \times 10^7\,\text{dyn cm}^{-2}$ in the rubber at the temperature 20 °C. Assume that the rubber band obeys the affine model.

(i) What is the relative elongation λ of the rubber band?
(ii) How many moles of network chains ν are there per cubic centimeter?
(iii) What is the number-average molar mass M_s between crosslinks, if the density of rubber is $\rho = 1\,\text{g cm}^{-3}$?
(iv) What is the mass m of the steel ball?
(v) What engineering stress σ_1 is required to stretch the rubber to a length 30 cm at 20 °C?
(vi) What mass m_1 do we need to attach to the rubber band to develop this stress σ_1 at 50 °C?

7.12 A strip of elastomer $1\,\text{mm} \times 1\,\text{mm} \times 10\,\text{cm}$ that obeys the affine network model is stretched to 40 cm length at $T = 300\,\text{K}$ at the engineering stress 1×10^7 Pa. The volume occupied by each monomer is $b^3 = 80\,\text{Å}^3$.

(i) What is the relative elongation λ?
(ii) Find the shear modulus G.
(iii) How many moles of network strands are in this rubber strip?
(iv) Estimate the number of monomers between crosslinks.

7.13 Two identical 10 cm long rubber bands, A and B, are tied together at their ends, stretched to a total length of 80 cm and held in this stretched state. Rubber bands A and B are held at different temperatures T_A and T_B.

(i) Is the true stress σ_{true} the same for the two bands? Explain.
(ii) Is the engineering stress σ_{eng} the same for the two bands? Explain.
(iii) What is the temperature T_B of band B if the length of rubber band B is $L_B = 38\,\text{cm}$ and the temperature of band A is 10 °C. Assume the classical form for the stress-elongation relation of the rubber band.

7.14 To stretch a rubber band by the factor of $\lambda = 2$ requires stress $\sigma_1 = 1.5 \times 10^7\,\text{dyn cm}^{-2}$ at 0 °C and stress $\sigma_2 = 1.65 \times 10^7\,\text{dyn cm}^{-2}$ at 30 °C. Assume that the rubber band obeys the affine model.

(i) Estimate the entropic and energetic components of the stress at 30 °C.
(ii) What is the entropic part of the modulus of the rubber band at 30 °C?
(iii) What is the number-average molar mass of chains between crosslinks, if the elastomer density is $\rho = 1.1\,\text{g cm}^{-3}$?

7.15 A rubber band with molar mass between crosslinks $M_s = 3000\,\text{g mol}^{-1}$ is uniaxially stretched to three times its original length. After achieving equilibrium at 21 °C it is allowed to contract adiabatically back to the unstretched state.

(i) Is the final temperature higher or lower than 21 °C? Why?
(ii) Estimate the temperature change of this rubber band if its heat capacity is $C_p = 1700\,\mathrm{J\,kg^{-1}\,K^{-1}}$. Assume the classical form for the stress-elongation relation of the rubber band.

7.16 What is the molecular origin of strain hardening at large elongations of polymeric networks that do not crystallize on stretching?

7.17 Demonstrate that the true stress in uniaxially deformed incompressible networks is the derivative of the free energy per unit volume F/V with respect of the logarithm of deformation λ:

$$\sigma = \left.\frac{\partial(F/V)}{\partial(\ln\lambda)}\right|_V. \tag{7.160}$$

Section 7.3

7.18 Demonstrate that I_1, I_2, and I_3 are invariants by changing the coordinate system and proving that the quantities are not affected by this change.

7.19 Consider the Pincus blob picture of stretching an ideal chain, discussed in Section 2.6.1. For each Pincus blob there is of order kT of entropic free energy stored in the stretched chain. The chain is a sequence of *trans*, *gauche*$_+$, and *gauche*$_-$ states (see Fig. 2.1) with the energy difference between *trans* and *gauche* states of order kT. Can the stretching free energy per Pincus blob be thought of as forcing the chain to make one extra trans state (going forward between neighbouring Pincus blobs)? Indeed, at maximum extension, the chain is in the all-*trans* conformation (Fig. 2.2). Why is there no significant energetic contribution to stretching an ideal chain comparable to the entropic contribution (of order kT per Pincus blob)?

7.20* Consider a non-affine tube model, with the number of monomers in the virtual chains changing with network deformation as $n_i = \lambda_i^2 n_{i0}$, where n_{i0} is the number of monomers in virtual chains constraining fluctuations in the i direction in the undeformed state.

(i) Start with virtual chains with $n_{i0} \approx N_e$ virtual monomers in the undeformed state, with the points of attachments to the network chains separated by N_e real monomers. Demonstrate that after elongation by a factor $\lambda_x > 1$ in the x direction, the affine strand in the x direction contains $\lambda_x N_e$ real monomers. The affine strand is defined as the smallest section of a network strand that deforms affinely. The entire network deforms affinely on length scales larger than the affine strand. Sections of network chain that are smaller than the affine strand are deformed non-affinely.

Hint: Use the invariance of confinement upon appropriate simultaneous change of the length and the number of virtual chains [Eq. (7.61)].

(ii) Derive the following result for the size of the affine strand in the elongation direction:

$$R_{af}(\lambda_x) \approx b\sqrt{N_e}\lambda_x^{3/2} \quad \text{for } \lambda_x > 1.$$

(iii) Prove that the distance between entanglements that are separated by N_e monomers along the deformed affine strand is

$$a_x \approx b\sqrt{N_e}\lambda_x^{1/2}.$$

Compare this distance between entanglements with the root-mean-square fluctuations of the affine strand. Explain this result.

Hint: Assume that the affine strand is uniformly stretched.

(iv) Show that the contribution to the free energy density from the elongation direction is linear in deformation:

$$\frac{F_x}{V} \approx \frac{\rho \mathcal{R} T}{M_e} \lambda_x$$

Hint: Consider the contribution from an affine strand.

(v) Derive the following result for the size of the affine strand in the compression (y) direction ($\lambda_y < 1$):

$$R_{af}(\lambda_y) \approx b\sqrt{N_e}\lambda_y^{1/2} \quad \text{for } \lambda_y < 1.$$

Show that the affine strand has N_e/λ_y monomers.
Hint: Use the invariance of confinement upon appropriate simultaneous change of the length and the number of virtual chains [Eq. (7.61)].

(vi) Show that the free energy density contribution from the direction of confinement is

$$\frac{F_y}{V} \approx \frac{\rho \mathcal{R} T}{M_e} \frac{1}{\lambda_y}.$$

(vii) Assume that the free energy density cost for each component can be approximated by the expression

$$\frac{F_i}{V} \approx \frac{\rho \mathcal{R} T}{M_e}\left(\lambda_i + \frac{1}{\lambda_i}\right), \tag{7.161}$$

and the total free energy density of the network can be approximated by the sum of the phantom and entanglement contributions

$$\frac{F}{V} \approx \frac{\rho \mathcal{R} T}{M_x}\sum_i \frac{\lambda_i^2}{2} + \frac{\rho \mathcal{R} T}{M_e}\sum_i \left(\lambda_i + \frac{1}{\lambda_i}\right). \tag{7.162}$$

Demonstrate that for uniaxial deformation of an incompressible network, the stress is given by Eq. (7.64) where the crosslink and entanglement moduli G_x and G_e, respectively, are defined in Eqs (7.43) and (7.47).

7.21* Consider a combined linear chain consisting of a 'real' N-mer and a 'virtual' m-mer. The ends of this combined chain are attached to an elastic non-fluctuating background. The x coordinate of the attachment points in the undeformed state is X_1 at the virtual chain end and X_2 at the real chain end of the combined chain. The ends of the combined chain deform affinely with the elastic background $X_1' = \lambda X_1$ and $X_2' = \lambda X_2$.

(i) Show that if the stress were supported exclusively by the real chain it would be equal to

$$\sigma = \frac{3kT}{b^2 N}\langle (R' - X_2')^2 \rangle - kT.$$

(ii) Derive the expression of mean-square end-to-end distance of the N-mer part of the combined chain.

$$\langle (R' - X_2')^2 \rangle = \frac{N^2}{(N+m)^2}(X_2' - X_1')^2 + \frac{b^2 N m}{N+m}.$$

(iii) Show that the stress supported exclusively by the real chain is

$$\sigma = kT\frac{N}{N+m}\left(\frac{(X_2' - X_1')^2}{b^2(N+m)} - 1\right).$$

(iv) Assume that the number of monomers in the virtual chain changes as a power law of the deformation:

$$m = m_0\lambda^\alpha.$$

Show that the contribution of this combined chain to the stress is

$$\sigma = kT\left(\frac{3(X_2' - X_1')^2}{b^2(N+m_0\lambda^\alpha)} - 1\right)\frac{N}{N+m_0\lambda^\alpha} + kT\left(1 - \frac{\alpha}{2}\right) \tag{7.163}$$

Determine the exponent α for which the virtual chain does not contribute to the stress and all of the stress is supported by the real chain.

7.22 Consider a comb polymer with p Kuhn monomers of length b between neighbouring points of attachment of n-mer side branches. Assume the number of side branches is large and that the end of each side branch is randomly attached to the elastic non-fluctuating background. Show that the mean-square fluctuation of the junction points is $b^2\sqrt{pn}$.

Section 7.4

7.23 Consider a network formed by end-linking chains with degree of polymerization $N = 100$ and monomer volume $b^3 = 30\,\text{Å}^3$ in a dry melt state ($\phi_0 = 1$).

(i) What is the modulus $G(1)$ of the network at preparation (dry) conditions at room temperature?
(ii) What is the equilibrium swelling ratio of this network at the θ-temperature ($\theta = 35\,^\circ\text{C}$)?
(iii) What is the equilibrium swelling ratio of this network in an athermal (good) solvent?
(iv) What would be the modulus $G(1/Q)$ of the network in a fully swollen state in the athermal solvent?

7.24 (i) Calculate the concentration dependence of the osmotic pressure of a gel in an athermal solvent, being sure to include both mixing and strand elasticity parts of the free energy.
(ii) Plot the osmotic pressure of a gel prepared in the melt state ($\phi_0 = 1$) with $N = 100$ monomers between crosslinks and the osmotic pressure of a solution of very long linear chains as functions of volume fraction of polymer. Why is the osmotic pressure of the gel smaller than that of the solution?
(iii) At what concentration is the osmotic pressure of the gel zero? What is the physical meaning of this concentration?

7.25 Swelling a thin film network.

The photoactive elements in photographic film are dispersed in a crosslinked gelatin network. During processing, this network is swollen to allow the developer solution to enter the gel. Since the network is strongly bonded to a solid substrate, it is constrained to only swell in one dimension (perpendicular to the substrate) with the other two dimensions unchanged by swelling.

(i) Derive the expression below for the concentration dependence of the modulus of the swollen gel, assuming the developer solution is an athermal solvent and that the network is also prepared in an athermal solvent:

$$G(\phi) \approx \frac{kT\,\phi_0^{7/4}}{b^3 N\,\phi^{3/4}}. \tag{7.164}$$

(ii) Why does this modulus *increase* as the network is diluted?
(iii) Derive an expression for the equilibrium swelling.
(iv) For a photographic film with $N = 100$ Kuhn monomers between crosslinks, prepared at volume fraction $\phi_0 = 0.1$, what is the equilibrium swelling?

7.26 What is the true osmotic pressure of a polymer gel swollen to equilibrium in a good solvent?

7.27 Estimate the average number of monomers in a network strand for gels prepared in the dry state and swollen to equilibrium in a θ-solvent with

(i) $Q = 2$,
(ii) $Q = 4$

7.28 At room temperature, compare the equilibrium swelling, dry modulus and modulus at swelling equilibrium for a network with $N = 10$ Kuhn monomers of length $b = 4$ Å per strand prepared in the dry state, swollen in

(i) athermal solvent,
(ii) θ-solvent

7.29 The modulus of unentangled networks is kT per combined strand [Eq. (7.43)]. Explain why the stretching caused by isotropic swelling increases the contribution to the modulus from each combined strand. Why can the elastic modulus be approximated by an elastic energy density?

7.30 A network with strands of number-average degree of polymerization $N = 100$ has equilibrium swelling ratio $Q = 25$ in an athermal solvent. Assuming the network was prepared in an athermal solvent, estimate the preparation concentration.

7.31 Consider a PDMS network prepared in the dry state that swells to an equilibrium swelling ratio of $Q = 4$ in the concentrated regime (θ-like swelling). Estimate the dry modulus of the network at room temperature. Compare your result with Fig. 7.17 and estimate the numerical prefactor in Eq. (7.91).

7.32 Consider a PDMS network prepared in the dry state that swells in toluene at 25 °C to an equilibrium swelling ratio of $Q = 7$. Estimate the dry and fully swollen moduli if the boundary of the concentrated regime is $\phi^{**} \approx 0.2$ and $b = 13$ Å for PDMS.

Section 7.5

7.33 Langley used the mean-field percolation model to derive the entanglement trapping factor, assuming that the probability of entanglement between two network strands is proportional to the square of their concentration. The probability $\mathcal{P}_2$ that a randomly chosen monomer in a network strand is connected to the macroscopic gel along both linear chain paths emanating from it is determined by integrating the gel curve [Eq. (6.163)] for each direction over the entire strand:

$$\mathcal{P}_2 = \frac{1}{N}\int_0^N [1 - \exp(-spP_{\text{gel}})][1 - \exp(-[N-s]pP_{\text{gel}})]\,ds. \tag{7.165}$$

The integration variable s represents the contour coordinate that counts monomers along the strand (running from 0 at one end to N at the other end) and p is the probability that a monomer has been randomly crosslinked. This integration assures that each monomer in the strand of N monomers is connected in both directions to the gel.

(i) Obtain the probability $\mathcal{P}_2$ by integrating Eq. (7.165) and use Eq. (6.163) to write your result as a function solely of gel fraction.

(ii) For an entanglement to be permanently trapped by the crosslinking, all four strand ends in Fig. 7.9 must be connected to the macroscopic gel, making the entanglement trapping factor of Eq. (7.95) $T_e \approx (\mathcal{P}_2)^2$. If any of the four paths are simply a network defect (such as a dangling end or loop, see Fig. 7.7) the entanglement will eventually be abandoned and hence not contribute to the modulus of the network. Use the result from part (i) to derive the Langley prediction for the entanglement trapping factor:

$$T_e = \left[2 - P_{gel} + \frac{2P_{gel}}{\ln(1 - P_{gel})}\right]^2. \tag{7.166}$$

7.34

(i) Calculate the probability $\mathcal{P}_1$ that a randomly chosen monomer in a strand is connected to the macroscopic gel along only one of the linear chain paths emanating from it.

(ii) Calculate the probability $\mathcal{P}_0$ that a randomly chosen monomer in a strand is not connected to the macroscopic gel along either of the two linear paths emanating from it.

(iii) Show that the probabilities $\mathcal{P}_0$, $\mathcal{P}_1$, and $\mathcal{P}_2$ (from Problem 7.33) are properly normalized (i.e., that $\mathcal{P}_0 + \mathcal{P}_1 + \mathcal{P}_2 = 1$).

7.35 When a lightly crosslinked gel first swells in a solvent, it jumps around. Why does it do it?

Section 7.6

7.36 Stress relaxation.

(i) Use the following table of data for the shear stress relaxation modulus of a polymer melt to determine the viscosity η, the steady state compliance J_{eq}, and the longest relaxation time ηJ_{eq}. Be sure to include any graphs that may be relevant for these calculations.

t(s)	$G(t)$ (Pa)	t(s)	$G(t)$ (Pa)	t(s)	$G(t)$ (Pa)
0.0133	1.0×10^6	20.6	4.8×10^5	106	1.2×10^5
0.365	9.4×10^5	28.6	4.1×10^5	122	9.6×10^4
1.00	8.8×10^5	41.9	3.2×10^5	139	7.6×10^4
1.90	8.3×10^5	50.0	2.8×10^5	155	6.2×10^4
2.79	7.9×10^5	55.3	2.6×10^5	189	4.0×10^4
3.69	7.5×10^5	60.6	2.4×10^5	238	2.2×10^4
5.50	7.0×10^5	68.6	2.1×10^5	305	1.0×10^4
7.29	6.6×10^5	73.9	1.9×10^5	356	5.0×10^3
10.0	6.1×10^5	81.9	1.7×10^5	422	2.2×10^3
15.3	5.4×10^5	90.0	1.5×10^5	472	7.1×10^2

(ii) How does the longest relaxation time compare with the maxima in the functions $tG(t)$ and $t^2G(t)$?

(iii) Sketch the time dependences of the creep compliance and recoverable compliance that you would expect to see for the polymer melt in part (i), assuming creep and recovery were measured at the same temperature. Indicate values of the rubbery compliance and the steady state compliance on the plot.

7.37 Creep.

(i) Determine the viscosity η, the steady state compliance J_{eq}, and the longest relaxation time $\eta_0 J_{eq}$ from the following creep data on a polymer solution at a shear stress of 20 Pa:

Time (s)	100	200	300	400	500	600	700	800	900	1000
Strain	0.31	0.52	0.74	0.92	1.10	1.28	1.46	1.64	1.82	2.00

(ii) Small-angle scattering reveals that the polymer's radius of gyration in this solution is 400 Å. Individual chains in polymer liquids move randomly in solution by a process known as diffusion. For diffusive motion, the square of the typical distance x moved is proportional to the time t allowed for motion, with the coefficient of proportionality being the diffusion coefficient D:

$$D \approx \frac{x^2}{t}.$$

Use the fact that the polymer roughly diffuses a distance equal to its coil size during a time interval equal to its longest relaxation time, to estimate the diffusion coefficient of the polymer.

7.38 Determine the viscosity η, the steady state compliance J_{eq}, and the longest relaxation time $\tau \approx \eta J_{eq}$ from the following data for monodisperse linear polystyrene with $M = 60\,600\ \mathrm{g\,mol^{-1}}$ at 180 °C.

ω (rad s^{-1})	G' (Pa)	G'' (Pa)
57.54	17400	49000
36.31	7590	33100
22.91	3090	21900
14.45	1260	14100
9.12	525	9120
5.75	200	5750
3.63	83.2	3720
2.91	33.1	2900

7.39 At low frequencies G'' of a liquid contains information on viscosity η, while G' of a liquid contains information on recoverable compliance J_{eq}. At low frequencies G' of a solid contains information on its modulus G_{eq}. What does G'' tell us about the network at low frequency?

7.40 If it is necessary to signal average for three full cycles, how much time was required to obtain the lowest frequency data points of Fig. 7.28?

7.41 Boltzmann superposition in oscillatory shear.

Use the Boltzmann superposition integral to derive the storage modulus of a viscoelastic liquid as a sine transform of the stress relaxation modulus $G(t)$ [Eq. (7.149) with $G_{eq}=0$]. Also derive the loss modulus as a cosine transform of $G(t)$ [Eq. (7.150) with $G_{eq}=0$] for a viscoelastic liquid.

7.42 Oscillatory shear.
Show that the dissipated energy per unit volume in each cycle of oscillatory shear is $\pi\gamma_0^2 G''$.

7.43 Prove that, for an affine network in uniaxial tension, the ratio

$$\frac{\sigma_{true}}{\lambda^2 - 1/\lambda}$$

is the shear modulus defined in Eq. (7.98), making use of the fact that Young's modulus is three times the shear modulus.
Hint: Hooke's law in tension is $\sigma_{true}=E\varepsilon$, where $E=3G$ is Young's modulus and $\varepsilon=(L-L_0)/L_0$ is the extensional strain (L and L_0 are the final and initial lengths of the sample).

7.44* Use the Boltzmann superposition integral to derive Eq. (7.128) for the recoverable compliance of a viscoelastic liquid.

7.45 Diblock copolymers with roughly equal block lengths can microphase separate into a lamellar phase, with alternating layers of mostly A monomer and mostly B monomer. When quenched into the lamellar phase from the isotropic phase, these layers form roughly parallel to each other locally. A polydomain texture is created from this quenching, with a typical grain size of order 0.1 μm. The oscillatory shear response of such a quenched sample is observed to have $G' \sim G'' \sim \omega^{1/2}$ at the lowest measurable frequencies. Can this observed response be the real terminal response of the sample? Is this sample a viscoelastic solid or a viscoelastic liquid?

7.46 Consider a liquid with a single relaxation mode and stress relaxation modulus given by the Maxwell model:

$$G(t) = G_0 \exp(-t/\tau).$$

(i) Calculate the viscosity of this liquid.
(ii) Estimate the viscosity of the liquid using $\eta \approx G(\tau)\tau$ [Eq. (7.120)]. What is the relative error of this estimate?

7.47 Find the relation between creep compliance $J(t)$ and recoverable compliance $J_R(t)$ using the Boltzmann superposition principle.

7.48 Dielectric spectroscopy indicates that water molecules respond to an oscillating electric field at a frequency of 17 GHz at room temperature. Is water still a Newtonian liquid at this high a frequency or is it viscoelastic? If it is viscoelastic, at what time scales can viscoelasticity be observed?

7.49 The Voigt model is similar to the Maxwell model, but the elastic and viscous elements are in parallel instead of in series. In the Voigt model each element has the same strain and the stress is the sum of the stresses in the two elements.

(i) Derive the creep compliance of the Voigt model. What type of material does the Voigt model describe? What is the behaviour of the Voigt model during creep recovery?
(ii) Derive the stress relaxation modulus of the Voigt model. What goes wrong with the Voigt model in describing stress relaxation?
(iii) Derive the stress relaxation modulus of a series combination of the Voigt model (with modulus G_V and viscosity η_V) and an elastic element (with modulus G_E).
(iv) Describe in words what happens to the three elements in part (iii) as a function of time after the step strain.

(v) What is the relaxation time for the three-element model with constants described in part (iii) and what is its physical significance?

7.50 Consider a series combination of two Maxwell models, whose stress relaxation modulus is a simple sum:

$$G(t) = G_A \exp(-t/\tau_A) + G_B \exp(-t/\tau_B).$$

(i) Calculate the storage and loss moduli of this system.
(ii) What is the longest relaxation time of the system if $\tau_A > \tau_B$? What is the average relaxation time τ determined from Eq. (7.136)?
(iii) What are the viscosity and the recoverable compliance of the series combination of two Maxwell models?
(iv) Calculate the low frequency behaviour of the storage and loss moduli. Verify that $\omega = 1/\tau$ corresponds to the intersection of the extrapolations of the low frequency power laws of $G'(\omega)$ and $G''(\omega)$. Verify that $\tau = \eta J_{eq}$.

Bibliography

Boyd, R. H. and Phillips, P. J. *The Science of Polymer Molecules* (Cambridge University Press, Cambridge, 1993).

Doi, M. and Edwards, S. F. *The Theory of Polymer Dynamics* (Clarendon Press, Oxford, 1986).

Erman, B. and Mark, J. E. *Structures and Properties of Rubberlike Networks* (Oxford University Press, Oxford, 1997).

Ferry, J. D. *Viscoelastic Properties of Polymers*, 3rd edition (Wiley, New York, 1980).

Flory, P. J. *Principles of Polymer Chemistry* (Cornell University Press, Ithaca, New York, 1953).

Graessley, W. W. The entanglement concept in polymer rheology. *Advances in Polymer Science* **16**, 1 (1974).

Heinrich, G., Straube, E., and Helmis, G. Rubber elasticity of polymer networks: theories. *Advances in Polymer Science* **85**, 33 (1988).

Queslel, J. P. and Mark, J. E. Molecular interpretation of the moduli of elastomeric polymer networks of known structure. *Advances in Polymer Science* **65**, 135 (1984).

Staverman, A. J. Properties of phantom networks and real networks. *Advances in Polymer Science* **44**, 73 (1982).

Treloar, L. R. G. *The Physics of Rubber Elasticity*, 3rd edition (Clarendon Press, Oxford, 1975).

This page is intentionally left blank